DOI:10.14753/SE.2020.2446

SEMMELWEIS EGYETEM

DOKTORI ISKOLA

Ph.D. értekezések

2446.

KAZSOKI ADRIENN KATALIN

A gyógyszerészeti kutatások korszerű kutatási irányai

című program

Témavezető: Dr. Zelkó Romána, egyetemi tanár

Programvezető: Dr. Antal István, egyetemi tanár

DOI:10.14753/SE.2020.2446

FORMULATION AND MICROSTRUCTURAL DISTINCTION OF NANOFIBROUS DRUG DELIVERY SYSTEMS

Ph.D. thesis

Dr. Adrienn Katalin Kazsoki

Doctoral School of Pharmaceutical Sciences

Semmelweis University

Supervisor: Romána Zelkó, D.Sc., professor

Official reviewers:
Rita Ambrus, Ph.D., associate professor
Krisztina Ludányi, Ph.D., associate professor

Head of the Complex Examination Committee:
István Antal, Ph.D., professor

Members of the Complex Examination Committee:
Ildikó Bácskay, Ph.D., associate professor
László Tóthfalusi, Ph.D., associate professor

Budapest
2020

DOI:10.14753/SE.2020.2446

TABLE OF CONTENTS

DOI:10.14753/SE.2020.2446

DOI:10.14753/SE.2020.2446

LIST OF ABBREVIATIONS

API	active pharmaceutical ingredients
ASD	amorphous solid dispersion
CD	cyclodextrin
CP-MAS	cross polarization magic angle spinning
FTIR	Fourier transform infrared spectroscopy
HPC	hydroxypropyl cellulose
HP-β-CD	hydroxypropyl-beta-cyclodextrin
MH	metoclopramide-hydrochloride
o-Ps	ortho-positronium
PALS	positron annihilation lifetime spectroscopy
PS	polysorbate
PVA	poly(vinyl alcohol)
RH	relative humidity
ROESY	rotating-frame nuclear overhauser effect spectroscopy
SD	solid dispersion
SEM	scanning electron microscopy
SS	solid solution
(ss)NMR	(solid-state) nuclear magnetic resonance
t	time
XRD	powder X-ray diffraction

DOI:10.14753/SE.2020.2446

1. INTRODUCTION

Over the past few decades, nanotechnology has gained increasing attention, which is due to its various fields of applications such as medicine, molecular diagnostics electronics, energy, and environment (1-3). Their potential application as drug delivery, protein- and peptide delivery has become the focus of pharmaceutical research interests. It is a promising tool for overcoming the formulation problems of drugs of undesirable physicochemical properties (4, 5).

Multifarious nanosized drug delivery systems have been developed, but the significance of the solid lipid matrix-based formulations, inorganic nanoparticles, and the polymeric nanocarrier and nanofibers are the most decisive ones (6). Incorporation of drugs in nanosized systems offer several advantages, for example, the therapeutic efficacy can promote, the drug dissolution and consequently, the bioavailability can improve (6). Among the polymer-based nanocarriers, the formulation of nanofiber systems has become a very intensively researched field in recent years. Therefore, my thesis focuses on approaches based on the applications of the fibrous materials as drug delivery carriers (7, 8).

Several techniques exist for preparing fibrous materials. Rotary spinning, melt spinning and electrospinning are the most commonly used techniques for fabrication fibers of a monolithic structure. The latter method is able to form a fiber of core-shell structure by using a special coaxial or triaxial emitter (9).

1.1. Electrospinning technique

Electrospinning is a relatively simple, well-established, intensively investigated, and economical fiber fabrication technique, which is able to form continuous fibers in the submicron range under atmospheric pressure and without the use of high temperature, making the formulation of sensitive drugs possible.

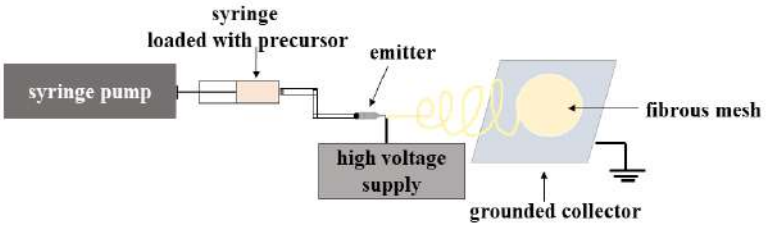

Figure 1 Construction of a lab-scale electrospinning device

Figure 1 illustrates the setup of a lab-scale electrospinning device schematically. It has three major parts: the high-voltage power supply, the spinneret (emitter, metallic-needle) and the grounded collector. The emitter is connected to the syringe through a Teflon tube. The prepared precursor (viscous polymer solution or melt) is transferred into a syringe, which is placed in a syringe pump that provides the continuous and controlled flow rate. Fabrication of fibrous materials is carried out by applying high-voltage and is based on the uniaxial stretching of the viscoelastic jet derived from the precursor system (10). During the process, the solvent or solvent mixture evaporates, leaving behind a solid fibrous mesh on the collector. Electrospinning is a continuous method, which makes it suitable for high-volume production. Its popularity is due to the fact that it is a well controllable method for preparing matrices of nano- and micrometer-sizes (11-14). The polymeric fibrous mesh can be prepared from a melt and also from solution precursor systems using an electric field (15-17). The fiber diameters can be controlled well by the process (flow rate, emitter to collector distance, applied voltage) (11, 18, 19) and environmental parameters (temperature, relative humidity) (20, 21, 18) and also by the spinnable precursor physicochemical properties (e.g. molecular weight of the polymer, concentration, surface tension, conductivity, rheological properties) (11, 22, 23, 18, 24-26). The possibility of fine-tailoring of the fiber characteristics through the optimization of process parameters has been discussed in several research papers (9). The major challenge is associated with the production rate, but its scale-up possibility has been investigated. Despite several solutions and implementations, it is still in its infancy, but due to the improvements, its industrial application is very promising (27-30).

1.2. Advantages and the related applications of micro- and nanofibrous systems

There is a wide range of properties of the fibrous materials that can be used in a broad range of biomedical and pharmaceutical applications (9). The unique properties of the random mesh of the nanofibers - high porosity, and the increased surface area to volume ratio - make them attractive as drug delivery vehicles (31). Due to their unique structure, the multifunction property, together with different drugs, can be embedded into nanofibers, and fibers can be prepared from a wide variety of polymers thus modifying the function-related characteristics which are commonly used in tissue regenerations and wound healing (32-35). The latter is based on the features and morphology of the

nanofibrous scaffolds that are very similar to the extracellular matrix, which has a crucial role in wound healing (36). Due to the this structural similarity, the fibrous scaffolds can stimulate cell proliferation and could help the wound healing process (37).

Besides the widespread biomedical applications of the nano- and microfibrous materials, their pharmaceutical applicability has become an intensively researched field. It has a particular role in the formulation of solid dispersions of drugs with poor water solubility. Solid dispersions are multicomponent solid products, where the active ingredient is embedded into an inert matrix, whose solubility is remarkably improved due to its more favorable wettability and fine particle-size distribution. The grouping of these systems is illustrated in **Figure 2**.

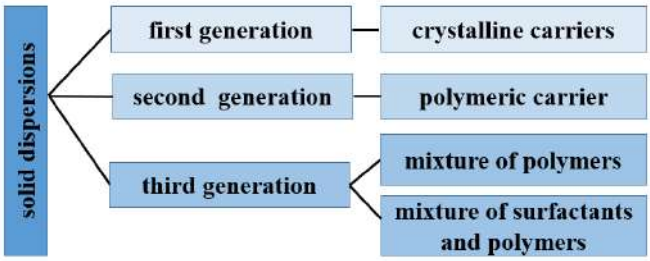

Figure 2 Grouping of solid dispersions (38)

In pharmaceutical applications, drugs and biologics are usually embedded into a polymer matrix. In the case of poorly water-soluble active ingredients, hydrophilic polymers are the most commonly used matrix. A further advantage of these systems is that with a rational choice of the polymer, the drug release kinetics can be designed to suit therapeutic requirements. The possibilities offered by electrospinning are based on the fact that as a result of the fiber fabrication process, the active pharmaceutical ingredients (APIs) can be embedded into the polymeric carrier in an amorphous state; and the amorphous materials' energy levels, which are higher than those of crystalline ones, may result in an enhanced apparent aqueous solubility and dissolution rate, and consequently, in increased bioavailability. It should be noted that in addition to amorphous drugs, crystalline APIs and biological materials can also be advantageously embedded in nanofibers (9).

1.3. Excipients modifying the drug-loaded fiber characteristics

There some other approaches in addition to the amorphization; for example, solubility can also be enhanced by using solubilizing agents. The use of surfactants is also providing

a solution for solubilizing lipophilic drugs. Polysorbate (PS) is a universal, non-ionic surfactant, which is widely used in the development of pharmaceutical formulation, as it is capable of improving the aqueous solubility of APIs and also acts as a permeability enhancer (39).

Very popular, but not universal solubilizers are cyclodextrins (CDs) and their derivatives (40, 41). CDs are cyclic oligosaccharides composed of glucopyranose units. Due to their unique truncated cone structure, hydrophilic exterior surface, and a nonpolar interior cavity (40), they provide drug-complexes of improved solubility properties. As cyclic host molecules with good water-soluble property, they can form inclusion complexes with nonpolar drugs of appropriate size, but besides that, formation of external adducts may also occur. As a result of the complex formation, the physicochemical properties of the drug can be modified. CDs can increase the aqueous solubility of the drug, promote the permeation and absorption of the API across biological membranes, and consequently, improve its bioavailability. They can enhance the physicochemical stability of the drugs via specific, non-covalent bond formations (40, 42). For the fiber formation by electrospinning, the use of uncharged CD derivatives are preferred (43-47), but electrospinning from the charged sulphobutyl-ether-β-CD containing precursor solution has already been described (48). Furthermore, the discussed solubilizing agents can promote the electrospinning process and act as plasticizers. Thus they can modify the mechanical properties of the fibers and enhance the final applicability of the fibrous materials (49).

1.4. Stability issues of amorphous materials

The enhanced apparent aqueous solubility of amorphous materials can be backtracked to their short-range order structural property. Although they have thermodynamically metastable nature (50), these systems are at a higher energy level, which can lead to their spontaneous recrystallization. Their enhanced thermodynamic potential, together with the increased molecular mobility, causes the physical and/or chemical instability of these systems (51). However, the stability and the possibilities for stabilization are a decisive issue for pharmaceutical products, because the product must provide the specified dose in proper quality. Predicting stability and examining the possibilities for stabilization is of huge importance during the formulation process. With the formulation of amorphous

solid dispersions or molecularly dispersed solid solutions, enhanced apparent aqueous solubility can be achieved, and the stability problems can be solved (52-54). Polymer macromolecules are able to form strong intermolecular interactions (e.g., hydrogen bonds) that may also lead to higher physicochemical stability. By a combination of the polymers with other excipients, for example, surfactants that can act as kinetic stabilizers, resulting in third-generation ASDs of improved stability property. Due to the exhibited secondary interactions, a complex molecular structure can be formed, which can reduce the probability of physical state changes of the amorphous API, as a result of the decreased molecular mobility (55).

Besides the embedded amorphous drug, the polymeric carriers are unstable also. Most of the polymers used for fiber formation are in an amorphous state, but if the polymeric carrier has semi-crystalline features that can promote the drug migration to the surface of the fiber, which can easily result in surface-crystallization (6). Aging-related processes can be related not only to the potential transition of the amorphous-crystalline form of the drug, but it can also entail the supramolecular alternations of the polymeric carrier as well. The long-term stability of polymer-based ASDs is determined by these two phenomena together, because they could affect the release characteristic and kinetics of the embedded drugs, which have a decisive impact on the bioavailability and therapeutic effect (51). Therefore, great attention should be paid to tracking the solid-state stability and monitoring the supramolecular changes of the drug-loaded nanofibrous mesh, since it is a critical point during the stability of these formulations (56). For investigating the complex micro- and macrostructural alterations, several techniques must be used, which can be classified into three groups: (i) imaging techniques, (ii) macrostructural, and (iii) microstructural characterization methods (56).

In the following, two techniques are discussed in detail. One of them is solid-state nuclear magnetic resonance (ssNMR), which is a very sensitive method, able to verify the nature of the amorphous systems and reveal the plasticizing mechanism. However, with this characterization technique, the free volumes are remaining invisible (57-61). In contrast, positron annihilation lifetime spectroscopy (PALS) is a sensitive method to determine the size distribution of free volume holes through ortho-positronium (o-Ps) lifetime distributions, which is able to follow the physical aging of the polymeric carrier (62-65).

1.5. Pharmaceutical application possibilities of nanofibrous systems

The nanofibrous formulations of required stability and desired function related properties are promising candidates for several dosage forms and pharmaceutical administration. A wide range of polymers can be used for solvent-based electrospinning, but the various polymers have different electrospinnable property. However, the low solubility of the drug in the fiber-forming solution limits the relative amount of drug in the nanofibers, and consequently the mass of the final product, as every polymer has an optimal concentration range where optimal fiber characteristic can be achieved. Therefore, the nanofiber-based formulations can be a potential product in the case of the API of a lower dose. The prepared nanofiber can be used as a final product, e.g., as buccal or sublingual sheets (66-68), wound bandage (69-72), or as intermediate product. After milling the fibers, an orodispersible (73) or a conventional tablet can be formed, but in the latter case great attention should be paid to monitoring changes in the physical state of the embedded drug(s), because changes may occur as a result of the milling process (74-77). Nanofibrous materials could be promising candidates for various administration routes; besides the most common *per os* application of the different formulations, the oral cavity is a possible site for the nanofiber-based controlled or fast release drug delivery systems for local therapy of the diseases of the oral cavity (78-80). In the case of this application, the most important factors are residence time and local drug concentration, because these influence the amount of the absorbed drug (81-83). The transmucosal routes offer an excellent alternative for systemic drug delivery of the APIs because of better patient adherence, ease of removal of the dosage form in emergencies, and good accessibility. That is due to the anatomic features of the mucosa: highly vascularized, rich in blood supply, and relatively permeable (84). However, permeation enhancers (e.g. PS, sodium lauryl sulfate, CDs) must be used to achieve the adequate level of bioavailability (85-87). Pharmaceutically luring advantages of the nanofibrous buccal formulations make them a very promising dosage form for diseases where the rapid onset (e.g., pain relief, nausea, migraine) is essential and in the case of APIs owing to the risk of potential liver damage. With nanofibers, the solubility related issue can be solved, whilst with the buccal administration route aims at the concerns associated with hepatic fist-pass metabolism and higher inter- and intraindividual varieties (88-94).

DOI:10.14753/SE.2020.2446

2. OBJECTIVES

The main objectives of my work were as follows.

- To formulate a papaverine-HCl-loaded nanofibrous sample for further buccal administration. For the bases of the formulation the first generation mucoadhesive hydroxypropyl cellulose (HPC) was chosen, but to improve its electrospinnability poly(vinyl alcohol) (PVA) was added to the system.

  - To determine the best composition for the fiber fabrication by electrospinning via preformulation study of different HPC-PVA mass ratios. (Besides, the total polymer concentration was kept constant.)
  - To investigate the effect of rheological properties and intermolecular interactions on morphological characteristics of the fabricated sample.
  - Supramolecular characterization and physicochemical investigation of the samples.
  - To examine the physicochemical stability of the drug-loaded nanofibers and to highlight how the physical aging of the polymeric carrier and the solid-state transition of the embedded drug take place.

- To prepare antiemetic drug (metoclopramide-HCl (MH) containing, PVA-based nanofibrous buccal sheets via electrospinning by using different permeability enhancer excipients: polysorbate 80 (PS 80) or hydroxypropyl-beta-cyclodextrin (HP-β-CD).

  - Morphological characterization of the electrospun sample.
  - To compare the mechanical features of the drug-loaded fibers containing PS 80 or HP-β-CD.
  - Solid-state characterization of the sample with particular attention paid to the investigation of the physical state of the embedded drug.
  - To obtain information on the plasticizing effect of the used excipients and to investigate the molecular mobility of the fibrous systems.
  - To study the dissolution profile of the formulations and to obtain information on drug distribution.
  - To examine the stress tolerance capacity, especially the supramolecular changing induced by elevated temperature and relative humidity.

DOI:10.14753/SE.2020.2446

3. RESULTS

3.1. Preformulation study of papaverine-HCl-loaded samples

3.1.1. Lorentz-Lorenz analysis of the precursor solutions used for electrospinning

Using the measured density and refractive index for precursor solutions of different HPC:PVA mass ratios, the R_m values, and space-filling factors were calculated. As a function of the PVA (as an auxiliary polymer) concentration of the precursor solutions (% w/w), the R_m values were plotted, and the slope of the fitted linear curve was 2.4024, and the linear regression accuracy value (R^2) was 0.9999. The R_c values of each viscous solution were calculated based on the linear regression. The space-filling factor were 0.224, 0.223, 0.223, 0.225 and 0.225 for precursor solution of HPC:PVA (m:m) of 5:5, 6:4, 7:3, 8:2 and 9:1, respectively. So a remarkable difference between these values was not found.

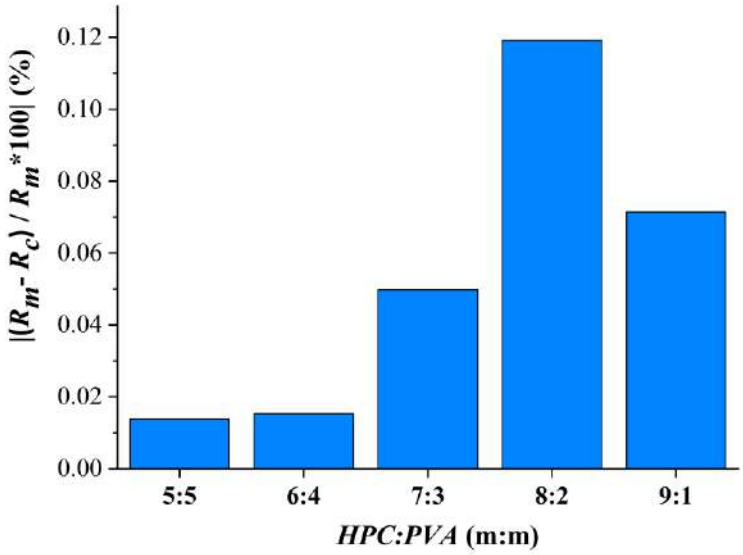

Figure 3 Lorentz-Lorenz plot values of papaverine-HCl loaded precursor solutions of different HPC:PVA mass ratios
(R_m is a measured and R_c is a calculated molar refraction index)

Figure 3 represents the Lorentz-Lorenz plot values of the drug-loaded precursor solutions as a function of their HPC:PVA mass ratio. It can be observed that with the increasing HPC ratio, the R_m and R_c values decrease continuously.

DOI:10.14753/SE.2020.2446

3.1.2. Rheological investigations of the polymer precursors

The viscoelasticity of the precursor solutions fundamentally determines the jet formation and stability; thus, it is a very critical parameter for the fiber formation process.

The storage and loss moduli were determined by oscillatory test measurements. The achieved moduli values were compared at different frequency values, but their ratio showed the same tendency; thereby, only the *G''/G'* dynamic moduli ratio results relating to 1.995 s^{-1} value were evaluated after this (**Figure 4**).

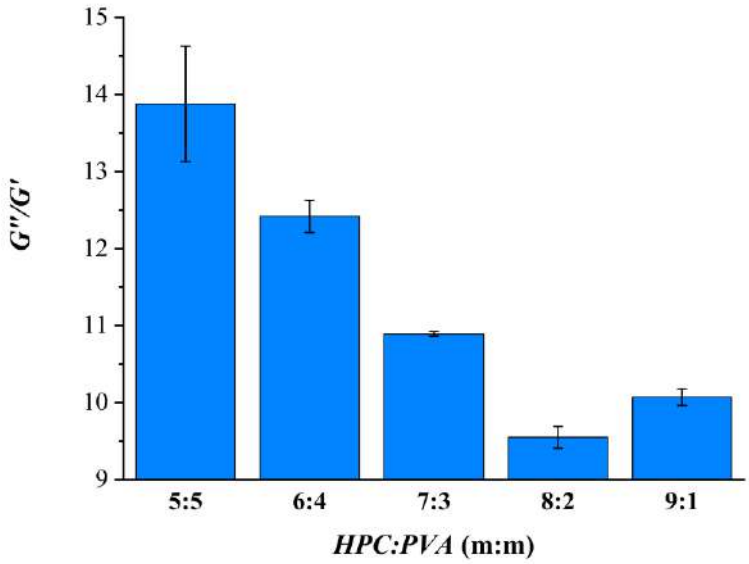

Figure 4 Ratio of loss (*G''*) and storage (*G'*) moduli of papaverine-HCl loaded precursor solutions as a function of HPC:PVA mass ratio (dynamic moduli measured at a frequency 1.995 Hz)

On the dynamic moduli ratio vs. HPC:PVA mass ration diagram can be seen unambiguously that it has a local minimum at a sample of HPC:PVA=8:2 mass ratio. With the increasing HPC ratio, the *G''/G'* value decrease monotonically, reaching a minimum, and after that, an increase can be observed.

3.1.3. Morphology study of the electrospun samples

The prepared papaverine-HCl-loaded HPC:PVA viscous solutions of constant 15 %(w/w) polymer concentration, but with different polymer ratios were used for the electrospinning process. Each of the five precursor solutions of different polymer compositions was suitable for electrospinning, but with varying degrees of success. The

electrospinning of the precursors resulted in well-defined, round samples on the collector, from where the samples could be easily peeled off. This is particularly advantageous for further processability and also from the point of the final applicability. The composition of HPC:PVA 9:1 was the exception only, where the removal was inhibited by firm adhesion.

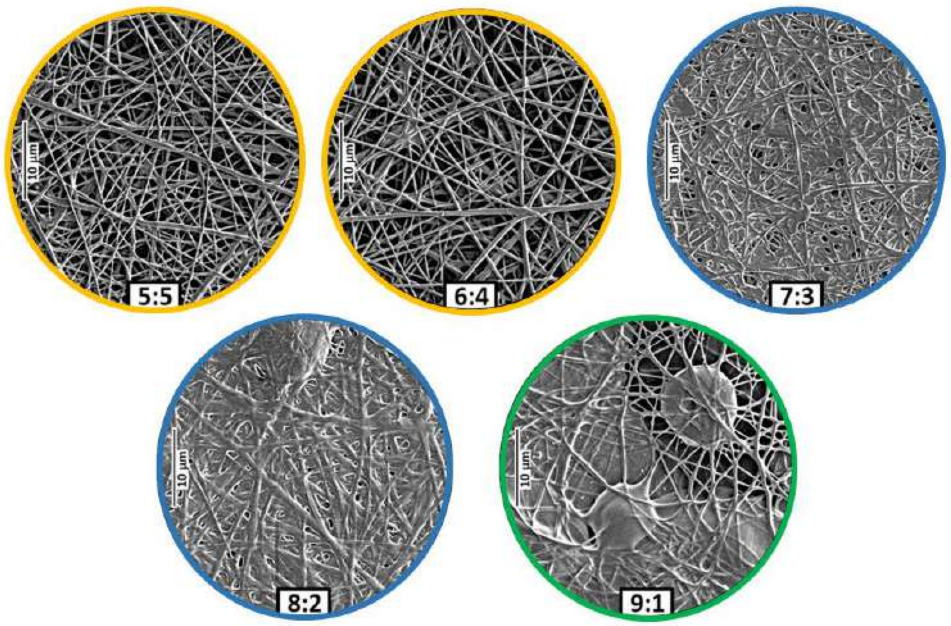

Figure 5 SEM images of the papverine-HCl-loaded electrospun samples as a function of HPC:PVA mass ratio 5:5 (**A**), 6:4 (**B**), 7:3 (**C**), 8:2 (**D**), 9:1 (**E**)

The morphology of the electrospun samples are shown in **Figure 5**. With the increasing HPC ratio to PVA morphology changes were obtained; spray-dried film-like structures, fibrous films, and clearly fibrous samples can be observed in the SEM images. At 9:1 HPC:PVA mass ratio, partial spray-dried film formation, and beaded fiber can be observed (**Figure 5E**). Electrospinning and electrostatic spraying co-occurred, which resulted in beaded fibers combined with film elements. In the case of 8:2 and 7:3 ratios, fibrous film morphology characteristics were obtained (**Figure 5D and C,** respectively), but in the latter case, the fibrous structure characterizes the whole fibrous film sample. SEM images of the electrospun samples of the two lowest (5:5 and 6:4) HPC ratio showed that random orientated, clearly fibrous structure without beads and film-like elements were achieved (**Figure 5A and B**, respectively).

As the HPC ratio was decreased, the fibrous characteristic became the dominant feature. The transition of a predominantly fibrous system from film formation was initiated at 8:2 HPC:PVA ratio, and was completed by 6:4 ratio. With the decreasing HPC ratio of the precursor solution, the fibrous part of the electrospun samples noticeably increased.

3.2. Solid-state characterization of the papaverine-HCl containing samples

3.2.1. Results of the FTIR analysis

FTIR measurements were carried out with the aim of characterizing the physical state of the API of the electrospun samples. The FTIR spectra of the electrospun samples, the physical mixture, and the solid components of the precursor solution are shown in **Figure 6.** In the spectra of the papaverine-HCl, the broad band system of the protonated amines can be observed between 2200-2800 cm^{-1}, with a maximum at 2495 cm^{-1}. The medium intensity bands are appearing above 3220 cm^{-1} are aromatic C-H vibrations, while the peaks at 2967-2840 cm^{-1} belonging to aliphatic C-H vibrations. The characteristic peak of the model drug between 2200-2800 cm^{-1} can be observed clearly in the physical mixture. These characteristic peaks were found to be selective, thus able to verify the physical state of the drug. Regardless of the polymer ratios, peaks belonging to the papaverine salt could not be observed.

DOI:10.14753/SE.2020.2446

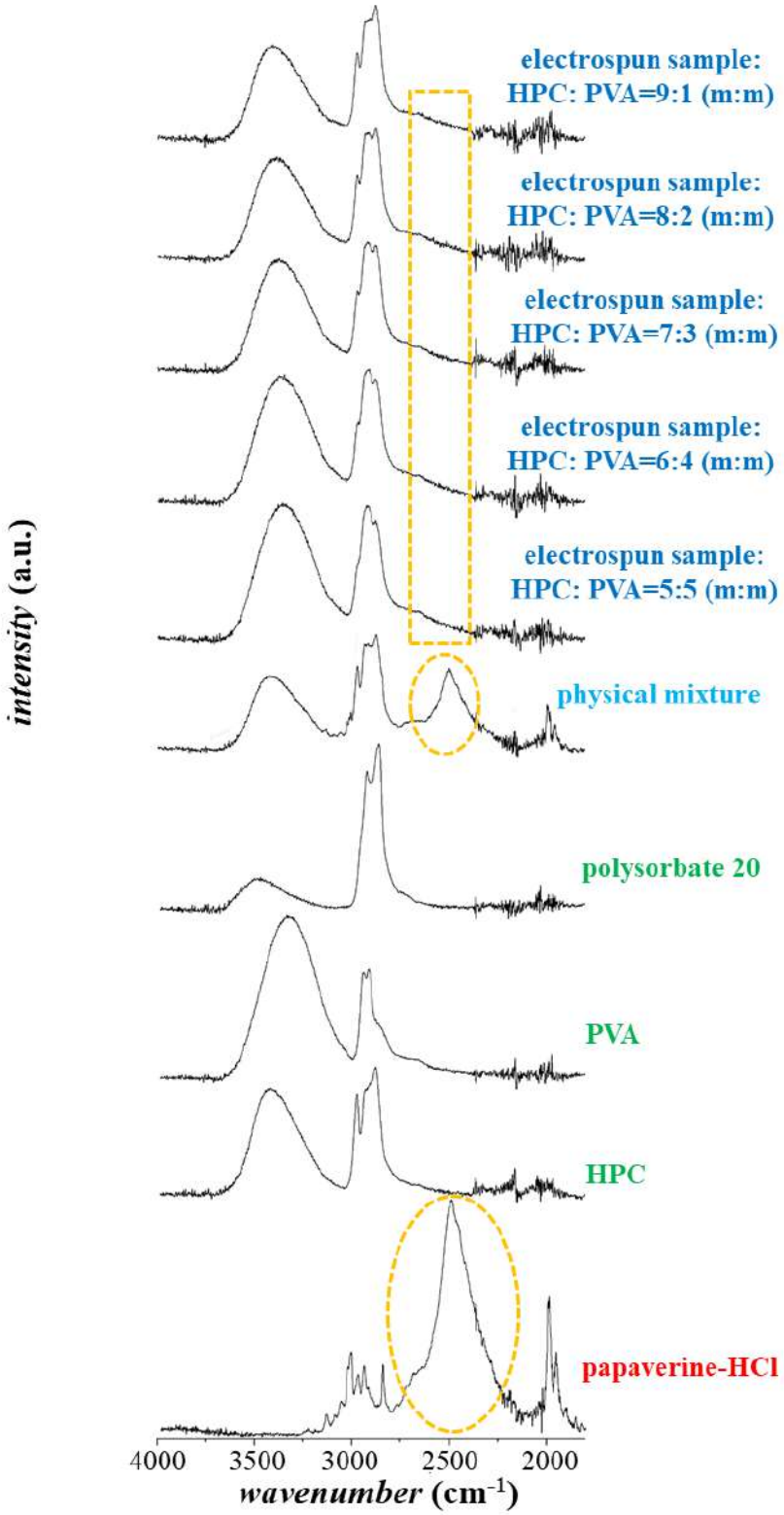

Figure 6 FTIR spectra of the components, physical mixture of the components and the drug-loaded electrospun sample of different hydroxypropyl cellulose (HPC) : poly(vinyl alcohol) PVA ratio

3.2.2. Microstructural distinction by PALS measurements

In order to monitor the supramolecular alternations of the electrospun samples and the corresponding physical mixtures, PALS measurements were carried out.

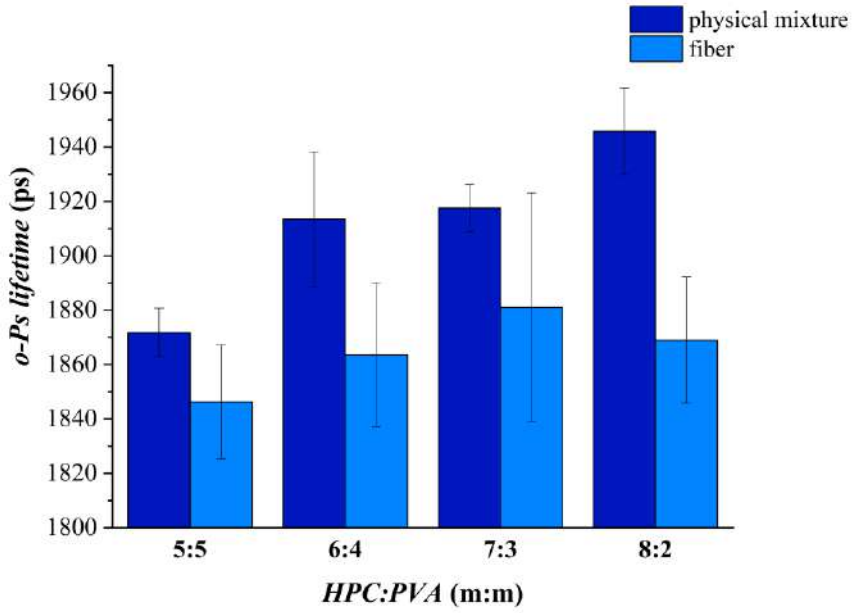

Figure 7 Ortho-positronium (o-Ps) lifetime values of papaverine-HCl loaded electrospun fibrous samples of different HPC:PVA mass ratio and the corresponding physical mixtures

Figure 7 shows the average discrete o-Ps lifetime values of the nanofibers electrospun from precursors of different HPC:PVA ratios and the corresponding physical mixtures. (The electrospun sample of HPC:PVA 9:1 ratio was not suitable for this investigation.) For each composition, decreased o-Ps values for electrospun samples can be observed in contrast to the corresponding physical mixtures.

3.3. Accelerated stability test of the papaverine-HCl containing electrospun sample of HPC:PVA 6:4 mass ratio

3.3.1. Morphology study of the stored electrospun samples

The stress induced morphological changes of the fibrous sample of HPC:PVA 6:4 mass ratio were tracked by SEM measurements. The time-dependent morphological changes can be seen unambiguously in the SEM images of the stored samples (**Figure 8**).

DOI:10.14753/SE.2020.2446

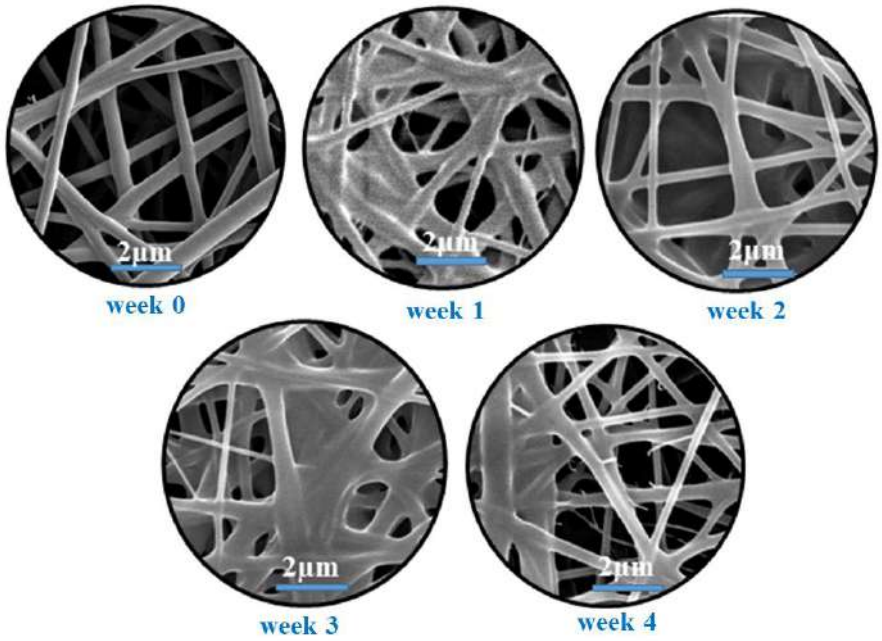

Figure 8 SEM morphology of the freshly prepared (unstored) and the stored papaverine-HCl loaded electrospun sample of HPC:PVA 6:4 (m:m)

Despite that the fibrous structure was basically preserved until the end of the stability test; remarkable structural changes took place. The fibrous structure was deteriorated by the stress conditions in two major steps. Firstly, the merging and broadening of the individual fibers can be observed, and thus the fiber-film like transition was started, which became more pronounced as storage time progressed. Secondly, fragmentation occurred, which was manifested in the formation of tenuous initiative scraps.

3.3.2. Micro-and macrostructural investigation of the stored under stress condition

FTIR measurements were carried out with the goal of the monitoring the physical state of the embedded drug. FTIR spectra of papaverine-HCl loaded electrospun samples as a function of storage time can be seen in **Figure 9**.

DOI:10.14753/SE.2020.2446

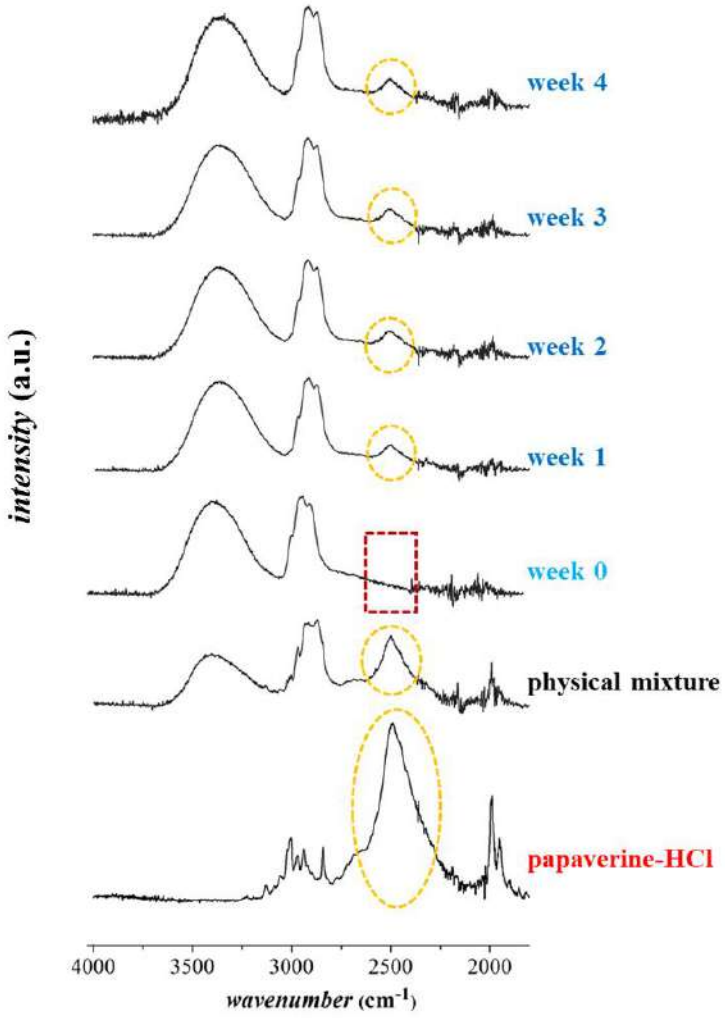

Figure 9 FTIR spectra of papaverine-HCl, the physical mixture, the freshly prepared and the stores (week1-4) electrospun sample of HPC:PVA=6:4 (m:m)

On the spectra of the freshly prepared sample, high-intensity selective characteristic peaks related to the API around 2500 cm^{-1}, which belonging to the protonated amine group of the API, could not be observed. Some peaks were merging and broadening, as was expected based on the preliminary study (which was discussed in detail in 3.2.1 chapter).

Unexpectedly, already after one week of storage, the peaks around at 2500 cm^{-1} appeared, which was possibly related to the API and persisted until the end of the stability test. In the case of all the sampling points, the relative intensity of this peak remained nearly constant.

DOI:10.14753/SE.2020.2446

Raman spectroscopy analysis were performed to monitoring the stress tolerance capacity of the formulation. The vibrational characterization of the samples can be seen in **Figure 10 and Figure 11**.

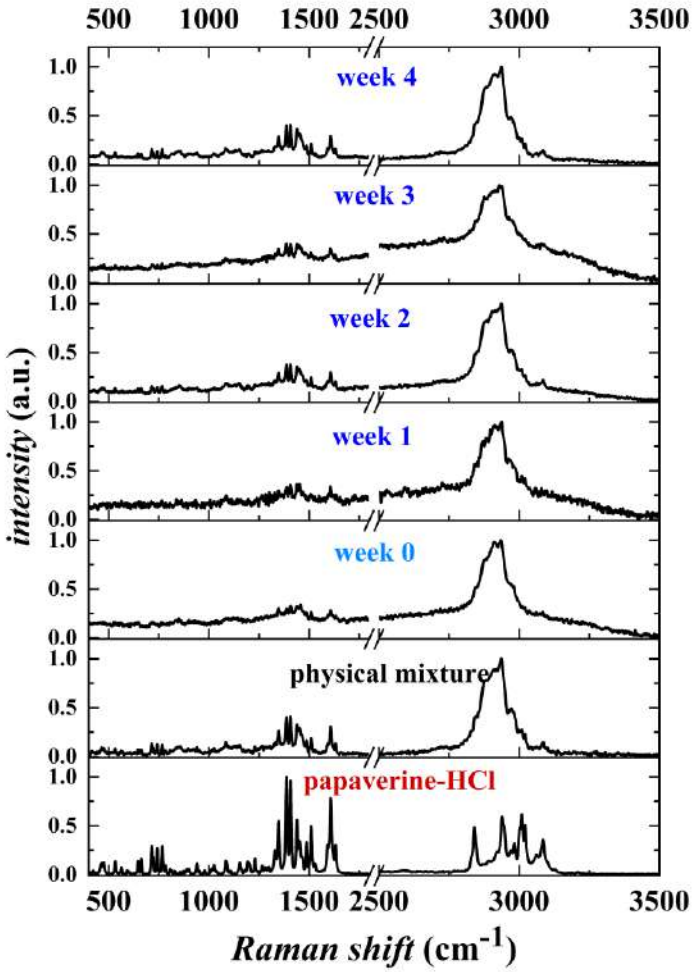

Figure 10 Raman spectra of the samples between 400 and 3500 cm^{-1}

Visible characteristic peaks of the API appeared in the spectrum of the physical mixture, which is referred to the crystalline state of the drug. In contrast to the freshly electrospun sample, where the merged spectral pattern could be observed, spectra of the stored samples showed a progressive change until it reached a profile like the physical mixture. Consequently, the crystallization process had a time-dependent nature.

DOI:10.14753/SE.2020.2446

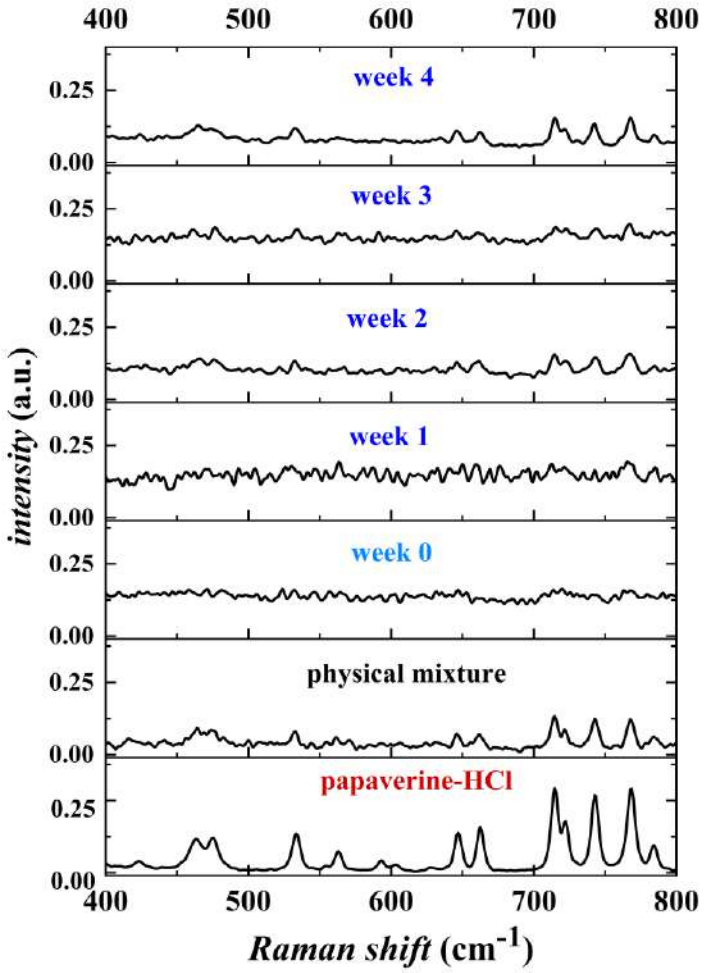

Figure 11 Raman spectra of the samples between 400 and 800 cm^{-1}

The shifting of the peak was notable only in one case; the CH-stretching vibrations of the API around at 2938 cm^{-1} wavenumber. Along with the storage time, the peak shifts were the following: -4.9 cm^{-1}, -1.9 cm^{-1}, -2.9 cm^{-1}, -2.9 cm^{-1} and -2.9 cm^{-1} for week 0, 1, 2, 3, 4, respectively.

DOI:10.14753/SE.2020.2446

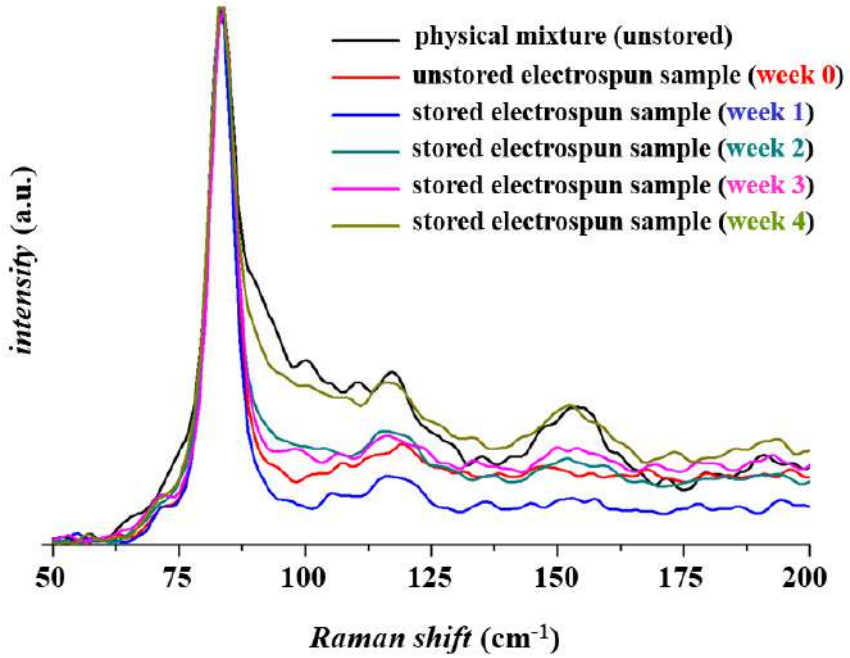

Figure 12 The shape of the Raman spectra of the region between 50 and 200 cm^{-1}

After a more thorough examination of the region of 50–200 cm^{-1} assigned as lattice vibration, a time-dependent process can be inferred related to the solid-state changes of the drug-containing polymeric system (**Figure 12**).

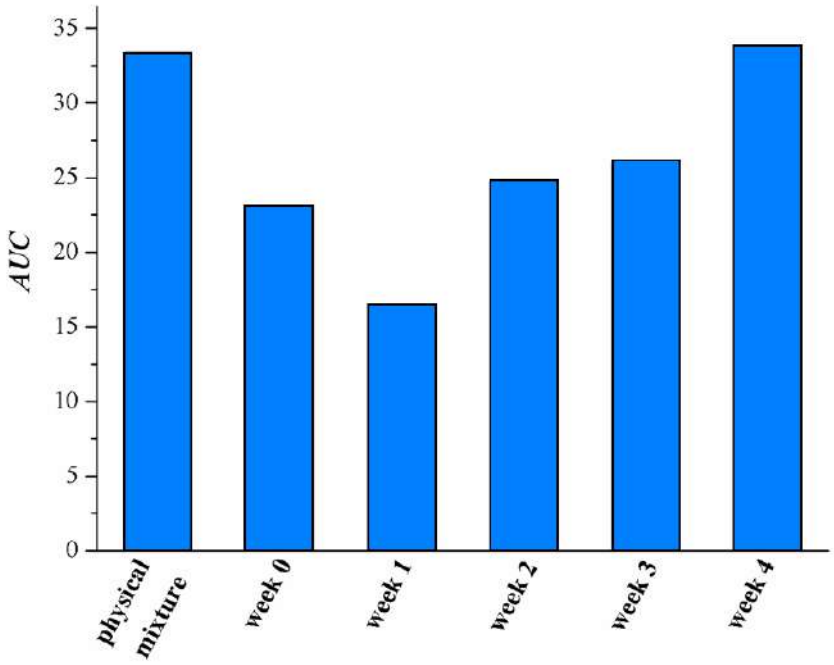

Figure 13 Integrated area of the Raman peak (at 85 cm^{-1}) of the physical mixture, freshly prepared and stored (weeks 1-4) papaverine-HCl loaded electrospun samples of HPC:PVA=6:4 mass ratio between

The spectral profile and the integrated area of the region between 50 and 200 cm^{-1} were becoming more and more similar to the characteristic feature of the physical mixture, which indicated that the amorphous to crystalline transition of the drug took place as a result of the exposition to stress conditions (**Figure 13**).

It was also observed that the characteristic peaks in the region of 700–780 cm^{-1} related to the benzene and isoquinoline ring out of plane deformation and the C-C-C bond (which connects the two rings) deformation merged into the baseline, and then along with the storage time, these peaks were re-separated (95).

After a detailed analysis of the spectra in the region of 430–700 cm^{-1}, where peaks of the wagging vibrations of methoxy moieties (463 cm^{-1} and 473 cm^{-1}), out of plane deformations of the rings (533 cm^{-1}, 563 cm^{-1}), in-plane and out of plane deformations of the rings and twisting vibrations of methoxy moieties (647 and 662 cm^{-1}, respectively) can be noticed (**Figure 11**) (95).

The aging related microstructural changes of the drug-loaded fibrous sample of HPC:PVA 6:4 mass ratio was detected by PALS measurements. The average discrete o-Ps lifetimes as a function of storage time showed a two-step process of a supramolecular alternation. One week storage in stress conditions resulted in the increase of third-lifetime value and thus larger free volume holes. After that, a sharp drop can be observed, and then a consecutive remarkable increase in o-Ps lifetime values can be noticed.

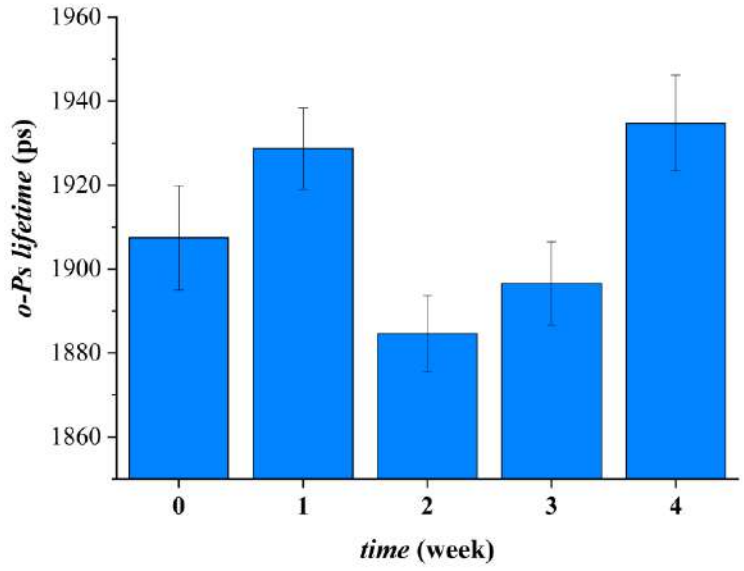

Figure 14 Average discrete ortho-positronium (o-Ps) lifetimes of the papaverine-HCl loaded electrospun nanofibers of HPC:PVA=6:4 mass ratio as a function of storage time

The two-step aging process was obviously detectable in the distribution curves of o-Ps lifetimes (**Figure 14**), implying multiple supramolecular changes throughout the stability test.

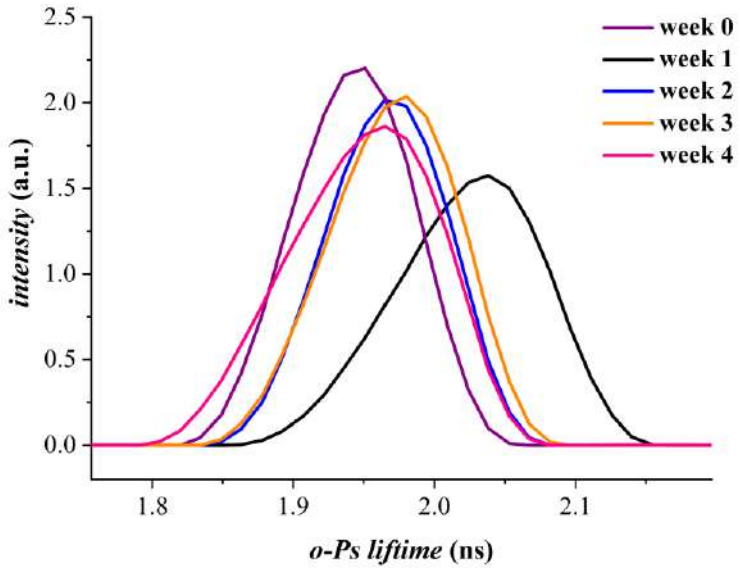

Figure 15 The ortho-positronium (o-Ps) lifetime distributions in the papaverine-HCl-loaded electrospun nanofibers of HPC:PVA=6:4 mass ratio, after 0, 1, 2, 3, 4 weeks of storage (t_0, t_1, t_2, t_3, t_4)

A definite change could be observed in the distribution in terms of the width as well in the average values after one week of storage. This process was followed by a second rearrangement, where backward shift and narrowing of the distributions could be noticed unambiguously. With the progressed storage time, the peak at 1.951 ns, indicative of o-Ps atoms shifted towards longer lifetimes (o-Ps=2.038 ns after one week), which referred to the increase of free volume holes in size and could arise as a consequence of the relaxation of the structure (**Figure 15**).

3.4. Morphology, topography and mechanical properties of the MH-loaded fibrous samples

MH-loaded, aqueous viscous PVA solutions of two different compositions were prepared, and fibrous samples were manufactured with electrospinning. After the optimization of the fiber formation process parameters and compositions of the viscous

solutions for the electrospinning process, well-defined, round-shaped samples were achieved on the collector. Randomly oriented, clear fibrous structure without any beads and film-like areas can be observed in the SEM images of each sample (**Figure 16**).

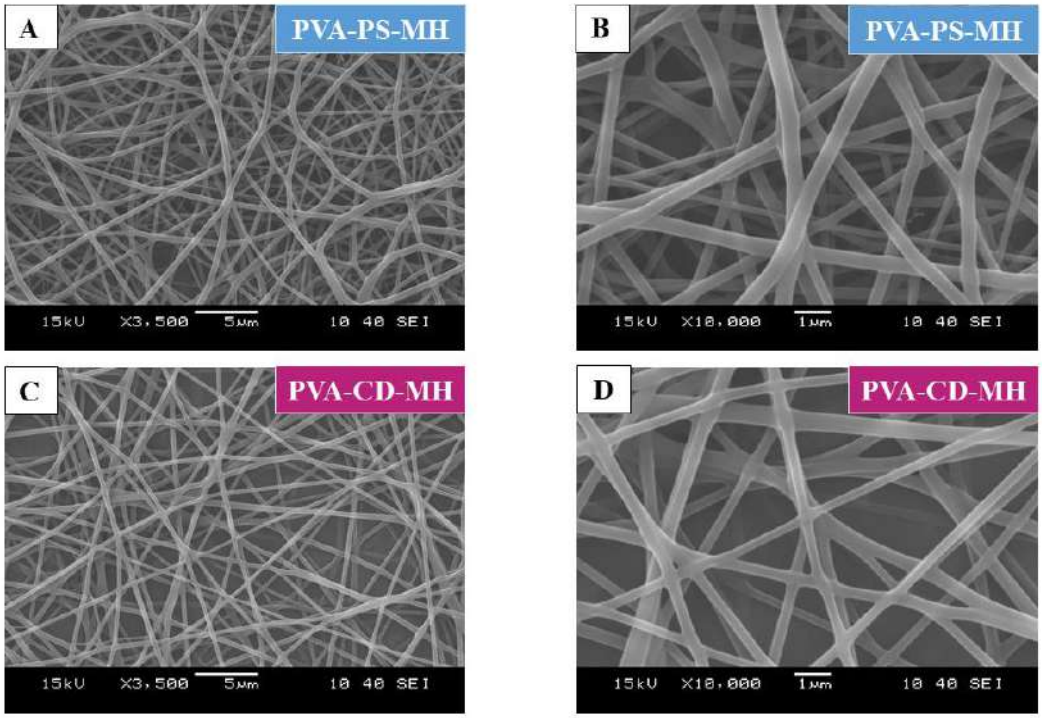

Figure 16 SEM photos of the poly(vinyl alcohol)-based, metoclopramide-HCl-loaded electrospun sample either containing polysorbate 80 (PVA-PS-MH) (**A, B**) or hydroxypropyl-β-cyclodextrin (PVA-CD-MH) (**C**, **D**)
(Magnification: 3500× (**A**, **C**) and 10000× (**B**, **D**)

On the SEM images, clusters or any visible signs of heterogeneity could not be detected in either sample e.g., surface crystallization of the active pharmaceutical ingredient and other artifacts was missing. In the case of the PVA-PS-MH sample, a more densely packed fibrous structure was achieved, while a sparse coverage was obtained for PVA-CD-MH fibers.

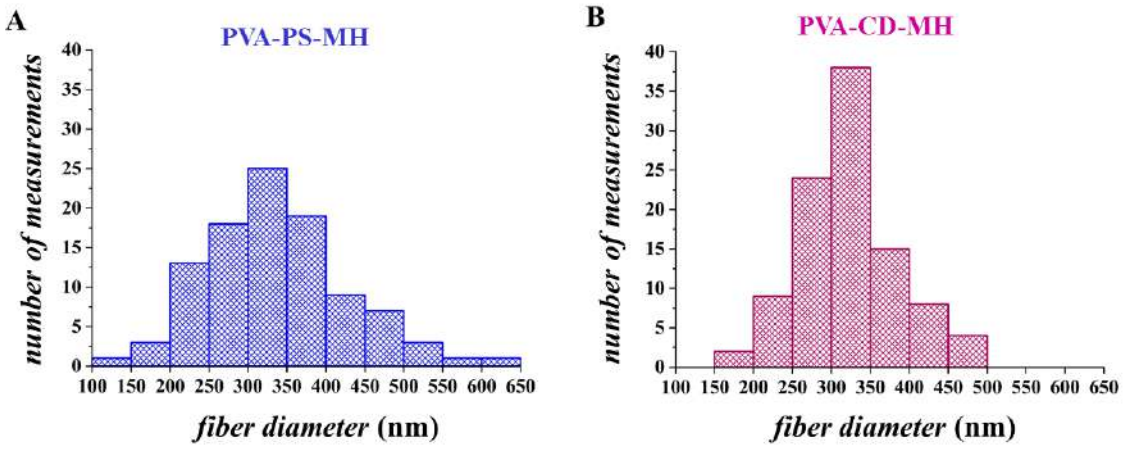

Figure 17 Histograms of the fiber diameter distribution of metoclopramide-HCl-loaded electrospun sample either containing polysorbate 80 (PVA-PS-MH) (**A**) or hydroxypropyl-β-cyclodextrin (PVA-CD-MH) (**B**)

336±88 nm and 323±62 nm (mean ±SD) average fiber diameter values were achieved for PVA-PS-MH and PVA-CD-MH electrospun samples, respectively. In the case of the PVA-PS-MH sample, a slightly wider fiber distribution was obtained than that of the PVA-CD-MH fibers with a more uniform structure (**Figure 17**).

Fiber diameter distributions of the two electrospun samples were investigated using the Kolmogorov–Smirnov test, which indicated that distributions of PVA-PS-MH and PVA-CD-MH fibers were normal (p = 0.844 and 0.416, respectively). A one-way analysis of variance (ANOVA) revealed that no significant difference between the diameter of the two formulations was found (p=0.211).

DOI:10.14753/SE.2020.2446

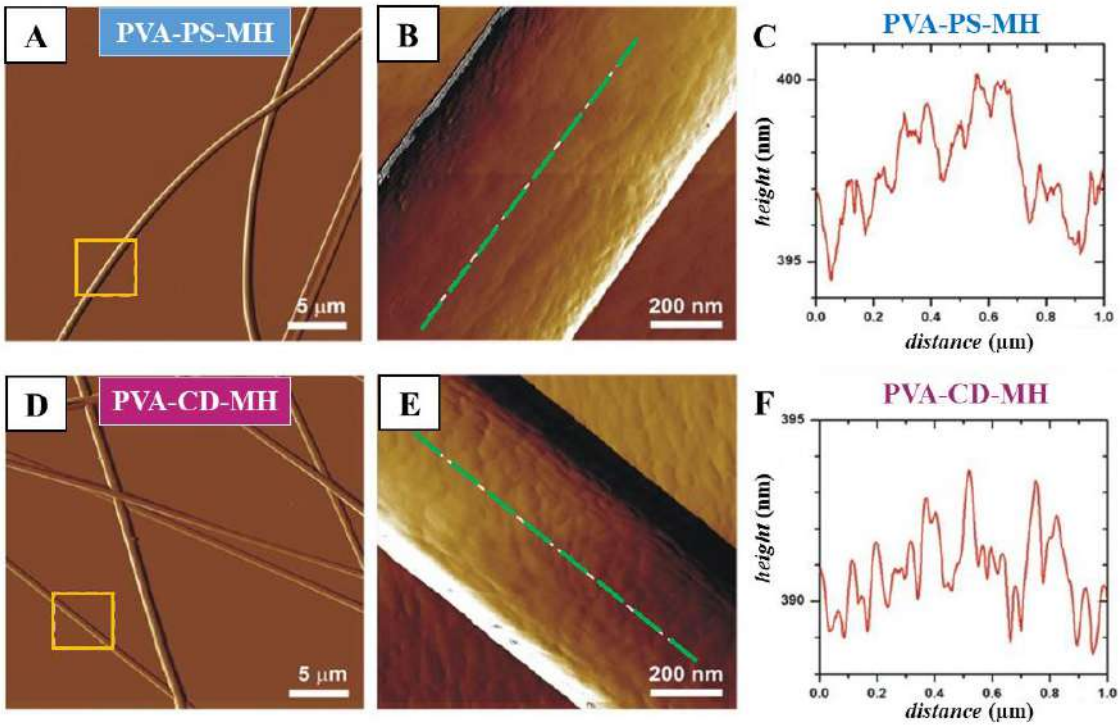

Figure 18 AFM amplitude-contrast images of poly(vinyl alcohol)-based, metoclopramide-HCl-loaded, either containing polysorbate 80 (PVA-PS-MH) (**A**, **B**, **C**) or hydroxypropyl-β-cyclodextrin (PVA-CD-MH)(**D**, **E**, **F**) nanofibers. Panel **B** and **E** are higher resolution images of areas indicated by yellow rectangles on panel **A** and **D**, respectively. Height sections (**C**, **F**) taken alongside the green dashed line in panel **B** and **E**, respectively.

AFM topography of both PVA-PS-MH (**Figure 18A and B**) and PVA-CD-MH (**Figure 18D and E**) fibrous sample appeared similar to those seen in SEM images (**Figure 16**). The PVA-CD-MH fibers appeared as long, curved, continuous, cylinders. In the case of PVA-PS-MH fibers, some ribbon-like, flat structure can also be observed (see top left and bottom right corners in **Figure 18A**).

The height of the investigated regions of the fibers varied between 330-360 nm and 300-450 nm for PVA-PS-MH and PVA-CD-MH fibers, respectively. Relatively smooth fiber surface with only a few nm height variations was observed in the case of both MH-loaded nanofibrous formulations. The height profile of PVA-PS-MH fibers (**Figure 18C**) showed sharper peaks than the cyclodextrin containing ones, which had a more rounded profile plot (**Figure 18F)**, indicating that PVA-PS-MH fibers display a bit coarser surface.

For the investigation of the mechanical properties of the PVA-based nanofibers formulated with different excipients by AFM, 100 nN, 500 nN, 1 µN and 5 µN loads were

applied at well-defined points of the fiber surface, that was pressed and retracted with the AFM tip at a constant 1 μm/s velocity.

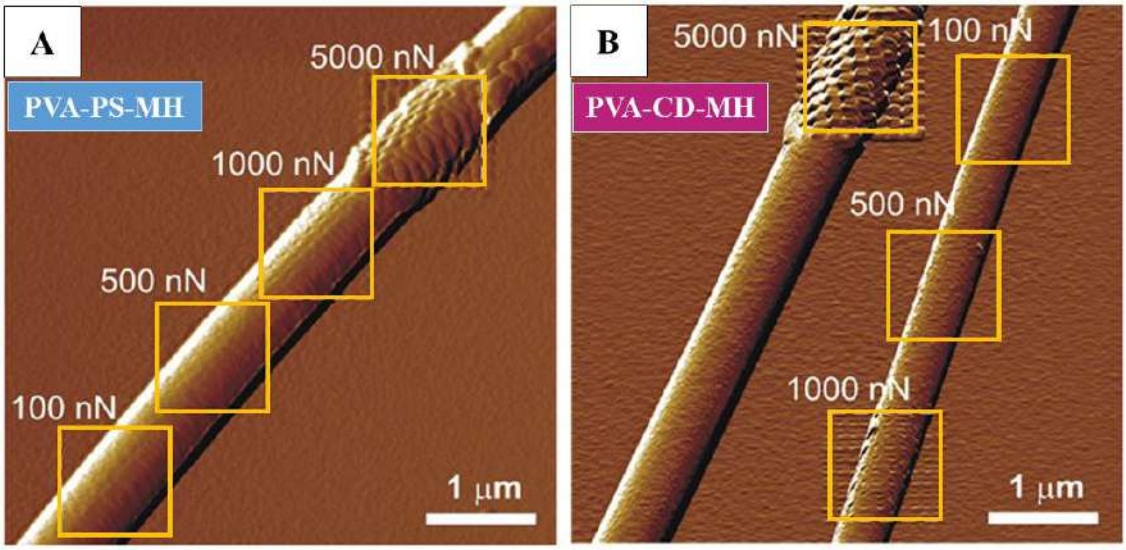

Figure 19 Effect of the mechanomanipulation: AFM-amplitude contrast images of metoclopramide-HCl-loaded electrospun fibers either containing polysorbate 80 (PVA-PS-MH) (**A**) or hydroxypropyl-β-cyclodextrin (PVA-CD-MH) (**B**) taken after force spectroscopy. The yellow rectangles indicate areas where force maps (10 × 10 force curves) were taken from. The maximum load applied in each region is written next to the rectangles.

The manipulated area was re-scanned. No noticeable alternations were found in regions loaded with 100 nN forces (**Figure 19)**. At 500 nN load, few small depressions were seen for PVA-CD-MH fibers, while in the case of the PVA-PS-MH sample, no effect was detected.

Nevertheless, in both formulations at 1 μN and 5 μN loads, permanent surface depressions were observed; thus, these forces enabled plastic deformation. Shallower and blurred depressions were obtained in PVA-PS-MH fibers (**Figure 19A**), while in PVA-CD-MH fibers, those were deeper and had a more definite profile reflecting the shape of AFM tips (**Figure 19B**).

Figure 20 shows the representative force curves that were taken at different maximum loads.

DOI:10.14753/SE.2020.2446

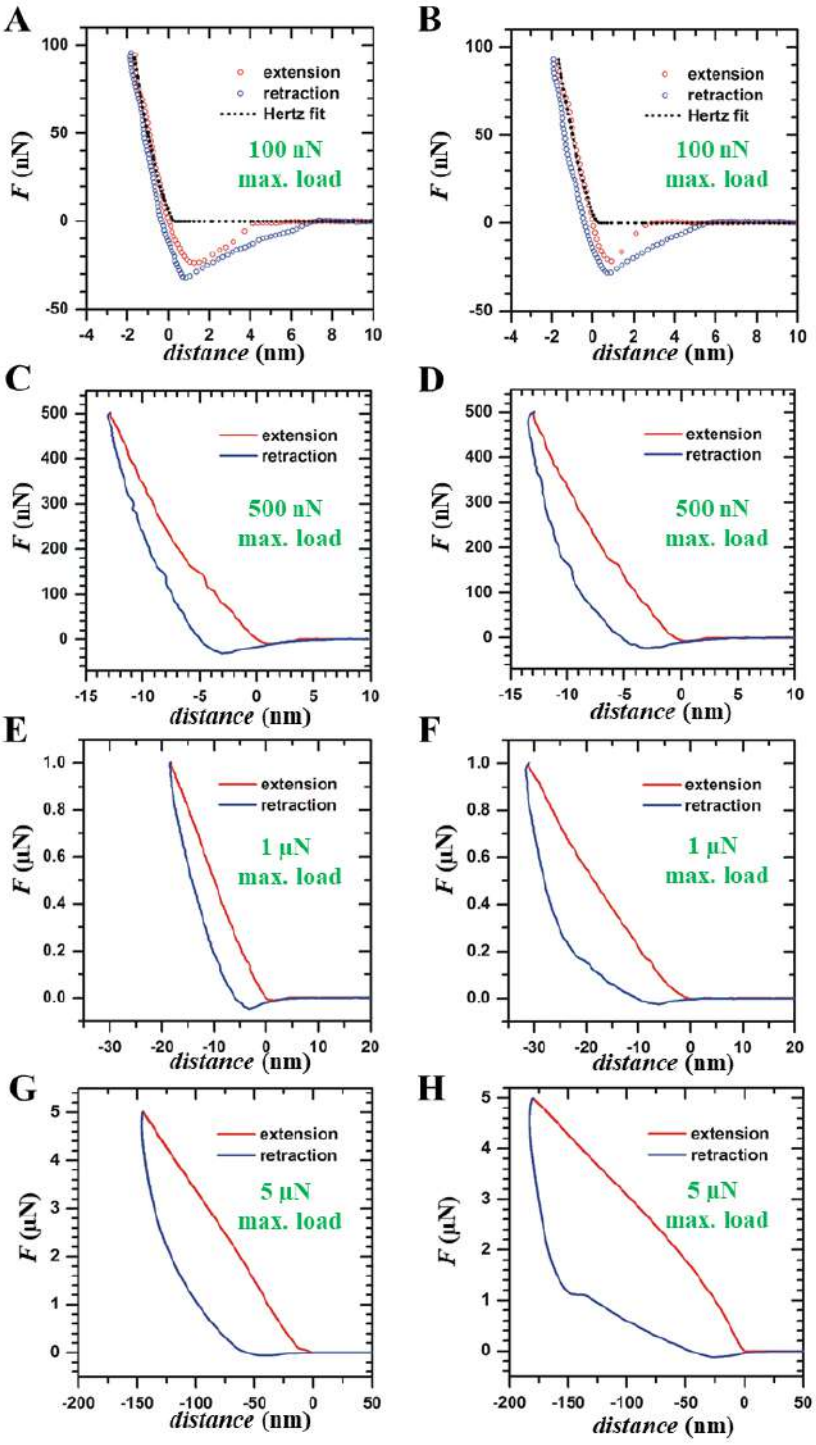

Figure 20 Representative force curves taken from metoclopramide-HCl-loaded either polysorbate 80 containing (**left panels**) or hydroxypropyl-β-cyclodextrin containing (**right panels**) nanofibers at 100 nN (**A**, **B**), 500 nN (**C**, **D**), 1 µN (**E**, **F**), 5 µN (**G**, **H**) maximum loads. Horizontal axes show the distance from the fiber surface.

The negative peak in approach curves in case of 100 nN maximum load can refer to a considerable attractive interaction between the fibers and the tip.

At 0 nm distance, where the fiber surface was reached, the force followed an apparent linear increase up to the threshold load (~100 nN), which is a sign of the elastic response. When the tip was retracted, the force was decreased, and the retraction curve was roughly parallel to the approach curve. Only a minimal hysteresis can be observed between the two curves, suggesting that at this load there was no plastic deformation.

The large negative force peak of the retraction curve is the consequence of the tip-fiber adhesion, and then the force reached 0 as the tip was drawn farther from the fiber surface. The ascending force region of approach curves was fitted with the Hertz-model of elasticity (96) that adapted to AFM force spectroscopy (**Figure 20A and B** dotted lines). According to distributions of Young's modulus calculated from the fits, in both cases apparent normal distribution was achieved, and for PVA-PS-MH and PVA-CD-MH fibers, the mean±SD values were 3.26±1.74 GPa and 1.48±0.90 GPa, respectively (**Figure 21A**).

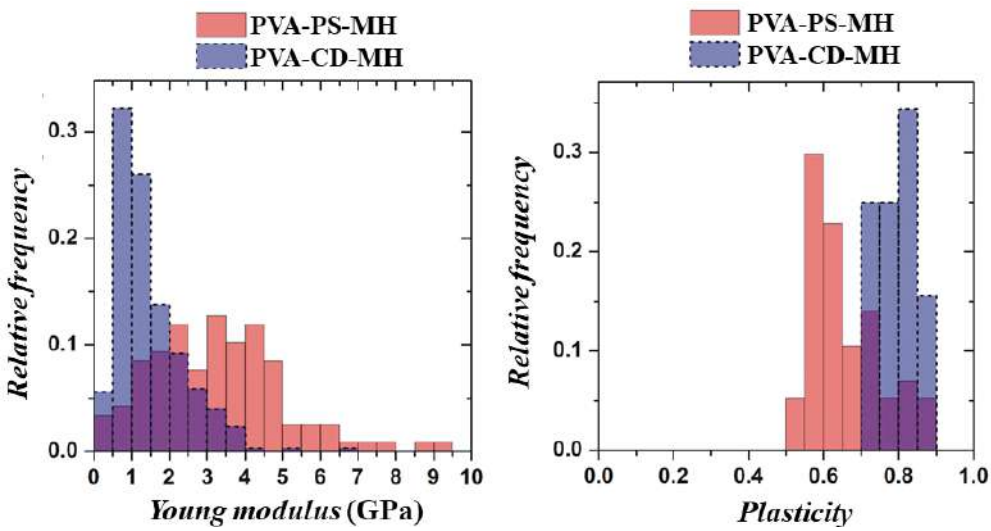

Figure 21 Histogram of Young-moduli and plasticity of the metoclopramide-HCl-loaded fibers formed either polysorbate 80 containing (PVA-PS-MH) or hydroxypropyl-β-cyclodextrin (PVA-CD-MH)

With the increasing loads, the hysteresis area between the approach and the retraction curves was larger, which was referred to as a plastic deformation of the fibers. In the case of the PVA-CD-MH sample, a larger hysteresis area can be observed at each applied load;

thus, this fibrous formulation is more plastic (plasticity distributions at 5 μN load can see in **Figure 21B**, as it was concluded from **Figure 19.**

3.5. Solid-state characterization of the MH-loaded electrospun samples

PALS measurements were performed to monitor supramolecular changes through changing of the o-Ps lifetime values of the physical mixtures, electrospun neat- and drug-loaded fibrous samples. The o-Ps lifetimes of the physical mixtures were found to be roughly the same regardless of the used excipients. The o-Ps lifetime values of PS containing nanofibrous samples (PVA-PS and PVA-PS-MH samples) were increased relative to the physical mixture (**Figure 22).**

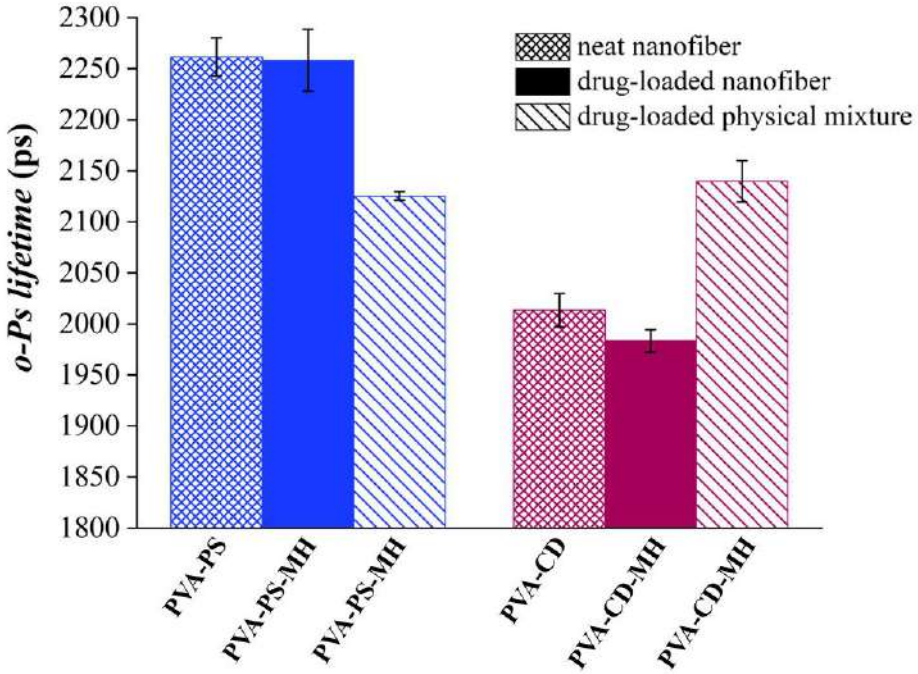

Figure 22 Average discrete ortho-positronium (o-Ps) lifetimes of either polysorbate or cyclodextrin containing neat samples, drug-loaded nanofibers, and related physical mixtures

The presence of the embedded drug does not modify the average free volume holes appreciably and thus the supramolecular structure; while the o-Ps lifetime of PVA-CD and PVA-CD-MH, neat and drug-loaded electrospun samples remarkably decreased compared to the physical mixture. The drug incorporation into the fibers caused a further slight reduction in the third-lifetime value.

DOI:10.14753/SE.2020.2446

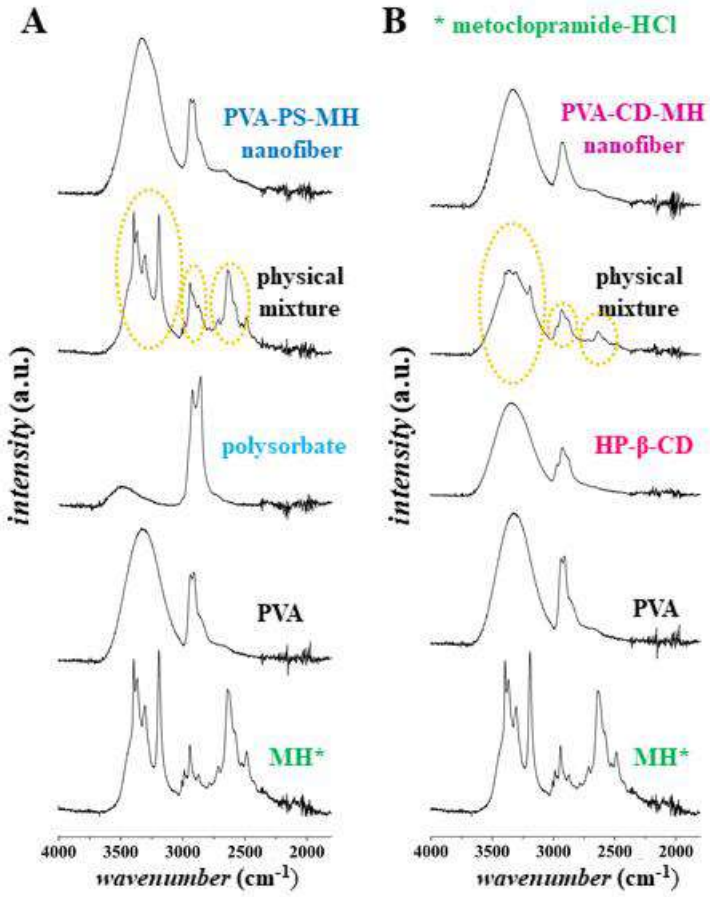

Figure 23 FTIR spectra of the solid components (metoclopramide-HCl (MH), poly(vinyl alcohol) (PVA), hydroxypropyl-β-cyclodextrin (HP-β-CD)) and the drug-loaded polysorbate (PVA-PS-MH) and hydroxypropyl-β-cyclodextrin (HP-β-CD) containing nanofibrous samples and the corresponding physical mixtures

Figure 23 shows the FTIR spectra of the starting materials used for precursor preparation, electrospun samples, and the corresponding physical mixtures. Characteristic peaks relating to the OH- (at 3320-3340 cm-$^{-1}$), NH-(at ~3190 cm^{-1}), CH- (at 2910-2940 cm^{-1}) bending and NH-stretching (at around 2635 cm^{-1}) vibrations of the MH can be observed clearly in the physical mixture. As the other characteristic peaks of MH overlapped with peaks attributed to functional groups of the excipients, the changes of NH signs were evaluated to verify the solid-state transition of the model drug (MH). In the spectra of the fibrous samples, the high-intensity characteristic peaks of the NH-groups disappeared.

DOI:10.14753/SE.2020.2446

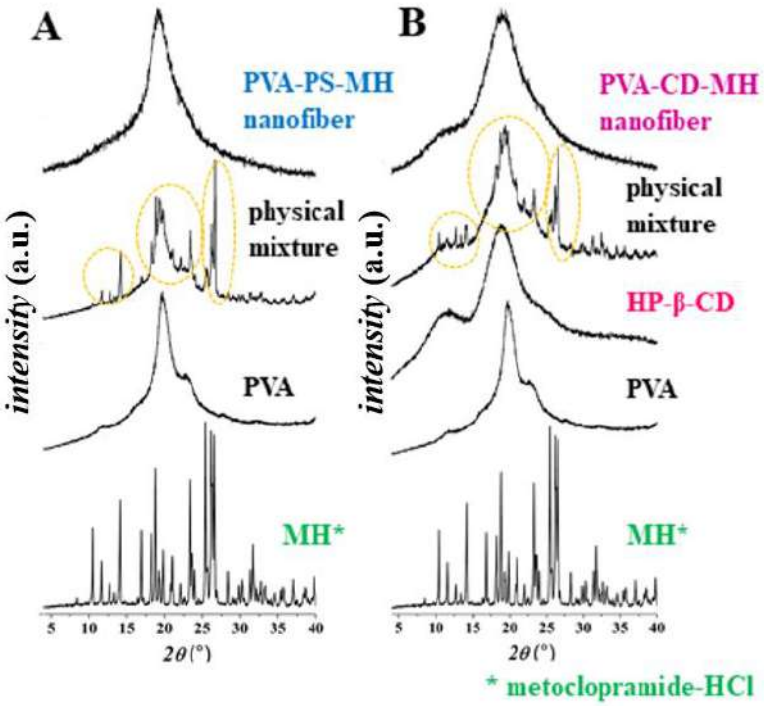

Figure 24 Power X-ray patterns of the solid components (metoclopramide-HCl (MH), poly(vinyl alcohol) (PVA), hydroxypropyl-β-cyclodextrin (HP-β-CD)) and the drug-loaded polysorbate (PVA-PS-MH) and hydroxypropyl-β-cyclodextrin (HP-β-CD) containing nanofibrous samples and the corresponding physical mixtures

Characteristic peaks of the MH and the broad peak of the PVA and CD appeared in the X-ray diffractograms of the physical mixture (**Figure 24**). While the XRD patterns of the drug-loaded fibrous samples could be characterized by diffuse peaks, high-intensity characteristic peaks relating to the MH did not appear.

The local anesthetic agent lidocaine is a substituted benzamide derivate as the model drug, but its inclusion complexation with HP-β-CD has already been described and widely studied in the literature (97). Due to the structural similarity of the two drugs, interactions between MH and the randomly substituted HP-β-CD at an atomic level was investigated by two dimensional rotating-frame nuclear overhauser effect spectroscopy (2D ROESY) NMR measurement.

DOI:10.14753/SE.2020.2446

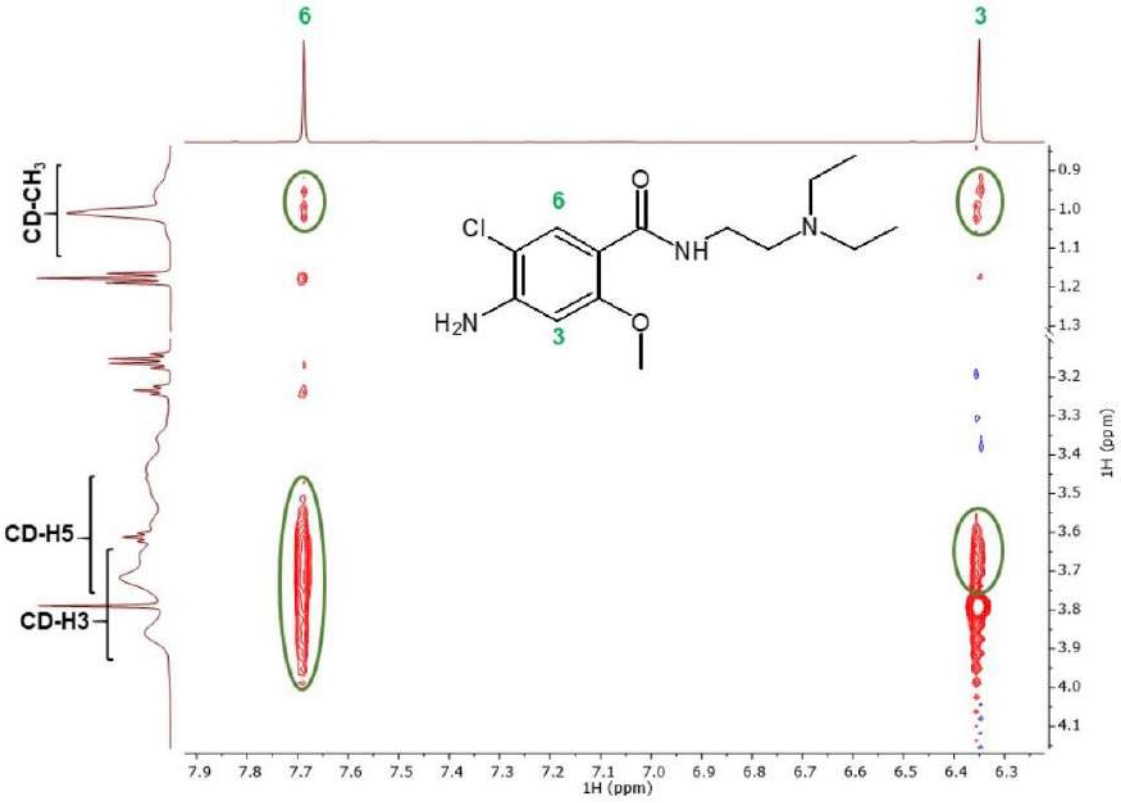

Figure 25 Partial 2D ROESY NMR spectrum of metoclopramide-HCl and randomly substituted hydroxypropyl-β-cyclodextrin (HP-β-CD)

Figure 25 represents a partial ROESY spectrum of the MH-HP-β-CD system, where between the aromatic ^{1}H resonances of MH and the inner cavity protons of HP-β-CD (CD-H3 and CD-H5) intense cross-peaks were clearly depicted. Cross-peaks can be observed between the resonances of the aromatic moiety of MH and the hydroxypropyl chains of the CD.

ssNMR measurements were performed with that goal to characterize the PVA-based nanofibrous systems. In the case of the measurement of MH, a well-resolved NMR spectrum typical for crystalline materials built up of small molecules was achieved.

Based on the single pulse experiment with 600 s of recycling delay, all of the resonance could be assigned to one carbon atom. In the crystalline structure, the N-ethyl groups have a different environment; therefore, their signals differ remarkably from those obtained in the solution NMR spectra, allowing them to be differentiated and assigned.

DOI:10.14753/SE.2020.2446

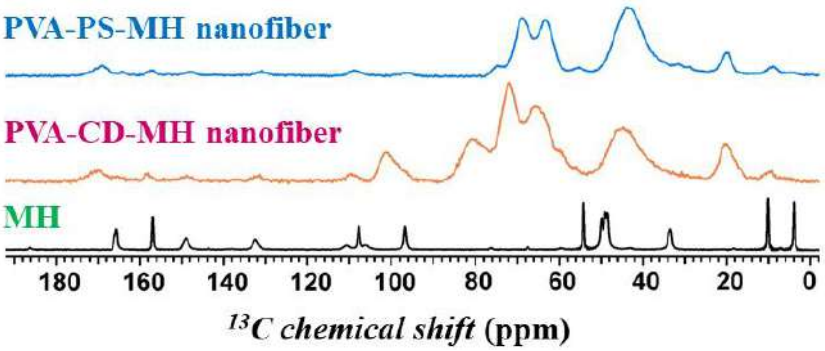

Figure 26 Solid-state NMR spectra of metoclopramide-HCl (MH) and the nanofibers

Signals of the methyl groups at 9.9, and 3.7 ppm were found to be especially sensitive for the detection of the even low ratio of crystalline ordering in the complex matrix systems. The spectra of the electrospun fibrous samples only showed broadened signals in a wide range (**Figure 26**). The resonance of MH overlapped with the signals of polymeric matrices. The exceptions were only the methyl and some aromatic signals of the model drug. The sharp MH signals of the crystalline materials (that were used for the precursor preparation for the electrospinning process) were merged and broadened in the spectra of the fibrous samples that unequivocally indicate that the MH has no crystalline structure in the fibers.

On the spectra, a slightly shifted signal can be observed instead of the two methyl resonances; thus, the short-range order could be ruled out on an nm scale.

Information can be obtained with the evaluation of the proton environment of the carbon atoms and their mobility by the analysis of the shapes of the CP build-up curves, which are constructed by varying the contact time and plotting signal intensity vs. contact time.

Fitting of the build-up curves by a simplified expression determination of changes in the chemical environment and relaxation of carbons (according to the **Equation 2**) was possible:

$$M(t) = \lambda^{-1} M_0 [1 - \exp(-\lambda t / T_{CH})] \exp(-t / T_{1\rho}) \qquad (2)$$

where $\lambda = 1+(T_{CH}/T_{1\rho})-(T_{CH}/T_{1\rho})$, $M(t)$ is the magnetization at contact time t, M_0 is the initial magnetization, T_{CH} is the time coefficient of the CP (the time it takes for

magnetization to be transferred from ^{1}H to ^{13}C), and $T_{1\rho}$ is the relaxation time of the carbon in the rotating frame. This equation is valid only in a regime of fast molecular motion, but it qualitatively describes the experimental CP build-up curves and permits a comparison of the fitted parameters.

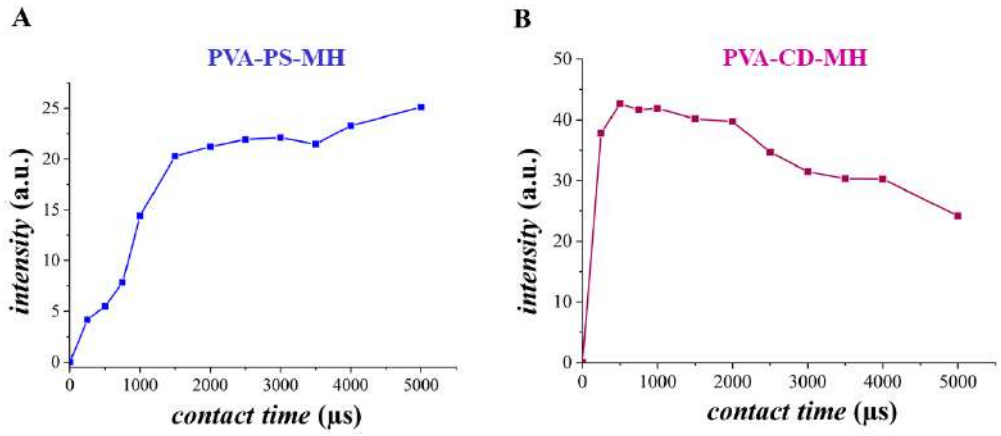

Figure 27 ^{13}C cross-polarization Magic Angle Spinning build-up curve of the metoclopramide-HCl loaded polysorbate (PVA-PS-MH) (**A**) and hydroxypropyl-β-cyclodextrin (PVA-CD-MH) (**B**) containing nanofibers

This equation is valid only for fast molecular motion, but qualitatively describes the experimental CP build-up curves and allows comparison of the fitted parameters (**Figure 27**).

The more mobile a carbon, the more slowly it relaxes, so the plasticizing effect of the excipients could be efficiently tracked. Because of the numerous overlaps of the signals, only the signal of PVA at 43.3 ppm was analyzed in detail. The resonance (at 75.3 ppm) attributed to the crystalline PVA decreases or even disappears in the plasticized samples (98).

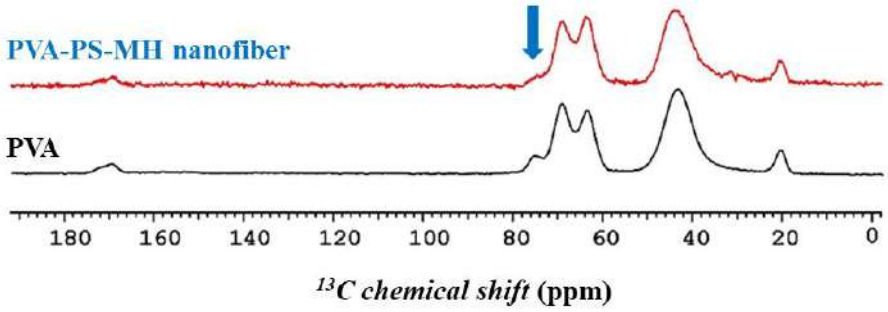

Figure 28 Solid-state NMR spectra of poly(vinyl alcohol) (PVA) and metoclopramide hydrochloride-loaded, polysorbate 80 containing fibrous sample (PVA-PS-MH)

This effect is clearly observable on the ^{13}C NMR spectra of the PVA-PS-MH sample (**Figure 28**), but it is not recognizable on the PVA-CD sample, because of the overlapping signals.

The H-bond structure remained unaltered; consequently, the hydrogen environment did not change significantly around the CH_2 groups; thus, the T_{CH} parameter did not change remarkably. The H-bonds formed between the adjacent chains exchanged to H-bonds between PVA and plasticizer molecules in the plasticized electrospun PVA-based fibrous samples. The mobility changes are more explicit, so the plasticization effect reflected in the T_{1rho} relaxation parameter is evident (**Figure 29**). The mobility of PVA chains was found to be similar in both fibrous samples. In the case of the MH-loaded fibrous samples, the chain mobility increased further, indicating that the API also acts as a plasticizer.

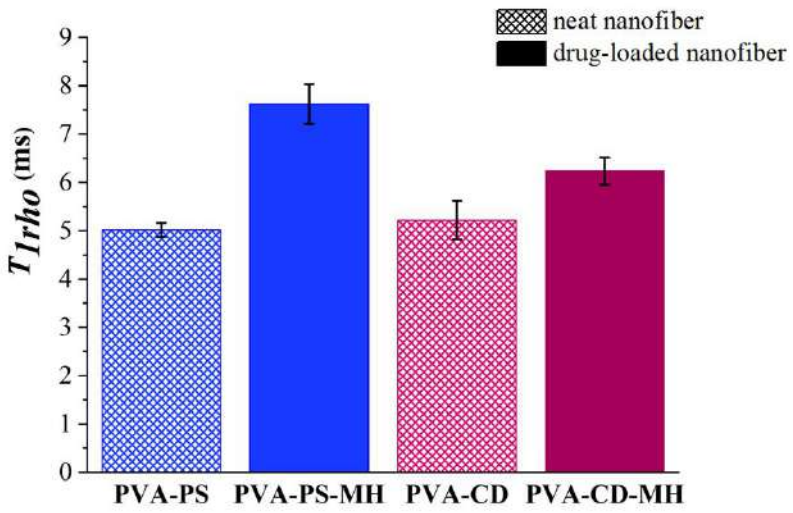

Figure 29 Solid-state NMR relaxation times of neat- and MH-loaded polysorbate (PS) or cyclodextrin(CD) containing nanofibrous sample

The amorphous nature of the electrospun PVA-based ASDs was characterized by the sensitive ssNMR method through the tendency of T_{1rho} values. A slight difference was achieved between the T_{1rho} values of the CD containing neat (PVA-CD) and drug-loaded (PVA-CD-MH) samples, while the relaxation time difference was remarkably higher between the PVA-PS and the PVA-PS-MH samples.

DOI:10.14753/SE.2020.2446

3.6. Stability investigation of the MH-loaded electrospun samples

The ASDs, e.g., the polymeric-based amorphous drug-loaded electrospun nanofibrous systems, have a thermodynamically metastable nature, thus achieving long term stability of these systems, their physicochemical stabilization has a great impact and special interest.

Accelerated stability tests of the electrospun samples are described in this chapter. In the case of each formulation, the stress indicated solid-state stability, and supramolecular changes of the stored samples were investigated with image techniques (SEM), macrostructural (DSC, XRD), and microstructural characterization methods (PALS, FTIR).

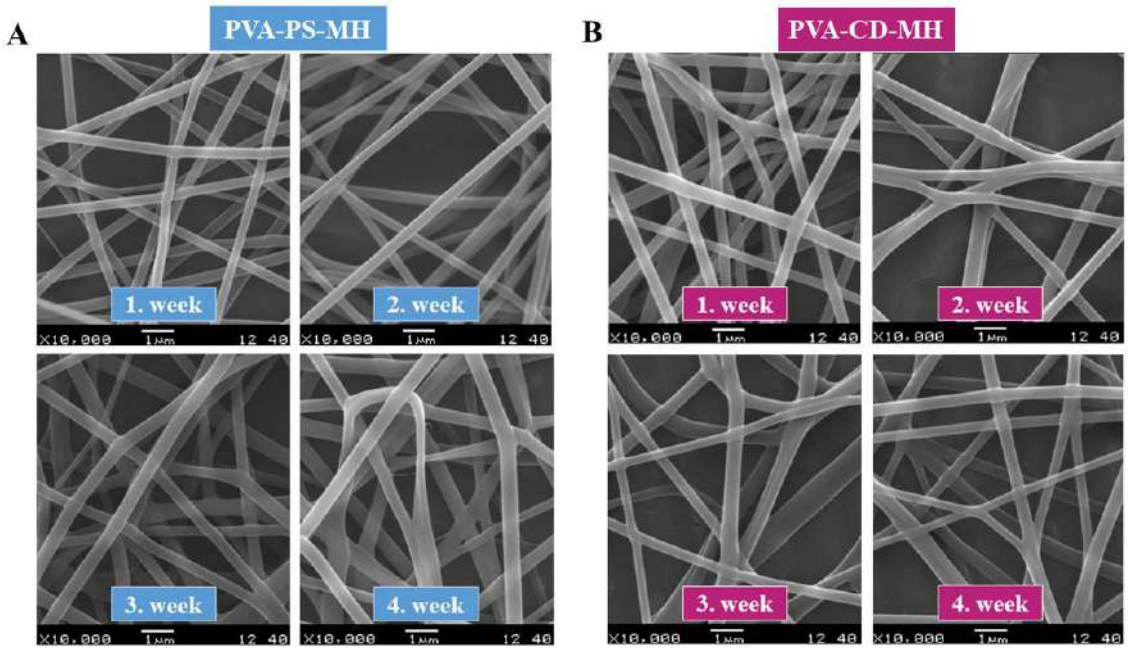

Figure 30 SEM photos of the stored (1-4 weeks) of the metoclopramide-HCl loaded polysorbate (PVA-PS-MH samples) (**A**) or hydroxypropyl-β-cyclodextrin (PVA-CD-MH samples) (**B**) containing nanofibers

The stress-induced time-dependent morphological changes of the MH-loaded fibrous samples were tracked by SEM measurements, and no remarkable changes in the morphological features of the electrospun samples have been detected (**Figure 30A** for PVA-PS-MH and **Figure 30B** for PVA-CD-MH sample). For either formulation, no fiber-to film transition or fragmentation could be observed. The integrity of the fibrous

structure was maintained for the four weeks of storage. On the images of the oldest PVA-PS-MH sample, slightly merged and broadened fiber segments could be seen.

The macrostructural alterations were monitored by XRD measurements.

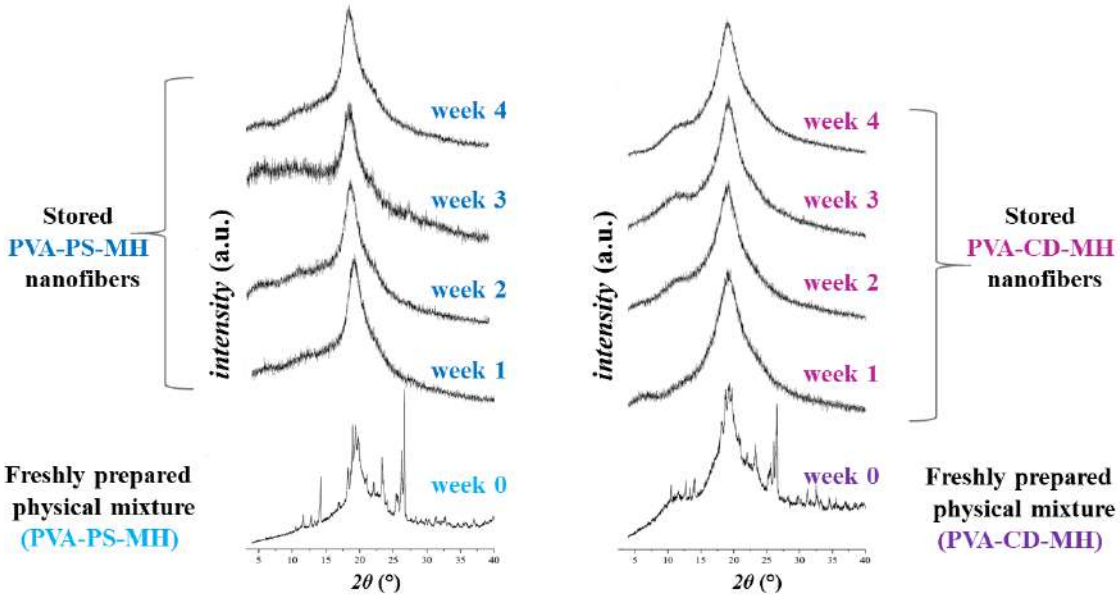

Figure 31 Power X-ray patterns of the stored (1-4 weeks) of the metoclopramide-HCl loaded polysorbate (PVA-PS-MH) or hydroxypropyl-β-cyclodextrin (PVA-CD-MH) containing nanofibers and the corresponding freshly prepared physical mixtures

In the course of the storage, no characteristic peaks of the API appeared on the diffractograms of the stored fibrous samples (**Figure 31A** for PVA-PS-MH and **Figure 31B** for PVA-CD-MH).

DOI:10.14753/SE.2020.2446

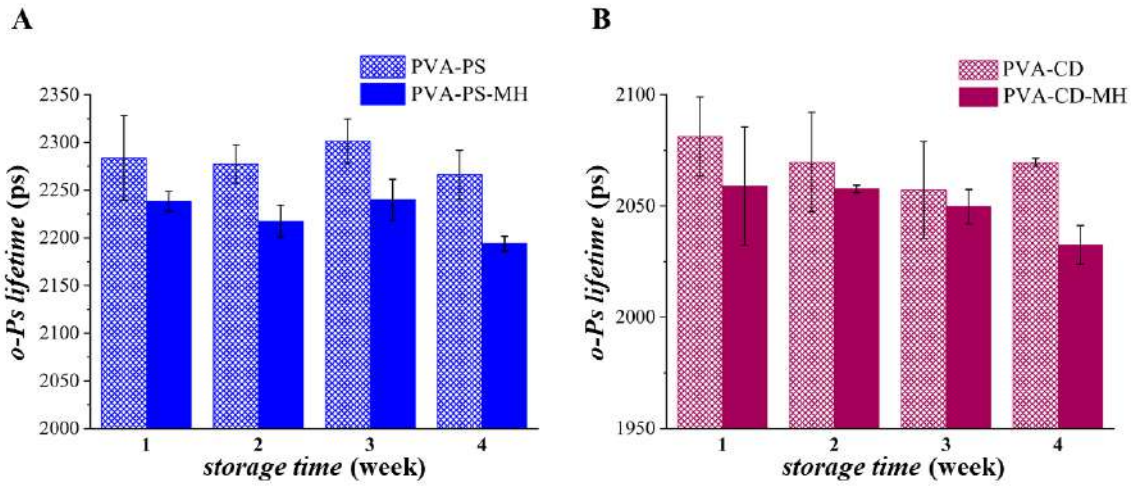

Figure 32 Discrete ortho-positronium (o-Ps) lifetimes of the stored (1-4 weeks) neat- and metoclopramide-HCl loaded polysorbate (PVA-PS and PVA-PS-MH, respectively) or hydroxypropyl-β-cyclodextrin (PVA-CD and PVA-CD-MH, respectively) containing nanofibers

The PALS method was chosen for tracking the aging-related changes of the polymer-based drug carriers. As the storage proceeded, the observed difference between the o-Ps values of the neat and drug-loaded PS containing stored fibrous samples became slightly larger: 0.046 ns, 0.059 ns, 0.062 ns, and 0.072 ns for week 1, 2, 3 and 4, respectively (**Figure 32A**). In the case of the HP-β-CD containing PVA-CD and PVA-CD-MH samples, the o-Ps lifetimes and consequently the average free volume holes were found to be nearly the same during the storage period (**Figure 32B**).

3.7. Results of the *in vitro* study of the MH-loaded electrospun nanofibrous sheets

For the PVA-PS-MH and PVA-CD-MH electrospun samples, 16.45±0.25 % (w/w) and 14.24±0.27 % (w/w) drug content was achieved, respectively.

The MH distributions in the nanofibrous orally dissolving webs and the corresponding physical mixtures, which could be the base of a tablet formulation, were investigated by Raman mapping. As the amorphous form of the API as a pure component was not available for the analysis and the evaluation, thus, to extract the missing amorphous spectral profile of the MH from the polymeric matrices, the MCR-ALS method was applied.

DOI:10.14753/SE.2020.2446

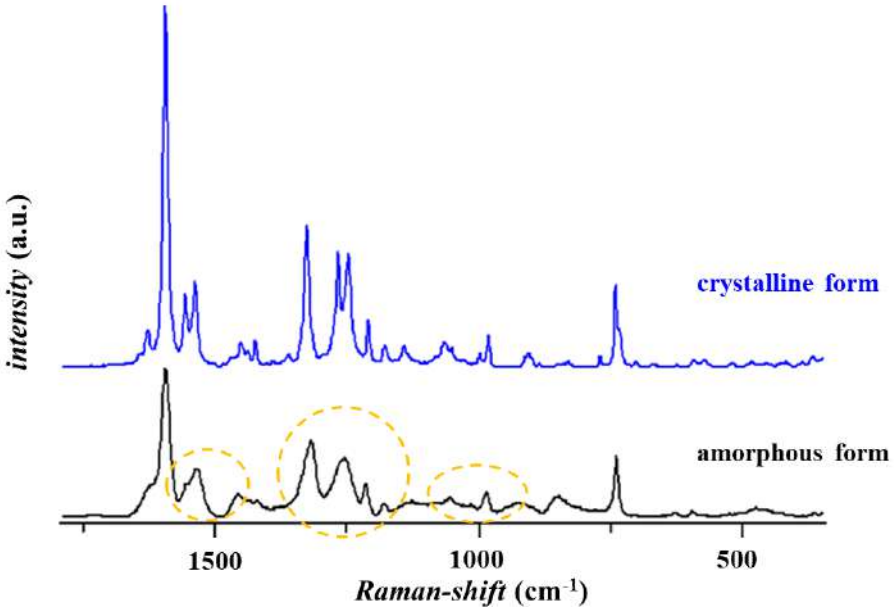

Figure 33 Raman spectra of the crystalline and amorphous metoclopramide-HCl

The Raman spectra of the crystalline form and the amorphous form of the API (as a result of the chemometric analysis) are shown in **Figure 33,** where the detectable difference between the forms could be tracked. On the spectra of the amorphous reference form, the broadened and merged signals could be seen.

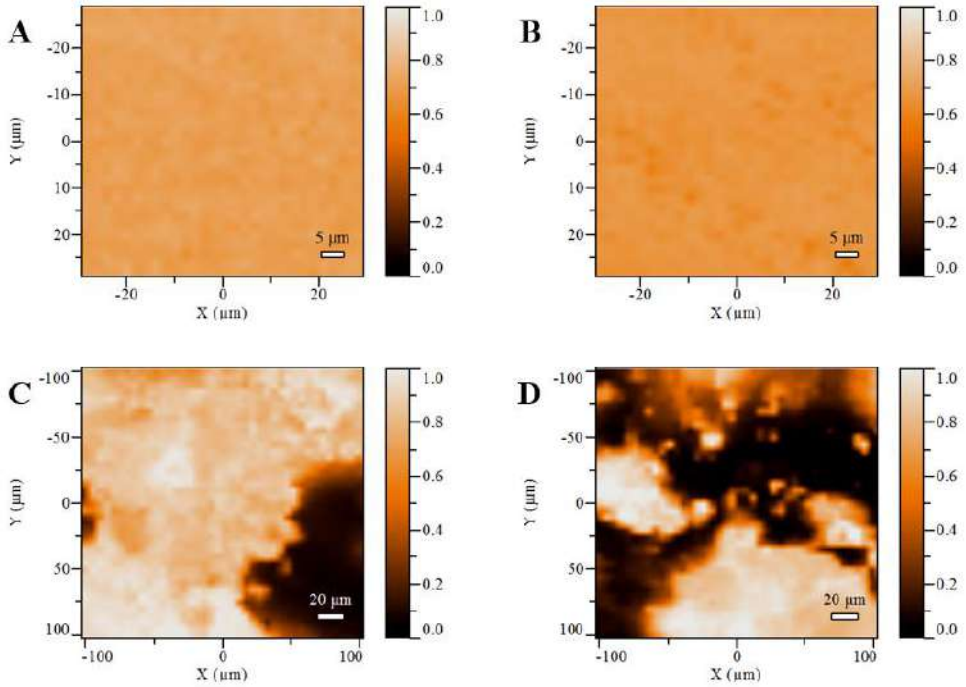

Figure 34 Raman maps of polysorbate (A) and cyclodextrin (B) containing metoclopramide-HCl-loaded fibers and the corresponding physical mixtures (C, D)

The Raman map of the PVA-PS-MH electrospun sample and the corresponding physical mixture can see in **Figure 34A** and **C** respectively, while **Figure 34B** and **D** represent the maps of the HP-β-CD containing the nanofibrous sample and the corresponding physical mixture. In the case of both nanofibrous samples, the relative MH concentration values were about the same in each sampling point; only a slight difference could be observed, while in the case of the physical mixtures, remarkable MH concentration fluctuation was achieved.

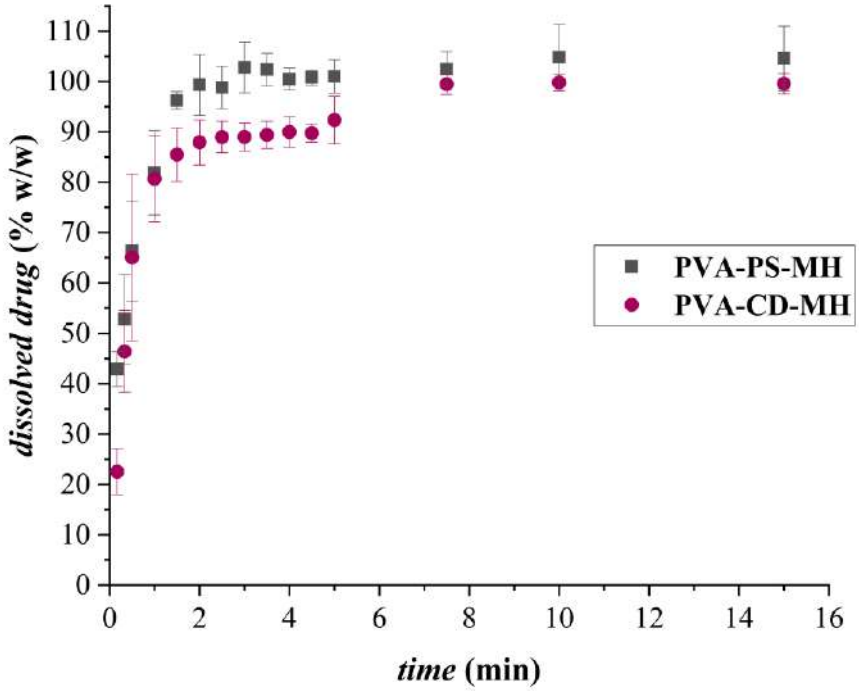

Figure 35 *In vitro* dissolution test of the metoclopramide-HCl loaded polysorbate (PVA-PS-MH) or hydroxypropyl-β-cyclodextrin (PVA-CD-MH) containing nanofibrous samples carried out at phosphate

Figure 35 shows the dissolution profile of the MH containing electrospun nanofibrous samples formulated with different excipients. As it is expected based on, e.g., our previously published study (68), rapid and complete *in vitro* drug release was achieved when the fibrous formulation contained PS. Slightly slower, but also complete dissolution characteristic of the PVA-CD-MH was observed.

DOI:10.14753/SE.2020.2446

4. DISCUSSIONS

4.1. Preformulation and characterization of papaverine-HCl-loaded samples

4.1.1. Preformulation study of papaverine-HCl-loaded samples

Some degree of overlap is required for successful electrospun fiber production. Optimal entanglement, where the contact between the polymeric chains resulting in a flexible supramolecular structure to the polymer precursor solution, is developed at a given concentration range and manifested in excellent fiber formation properties. If excessive chain entanglement takes place, which hinders the free movement of the polymer chains, the film formation becomes more pronounced instead of the randomly oriented individual fiber formation. The results can be explained by the change of the entanglements of polymeric chains. The reason is to be found in the dependence of the molar reflectance and rheological parameters of the inter- and intrachain interaction of polymers.

The molar reflectance measurements suggest that with the increasing HPC content, the entanglements of the polymer chains became more pronounced, which was disadvantageous from the point of the fiber formation process. From the nearly same space-filling factor values, similar molecular mobility can be inferred. The observed opposite trend in R values (R_m and R_c) and the HPC ratio implies that no specific intermolecular interaction between the polymers was established. Nonetheless, the observed divergence refers to a slight but non-specific intermolecular interaction, e.g., hydrogen bonding or altered chain entanglement, which was the most effective in the case of HPC:PVA 8:2, 9:1 and 7:3 mass ratios.

The smallest moduli ratio entails the most elastic behavior of the composite precursor solution relative to the other solutions of different polymer ratios. This indicated that the overwhelming viscoelasticity of the precursors could be disadvantageous from the point of fiber formation, because the applied electrical forces could not be transferred with adequate efficiency to the viscoelastic elongation of the polymer jets in the course of the electrospinning process. Polymeric precursors of the smallest *G”/G’* ratio, so with the most elastic behavior, resulted in film formation, while in the case of the less elastic behavior of the viscous solutions for the electrospinning more fibrous structures were obtained. It can be concluded that for successful fiber formation, the precursor solution

should have viscoelastic nature, on the other hand too high elasticity is unfavorable in this respect.

4.1.2. Micro-and macrostructural investigation of the papaverine-HCl containing samples

The FT-IR results suggest that the papaverine embedded into the fibers in an amorphous state regardless of the two polymer ratios.

According to the PALS results, denser supramolecular structures were formed as a result of the electrospinning process, which was indicated by the decreased o-Ps lifetime values of the electrospun sample of different polymer compositions and manifested in smaller free volume holes.

4.1.3. Accelerated stability test

The merged and broadened FTIR and Raman bands of the fresh sample indicated that the API embedded into the polymeric carrier in an amorphous state. The appearing characteristic peaks in the spectra of the stored samples suggested that the recrystallization of the API took place. The latter fact is in good agreement with the observed phenomenon of the morphological evaluation. It can track back to limited conformational and molecular mobility of the moieties of the crystalline materials, which were manifested in sharp characteristic peaks. In contrast, in an amorphous state, there are numerous allowed conformations, and the energy can be distributed between them and can lead to a merged and broadened spectral profile.

The effects of higher temperature and elevated humidity remarkably affect the molecular mobility and the secondary intermolecular interactions, namely, increasing the former and decreasing the latter. These changes can presumably predispose the ASD for the physical-state modification, and the escalation of the molecular mobility can make a significant contribution to the chances that amorphous APIs start to form crystals.

The preliminary study showed that only weak secondary inter- and intramolecular interactions occurred between the compound of the polymeric system, which also confirms that even a slight temperature rise can be sufficient to destroy or decrease these attractive forces. The established weak secondary interactions were beneficial for fiber formation because, in this case, optimum molecular entanglement was achieved. On the

other hand, these interactions were not strong enough to prevent the increase of the molecular mobility, thus could not able to keep the API in an amorphous state during the stress-induced stability test. It follows that this was a drawback for the solid-state stability.

The observed reduction in the intensity of the lattice vibrations could also be a consequence of the enhanced molecular mobility, which could lead to the recrystallization of the API via enthalpy relaxation.

These observations of the supramolecular characterization may be due to the combined effect of a number of factors, e.g., the phase transition and redistribution of the API, the supramolecular restructuration of polymeric chains and the fragmentation of the fibrous structure. After the first week of storage, as a consequence of the elevated temperature, the molecular mobility of the polymer chains could increase, and thus the original polymeric structure was destroyed, and a new one was created (t_1). The prolonged elevated temperature exposure of the fibers resulted in a different structure in the samples, which were stored for 2-4 weeks. The increase in temperature-driven mobility has sufficient force to overpower the intermolecular binding forces. The widening of the size distribution curves of the free volume holes without remarkable shifting towards larger holes (t_1-t_3) can be inferred that an intermediate structure was achieved. The fourth storage week induced widening of the o-Ps distribution curve, suggesting that a large fraction of "crosslinks" was destroyed by the enhanced molecular mobility, and the recrystallization of the API caused inhomogeneity in free volume hole size distributions.

4.2. Formulation and characterization of MH-loaded electrospun samples

4.2.1. Morphology and topography of the fibrous samples

SEM and AFM images obviously showed that regardless of the used excipient, a clearly fibrous structure with uniform fiber surface was formed. It can be deemed, the PVA is a convenient polymer to be as the base of the matrix and incorporate the MH.

The AFM measurements showed that loaded with relatively low forces (up to 100nN), largely elastic deformation was obtained. The achieved Young-moduli results: 3.26±1.74 GPa and 1.48±0.90 GPa mean±SD values for PVA-PS-MH and PVA-CD-MH fibers, respectively are in good accordance with trifluoroacetate-derived PVA films value of 1.5-3.75 GPa (99), that can be found in the literature. At this point, it should be mentioned that Young moduli of different PVA polymers that are reported previously vary in a very

broad range (e.g., 6.4 MPa (100) 1.8-4.7 GPa (101), 32.6 GPa (102), 50 GPa (103)), which could be a consequence of the different compositions, preparation techniques and the applied testing methods. When the fibers were subjected to higher loads (up to 5 μN), the resulted deformation was predominantly plastic. From the plasticity values that were calculated from force spectra and from that phenomenon, 500 nN load led to deformation only in PVA-CD-MH fiber. Thus it can be concluded that the PVA-CD-MH fibers are more plastic than the PS containing ones. By and large, the addition of PS80 resulted in two times stiffer, less plastic nanofibers than the use of HP-β-CD.

4.2.2. Solid-state characterization of the electrospun samples

The CP build-up curves indicated that the HP-β-CD behavior was found to be very similar to PVA (**Figure 27B**), in contrast with the liquid-like behavior of PS80 (**Figure 27A)** that indicates that HP-β-CD acts as an inner plasticizer, while PS80 acts an outer plasticizer (104).

The third lifetime values of the PALS results also revealed the different plasticizing effect of the used excipients; the ssNMR disclosed mobility and diffusibility differences of the nanofibrous samples (105). The enhanced mobility and diffusibility of the PVA-PS-MH sample caused by the PS80 manifested in the increased o-Ps lifetime value of the fibrous sample related to the physical mixture. The remarkable reduction in o-Ps lifetime values of the HP-β-CD containing electrospun samples, and consequently in the average size of the free volume holes, implied the supramolecular ordering of the polymeric chains, resulting in a more complex molecular packing.

The XRD characteristic of the fibrous samples, together with their FTIR spectra, indicated the absence of a long term order, thus suggested that as a result of the electrospinning process, the MH embedded into the fibers in the amorphous state, regardless of the formulations.

The ssNMR also verified the amorphous state of the API; furthermore, this method was suitable for clarifying the amorphous nature of the active agent. Nonetheless, this piece of information proved to be very useful during the formulation design, as the true solid solutions have thermodynamical stability alone; the nature of the amorphous systems is not widely studied and described in the literature (57, 58). The slight difference between the T_{1rho} relaxation parameters of the neat- and MH-loaded CD containing

formulations implied that the amorphous API in the PVA-CD-MH electrospun sample were molecularly dispersed. In contrast to the observed higher T_{1rho} relaxations difference in the case of the PS containing formulation, indicated that the amorphous drug distributed inhomogeneously in the matrix, which leads to the formation of clusters and amorphous solid dispersions.

The 2D ROESY NMR spectra indicated that the aromatic part of the API is in close proximity to the cavity of the CD, which suggests the formation of the inclusion complex. The cross-peaks between the hydroxypropyl chains of the CD and the MH shows that external complex formation also took place. From the very complex complexation results obtained in concentrated liquid solution together with that fact that the solvent evaporation during the electrospinning was extremely fast, we can assume that the formed structure probably also remained in the solid-state. In the case of the other formulation, based on the chemical structure of the compounds, only weaker secondary interaction formation is possible. Nonetheless, in both formulations, regardless of the used excipient, the established interactions were able to moderate the molecular mobility and obstruct the enthalpy relaxation. Thus the recrystallization of the amorphous drug could not occur, which may provide a clear explanation for why the MH remained in an amorphous form until the end of the four-week-long accelerated stability test.

4.2.3. Stability investigation of the MH-loaded electrospun samples

The PALS results of the stored samples indicated that the supramolecular structure of the drug-loaded HP-β-CD containing nanofibrous samples did not change remarkably. This could be attributed to the host-guest complexation and thus the molecular packing enhancer property of the CD. The observed o-Ps values of the stored PVA-PS-MH samples based on established weaker interaction formation ability of this sample, together with that fact that the PS, as a liquid-like plasticizer can migrate in the fiber and could destroy the already formed secondary-bonds was manifested in time-dependent structural changes, which started during the four-week storage period and is likely to become progressively even more pronounced.

4.2.4. *In vitro* study of the MH-loaded electrospun nanofibrous sheets

The spectrophotometric measurements that focused on the determination of the drug content of the electrospun samples indicated that the total amount of the MH incorporated into the fibers.

From the Raman maps, it can be deduced that the MH molecules were distributed homogenously in the electrospun nanofibrous sheets, which has obviously a crucial role in formulation development and which may derive from the fast solvent evaporation during the fiber formation process. The greater extent inhomogeneity of the physical mixtures than that of the fibrous samples, suggests that the latter is easier to dose, which could have great importance for low-dose and low therapeutic index drugs.

The fast and complete drug-release characteristic of PVA-PS-MH nanofibrous sample can be backtracked to the enhanced apparent aqueous solubility of amorphous drug delivery systems. This may also be due to the unique fiber characteristic (high surface area to volume ratio of fibers) and also to the wettability enhancing effect of the used surfactant. The slightly slower MH-release of the PVA-CD-MH sample can be attributed to the established stronger intermolecular interactions between the CD-MH-PVA.

The enhanced molecular mobility of the PVA may also contribute to achieving complete dissolution, because the release of MH from a more liquid-like polymer base is beneficial.

DOI:10.14753/SE.2020.2446

5. CONCLUSIONS

The hydrophilic polymer-based nanofibrous orally dissolving sheets prepared by electrospinning are promising candidates for rapid drug release. The *intraoral* (e.g., buccal) administration aims at the concerns associated with pre-systemic metabolism (e.g., first-pass metabolism) and the consequential oral bioavailability. The fibrous formulation solves the solubility related issues, which is due to the unique morphological properties of the fibers. Moreover, as a result of the fiber formation process, an amorphous drug delivery system can be formed. The short-term ordering of these systems is the most responsible for these physical- and /or chemical instability.

In my work, the primary focus was put into the more in-depth examination of the stress-indicated changes. Furthermore, I aimed to understand the stabilization opportunities of the electrospun samples based on the relationship between the precursor solution and the features of the resulting third-generation solid dispersions which can help in rational precursor design. Papaverine-HCl was chosen as a model drug, and HPC-PVA composite based nanofibrous sheets were prepared by electrospinning technique from aqueous precursor solutions. Based on the scientific literature, it was the first time that the fiber-forming capability of the poor electrospinnability HPC was improved with PVA, and the fiber formation was carried out without organic solvent usage. The combination of the two polymers allowed adequate composite fiber preparation with slightly different morphological features.

During the fiber formation, five different precursor solutions of HPC:PVA 9:1, 8:2, 7:3, 6:4, 5:5 mass ratios were successfully carried out. The optimum composition of the viscous solutions for the electrospinning process was selected by the combination of the dynamic moduli measurements and molar reflectance characterization with SEM investigation. It was the first published study when the Lorentz-Lorenz analysis was used to predict the success of the fibrous sample formation by electrospinning.

Along with changes in the polymer ratio, the rheological properties of the solutions, the established intra- and intermolecular interactions and the corresponding morphology of the electrospun sample were varied. With the decreasing HPC ratio, fiber formation became dominant. Polymeric precursors of the lowest elasticity and the smallest Lorentz-Lorenz plot values resulted in the best fiber characteristics of the electrospun samples. Thereby, the combination of these measurements made it possible to determine the most

suitable precursor composition. The electrospinning of polymer composite precursor solutions resulted in the formation of amorphous drug delivery systems and the supramolecular ordering of the polymeric chain structure, regardless of the composition of the solution used for fiber formation.

In the case of the investigated composite ratios, the formation of a clearly fibrous structure was observed only at HPC: PVA 5: 5 and 6: 4 ratios. As the HPC has a higher mucoadhesive property, the sample of 6:4 HPC: PVA ratio was chosen for the further study, and this system was subjected to an accelerated stability test. It was the first examination, to the best of our knowledge, in which the supramolecular changes during the physicochemical stability test of drug-loaded electrospun sheets through positron lifetime distribution was reported. Furthermore, the two-step aging process of the drug carrier was also demonstrated. Together with the additional Raman and FTIR measurements, the altered local chemical environment became detectable. Based on these, it can be concluded that the papaverine-HCl loaded nanofibers exhibited less appropriate stress tolerance capacity. The applied experimental setup was found to be suitable to track how the aging of the polymeric carrier reflected in the solid-state changes of the embedded drug.

As for fiber formation, the established weak secondary interactions (formed between the API and polymers) were beneficial, because in this case, the optimum molecular entanglement could be achieved; however, this was detrimental to stability.

It is also clear from the above that stability problems due to the metastable nature of amorphous materials are determinants that need to be emphasized during formulation development. To examine this issue in detail, the MH was chosen as a model drug, which was an excellent API due to its molecular structural features. It was successfully elucidated how the most commonly used solubilizing agent influenced the electrospinning process and the behavior of the nanofibrous sample.

Both of the examined excipients (HP-β-CD and PS80) enabled the formation of fibrous structure from the MH containing PVA-based aqueous precursor. The subtle changes attributed to the applied excipients were subjected to a state-of-the-art imaging and several solid-state characterization techniques. It was revealed that the use of polysorbate led to about two times stiffer, less plastic fibers than the addition of cyclodextrin. Consequently, PS80 advances elastic behavior, while the HP-β-CD

promotes the plastic features. MH-loaded nanofibers of different mechanical properties were prepared by electrospinning.

The major novelty of the work was the identification of the plasticizing effect of the nanofibrous samples by ssNMR measurements. The ^{1}H-^{13}C NMR cross-polarization build-up curves showed that cyclodextrin acts as an inner, while polysorbate acts as an outer plasticizer, and the latter can migrate in the polymer matrix, which is due to its "liquid-like" feature. The PALS measurements confirmed the ssNMR results; it was able to show the molecular mobility differences of the two formulations.

The solid-state methods with different sensitivity showed the short-term ordering of the embedded drug, so it suggests that amorphous drug delivery systems were formed regardless of the applied excipients, but with different homogeneities. The use of PS80 was prone to cluster formation, which could be disadvantageous from the point of the long-term stability of this system, as recrystallization of the API is easier in this case.

During the accelerated stability test, no change in the physical state of the MH, could be observed. Thus, it can be stated that the electrospun samples exhibited a large stress tolerance capacity. However, the use of PS80 resulted in time-dependent microstructural changes, which together with its enhanced cluster-formation ability can be the drawback of this formulation.

Homogenous drug distribution, together with the rapid and complete drug dissolution, made the electrospun samples suitable for application as orally dissolving webs. The established stronger interaction in the case of the CD-containing formulation reflected in the rapid, but a little bit slower drug release compared to the PS-containing one. The two-step dissolution profile of the PVA-CD-MH electrospun sample could be a consequence of the different dissolution rates of the complexed drug and the free amorphous drug part.

It can be established on the basis of the results presented in my dissertation that the complex physicochemical characterization of the polymer-based nanofibrous drug delivery systems it is of great importance. It contributes to a better understanding of material properties, including the supramolecular interactions of multicomponent systems, and consequently the rational design of drug-loaded nanofibrous carriers with the adequate stability and desired mechanical property.

DOI:10.14753/SE.2020.2446

6. SUMMARY

Papaverine-hydrochloride loaded electrospun fibers were prepared for further intraoral administration with the aim of improving the oral bioavailability of the drug. Bases of the formulation, HPC was chosen, but the addition of the PVA to the precursor was successful, from the point of the electrospinnability. Preformulation studies were carried out by monitoring the rheological properties and the molar reflectance of the precursor solution of five different polymer ratios at a constant total polymer concentration, as well as the fiber morphology. A relationship was found between the examined properties of the polymer solutions and their electrospinnability, and the consequent morphology of the samples. The best fiber performance was achieved when the lowest elasticity and the smallest intermolecular interactions were found. Nonetheless, the morphology of the sample changed with the polymer ratio, ASDs were formed with a supramolecular ordered structure in both cases. The electrospun sample of HPC:PVA 6:4 ratio was found to the best and was subjected to an accelerated stability test. The partial recrystallization of the drug indicates the moderate stress tolerance capacity of the ASD, while the PALS measurements revealed the two-step aging process of the drug carrier.

Several characterization techniques were used to investigate the effect of two different excipients on fiber formation properties, the behavior of the MH-loaded electrospun samples, and their stress-induced physical aging. The AFM measurements pointed out that clearly fibrous samples of viscoelastic nature were formed with different mechanical properties. The use of PS80 advances the elastic behavior, while the addition of the HP-β-CD enhances plastic features. The observed supramolecular changes suggest the molecular mobility differences of the two formulations. The ssNMR measurements revealed that the PS80 acts as an outer-, while the CD acts as an inner plasticizer. The liquid-like structure of the former ones caused the enhanced molecular mobility of this formulation and its less plastic behavior. The ssNMR results suggested that different amorphous drug delivery systems were formed. The molecularly dispersed PVA-CD-MH system was found to be beneficial for long-term stability. Nonetheless, during the 4-week-long storage under stress conditions, recrystallization of the API was not observed. However, the established stronger interactions in the case of PVA-CD-MH samples were reflected in the unchanged microstructure under stress condition and in the little bit slower, but fast and complete dissolution profile of this formulation.

7. REFERENCES

1. Jain KK. (2003) Nanodiagnostics: application of nanotechnology in molecular diagnostics. Expert Rev Mol Diagn, 3: 153-161.
2. Silva GA. (2004) Introduction to nanotechnology and its applications to medicine. Surg Neurol, 61: 216-220.
3. Wilkinson JM. (2003) Nanotechnology applications in medicine. Med Device technol, 14: 29-31.
4. Shi J, Votruba AR, Farokhzad OC, Langer R. (2010) Nanotechnology in Drug Delivery and Tissue Engineering: From Discovery to Applications. Nano Lett, 10: 3223-3230.
5. Suri SS, Fenniri H, Singh B. (2007) Nanotechnology-based drug delivery systems. J Occup Med Toxicol, 2: 16.
6. Szabo P, Zelko R. (2015) Formulation and Stability Aspects of Nanosized Solid Drug Delivery Systems. Curr Pharm Des, 21: 3148-3157.
7. Chen S, Li R, Li X, Xie J. (2018) Electrospinning: An enabling nanotechnology platform for drug delivery and regenerative medicine. Adv Drug Deliv Rev, 132: 188-213.
8. Sridhar R, Lakshminarayanan R, Madhaiyan K, Amutha Barathi V, Lim KHC, Ramakrishna S. (2015) Electrosprayed nanoparticles and electrospun nanofibers based on natural materials: applications in tissue regeneration, drug delivery and pharmaceuticals. Chem Soc Rev, 44: 790-814.
9. Sebe I, Szabó P, Kállai-Szabó B, Zelkó R. (2015) Incorporating small molecules or biologics into nanofibers for optimized drug release: A review. IInt J Pharm, 494: 516-530.
10. Li D, Xia Y. (2004) Electrospinning of Nanofibers: Reinventing the Wheel? Adv Mat, 16: 1151-1170.
11. Beachley V, Wen X. (2009) Effect of electrospinning parameters on the nanofiber diameter and length. Mater Sci Eng C, 29: 663-668.

12. Fridrikh SV, Yu JH, Brenner MP, Rutledge GC. (2003) Controlling the Fiber Diameter during Electrospinning. Phys Rev Lett, 90: 144502.

13. Garg K, Bowlin GL. (2011) Electrospinning jets and nanofibrous structures. Biomicrofluidics, 5: 013403.

14. Tiwari SK, Venkatraman SS. (2012) Importance of viscosity parameters in electrospinning: Of monolithic and core–shell fibers. Mater Sci Eng C , 32: 1037-1042.

15. Bhardwaj N, Kundu SC. (2010) Electrospinning: A fascinating fiber fabrication technique. Biotechnol Adv, 28: 325-347.

16. Hutmacher DW, Dalton PD. (2011) Melt Electrospinning. Chem Asian J, 6: 44-56.

17. Nagy ZK, Balogh A, Drávavölgyi G, Ferguson J, Pataki H, Vajna B, Marosi G. (2013) Solvent-Free Melt Electrospinning for Preparation of Fast Dissolving Drug Delivery System and Comparison with Solvent-Based Electrospun and Melt Extruded Systems. J Pharm Sci, 102: 508-517.

18. Robb B, Lennox B. 3 - The electrospinning process, conditions and control. In: LA Bosworth ,S Downes (szerk.), Electrospinning for Tissue Regeneration. Woodhead Publ Ser Biomater, 2011: 51-66.

19. Thompson CJ, Chase GG, Yarin AL, Reneker DH. (2007) Effects of parameters on nanofiber diameter determined from electrospinning model. Polymer, 48: 6913-6922.

20. Medeiros ES, Mattoso LHC, Offeman RD, Wood DF, Orts WJ. (2008) Effect of relative humidity on the morphology of electrospun polymer fibers. Can J Chem, 86: 590-599.

21. Pelipenko J, Kristl J, Janković B, Baumgartner S, Kocbek P. (2013) The impact of relative humidity during electrospinning on the morphology and mechanical properties of nanofibers. Int J Pharm , 456: 125-134.

22. Klossner RR, Queen HA, Coughlin AJ, Krause WE. (2008) Correlation of Chitosan's Rheological Properties and Its Ability to Electrospin. Biomacromolecules, 9: 2947-2953.

23. Regev O, Vandebril S, Zussman E, Clasen C. (2010) The role of interfacial viscoelasticity in the stabilization of an electrospun jet. Polymer, 51: 2611-2620.

24. Shenoy SL, Bates WD, Frisch HL, Wnek GE. (2005) Role of chain entanglements on fiber formation during electrospinning of polymer solutions: good solvent, non-specific polymer–polymer interaction limit. Polymer, 46: 3372-3384.

25. Son WK, Youk JH, Lee TS, Park WH. (2004) The effects of solution properties and polyelectrolyte on electrospinning of ultrafine poly(ethylene oxide) fibers. Polymer, 45: 2959-2966.

26. Yu JH, Fridrikh SV, Rutledge GC. (2006) The role of elasticity in the formation of electrospun fibers. Polymer, 47: 4789-4797.

27. Nagy ZK, Balogh A, Démuth B, Pataki H, Vigh T, Szabó B, Molnár K, Schmidt BT, Horák P, Marosi G, Verreck G, Van Assche I, Brewster ME. (2015) High speed electrospinning for scaled-up production of amorphous solid dispersion of itraconazole. Int J Pharm, 480: 137-142.

28. Vass P, Hirsch E, Kóczián R, Démuth B, Farkas A, Fehér C, Szabó E, Németh Á, Andersen SK, Vigh T, Verreck G, Csontos I, Marosi G, Nagy ZK. (2019) Scaled-Up Production and Tableting of Grindable Electrospun Fibers Containing a Protein-Type Drug. Pharmaceutics, 11: 329.

29. Vass P, Szabó E, Domokos A, Hirsch E, Galata D, Farkas B, Démuth B, Andersen SK, Vigh T, Verreck G, Marosi G, Nagy ZK. (2019) Scale-up of electrospinning technology: Applications in the pharmaceutical industry. Wiley Interdiscip Rev Nanomed Nanobiotechnol, 12: e1611.

30. Zhou F-L, Gong R-H, Porat I. (2009) Mass production of nanofibre assemblies by electrostatic spinning. Polym Int, 58: 331-342.

31. Sill TJ, von Recum HA. (2008) Electrospinning: Applications in drug delivery and tissue engineering. Biomat, 29: 1989-2006.

32. Agarwal S, Wendorff JH, Greiner A. (2008) Use of electrospinning technique for biomedical applications. Polymer, 49: 5603-5621.

33. Eatemadi A, Daraee H, Zarghami N, Melat Yar H, Akbarzadeh A. (2016) Nanofiber: Synthesis and biomedical applications. Artif Cells Nanomed Biotechnol, 44: 111-121.

34. Kai D, Liow SS, Loh XJ. (2014) Biodegradable polymers for electrospinning: Towards biomedical applications. Mater Sci Eng C**,** 45: 659-670.

35. Liang D, Hsiao BS, Chu B. (2007) Functional electrospun nanofibrous scaffolds for biomedical applications. Adv Drug Deliv Rev, 59: 1392-1412.

36. Rieger KA, Birch NP, Schiffman JD. (2013) Designing electrospun nanofiber mats to promote wound healing – a review. J Mater Chem B, 1: 4531-4541.

37. Yoo HS, Kim TG, Park TG. (2009) Surface-functionalized electrospun nanofibers for tissue engineering and drug delivery. Adv Drug Deliv Rev, 61: 1033-1042.

38. Vasconcelos T, Sarmento B, Costa P. (2007) Solid dispersions as strategy to improve oral bioavailability of poor water soluble drugs. Drug Discov Today, 12: 1068-1075.

39. Rahma A, Munir MM, Khairurrijal, Rachmawati H. (2015) The Influence of Non-Ionic Surfactant on the Physical Characteristics of Curcumin-Loaded Nanofiber Manufactured by Electrospinning Method. Adv Mat Res, 1112: 429-432.

40. Jambhekar SS, Breen P. (2016) Cyclodextrins in pharmaceutical formulations I: structure and physicochemical properties, formation of complexes, and types of complex. Drug Discov Today, 21: 356-362.

41. Loftsson T, Hreinsdóttir D, Másson M. (2005) Evaluation of cyclodextrin solubilization of drugs. Int J Pharm, 302: 18-28.

42. Webber MJ, Langer R. (2017) Drug delivery by supramolecular design. Chem Soc Rev, 46: 6600-6620.

43. Bazhban M, Nouri M, Mokhtari J. (2013) Electrospinning of cyclodextrin functionalized chitosan/PVA nanofibers as a drug delivery system. Chinese J Polym Sci, 31: 1343-1351.

44. Canbolat MF, Celebioglu A, Uyar T. (2014) Drug delivery system based on cyclodextrin-naproxen inclusion complex incorporated in electrospun polycaprolactone nanofibers. Colloids Surf B Biointerfaces, 115: 15-21.

45. Kayaci F, Uyar T. (2012) Encapsulation of vanillin/cyclodextrin inclusion complex in electrospun polyvinyl alcohol (PVA) nanowebs: Prolonged shelf-life and high temperature stability of vanillin. Food Chem, 133: 641-649.

46. Uyar T, Besenbacher F. (2009) Electrospinning of cyclodextrin functionalized polyethylene oxide (PEO) nanofibers. Eur Polym J, 45: 1032-1037.

47. Zhang W, Chen M, Diao G. (2011) Electrospinning β-cyclodextrin/poly(vinyl alcohol) nanofibrous membrane for molecular capture. Carbohydr Polym, 86: 1410-1416.

48. Borbás E, Balogh A, Bocz K, Müller J, Kiserdei É, Vigh T, Sinkó B, Marosi A, Halász A, Dohányos Z, Szente L, Balogh GT, Nagy ZK. (2015) In vitro dissolution–permeation evaluation of an electrospun cyclodextrin-based formulation of aripiprazole using μFlux™. Int J Pharm, 491: 180-189.

49. Ghosal K, Chandra A, G P, S S, Roy S, Agatemor C, Thomas S, Provaznik I. (2018) Electrospinning over Solvent Casting: Tuning of Mechanical Properties of Membranes. Sci Rep, 8: 5058.

50. Shahrin N. (2013) Solubility and Dissolution of Drug Product: A Review. 2013, 2: 9.

51. Baghel S, Cathcart H, O'Reilly NJ. (2016) Polymeric Amorphous Solid Dispersions: A Review of Amorphization, Crystallization, Stabilization, Solid-State Characterization, and Aqueous Solubilization of Biopharmaceutical Classification System Class II Drugs. J Pharm Sci, 105: 2527-2544.

52. Chiou WL, Riegelman S. (1971) Pharmaceutical applications of solid dispersion systems. J Pharm Sci, 60: 1281-1302.

53. He Y, Ho C. (2015) Amorphous Solid Dispersions: Utilization and Challenges in Drug Discovery and Development. J Pharm Sci, 104: 3237-3258.

54. Huang Y, Dai W-G. (2014) Fundamental aspects of solid dispersion technology for poorly soluble drugs. Acta Pharm Sin B, 4: 18-25.

55. Mah PT, Peltonen L, Novakovic D, Rades T, Strachan CJ, Laaksonen T. (2016) The effect of surfactants on the dissolution behavior of amorphous formulations. Eur J Pharm Biopharm, 103: 13-22.

56. Szabó P, Zelko R, Antal I. (2016) The Role of Solid State Characterization in Predicting Stability of Solid Dosage Forms. Curr Pharm Des, 22: 5019-5028.

57. Brettmann B, Bell E, Myerson A, Trout B. (2012) Solid-state NMR characterization of high-loading solid solutions of API and excipients formed by electrospinning. J Pharm Sci, 101: 1538-1545.

58. Brettmann BK, Myerson AS, Trout BL. (2012) Solid-state nuclear magnetic resonance study of the physical stability of electrospun drug and polymer solid solutions. J Pharm Sci, 101: 2185-2193.

59. Ito A, Watanabe T, Yada S, Hamaura T, Nakagami H, Higashi K, Moribe K, Yamamoto K. (2010) Prediction of recrystallization behavior of troglitazone/polyvinylpyrrolidone solid dispersion by solid-state NMR. Int J Pharm, 383: 18-23.

60. Pham TN, Watson SA, Edwards AJ, Chavda M, Clawson JS, Strohmeier M, Vogt FG. (2010) Analysis of Amorphous Solid Dispersions Using 2D Solid-State NMR and 1H T1 Relaxation Measurements. Mol Pharm, 7: 1667-1691.

61. Schachter DM, Xiong J, Tirol GC. (2004) Solid state NMR perspective of drug–polymer solid solutions: a model system based on poly(ethylene oxide). Int J Pharm, 281: 89-101.

62. Kiss D, Süvegh K, Zelkó R. (2008) The effect of storage and active ingredient properties on the drug release profile of poly(ethylene oxide) matrix tablets. Carbohydr Polym, 74: 930-933.

63. Süvegh K, Zelkó R. (2002) Physical Aging of Poly(vinylpyrrolidone) under Different Humidity Conditions. Macromolecules, 35: 795-800.

64. Szabó B, Süvegh K, Zelkó R. (2011) Effect of storage on microstructural changes of Carbopol polymers tracked by the combination of positron annihilation lifetime spectroscopy and FT-IR spectroscopy. Int J Pharm, 416: 160-163.

65. Szente V, Süvegh K, Marek T, Zelkó R. (2009) Prediction of the stability of polymeric matrix tablets containing famotidine from the positron annihilation lifetime distributions of their physical mixtures. J Pharm Biomed Anal, 49: 711-714.

66. Chen J, Wang X, Zhang W, Yu S, Fan J, Cheng B, Yang X, Pan W. (2016) A novel application of electrospinning technique in sublingual membrane: characterization, permeation and in vivo study. Drug Dev Ind Pharm, 42: 1365-1374.

67. Song Q, Guo X, Sun Y, Yang M. (2019) Anti-solvent Precipitation Method Coupled Electrospinning Process to Produce Poorly Water-Soluble Drug-Loaded Orodispersible Films. AAPS PharmSciTech, 20: 273.

68. Szabó P, Daróczi TB, Tóth G, Zelkó R. (2016) In vitro and in silico investigation of electrospun terbinafine hydrochloride-loaded buccal nanofibrous sheets. J Pharma Biomed Anal, 131: 156-159.

69. Chen J-P, Chang G-Y, Chen J-K. (2008) Electrospun collagen/chitosan nanofibrous membrane as wound dressing. Colloids Surf A Physicochem Eng Asp, 313-314: 183-188.

70. Haik J, Kornhaber R, Blal B, Harats M. (2017) The Feasibility of a Handheld Electrospinning Device for the Application of Nanofibrous Wound Dressings. Adv Wound Care, 6: 166-174.

71. Khil M-S, Cha D-I, Kim H-Y, Kim I-S, Bhattarai N. (2003) Electrospun nanofibrous polyurethane membrane as wound dressing. J Biomed Mater Res B Appl Biomater, 67B: 675-679.

72. Unnithan AR, Barakat NAM, Tirupathi Pichiah PB, Gnanasekaran G, Nirmala R, Cha Y-S, Jung C-H, El-Newehy M, Kim HY. (2012) Wound-dressing materials with antibacterial activity from electrospun polyurethane–dextran nanofiber mats containing ciprofloxacin HCl. Carbohydr Polym, 90: 1786-1793.

73. Casian T, Borbás E, Ilyés K, Démuth B, Farkas A, Rapi Z, Bogdan C, Iurian S, Toma V, Știufiuc R, Farkas B, Balogh A, Marosi G, Tomuță I, Nagy ZK. (2019) Electrospun amorphous solid dispersions of meloxicam: Influence of polymer type and downstream processing to orodispersible dosage forms. Int J Pharm, 569: 118593.

74. Démuth B, Farkas A, Szabó B, Balogh A, Nagy B, Vágó E, Vigh T, Tinke AP, Kazsu Z, Demeter Á, Bertels J, Mensch J, Van Dijck A, Verreck G, Van Assche I, Marosi G, Nagy ZK. (2017) Development and tableting of directly compressible powder from electrospun nanofibrous amorphous solid dispersion. Adv Powder Technol, 28: 1554-1563.

75. Hamori M, Nagano K, Kakimoto S, Naruhashi K, Kiriyama A, Nishimura A, Shibata N. (2016) Preparation and pharmaceutical evaluation of acetaminophen nano-fiber tablets: Application of a solvent-based electrospinning method for tableting. Biomed Pharmacother, 78: 14-22.

76. Hassounah IA, Shehata NA, Kimsawatde GC, Hudson AG, Sriranganathan N, Joseph EG, Mahajan RL. Chapter 11 - Designing and testing single tablet for tuberculosis treatment through electrospinning. In: AM Grumezescu (szerk.), Fabrication and Self-Assembly of Nanobiomaterials. William Andrew Publishing, 2016: 335-365.

77. Poller B, Strachan C, Broadbent R, Walker GF. (2017) A minitablet formulation made from electrospun nanofibers. Eur J Pharm Biompharm, 114: 213-220.

78. Chidambaram N, Srivatsava AK. (1995) Buccal Drug Delivery Systems. Drug Dev Ind Pharm, 21: 1009-1036.

79. de Vries ME, Boddé HE, Verhoef JC, Junginger HE. (1991) Developments in buccal drug delivery. Crit Rev Ther Drug Carrier Syst, 8: 271-303.

80. Shinkar DM, Dhake AS, Setty CM. (2012) Drug Delivery from the Oral Cavity: A Focus on Mucoadhesive Buccal Drug Delivery Systems. PDA J Pharm Sci Technol, 66: 466.

81. Hao J, Heng PWS. (2003) Buccal Delivery Systems. Drug Dev Ind Pharm, 29: 821-832.

82. Langoth N, Kalbe J, Bernkop-Schnürch A. (2003) Development of buccal drug delivery systems based on a thiolated polymer. Int J Pharm, 252: 141-148.

83. Rossi S, Sandri G, Caramella CM. (2005) Buccal drug delivery: A challenge already won? Drug Discov Today Technol, 2: 59-65.

84. Patel VF, Liu F, Brown MB. (2012) Modeling the oral cavity: In vitro and in vivo evaluations of buccal drug delivery systems. J Control Release, 161: 746-756.

85. Aungst BJ, Rogers NJ. (1989) Comparison of the effects of various transmucosal absorption promoters on buccal insulin delivery. Int J Pharm, 53: 227-235.

86. Nicolazzo JA, Reed BL, Finnin BC. (2004) Modification of buccal drug delivery following pretreatment with skin penetration enhancers. J Pharm Sci, 93: 2054-2063.

87. Siegel IA, Gordon HP. (1985) Surfactant-induced increases of permeability of rat oral mucosa to non-electrolytes in vivo. Arch Oral Biol, 30: 43-47.

88. Chinna Reddy P, Chaitanya KSC, Madhusudan Rao Y. (2011) A review on bioadhesive buccal drug delivery systems: current status of formulation and evaluation methods. DARU J Pharm Sci, 19: 385-403.

89. Mahajan P, Kaur A, Aggarwal G, Harikumar SL. (2013) Mucoadhesive drug delivery system: A review. Int J Drug Dev Res, 5: 11-20.

90. Manohar SD, Sridhar DA, Mallikarjuna SC. (2012) Drug delivery from the oral cavity: A focus on mucoadhesive buccal drug delivery systems. PDA J Pharm Sci Technol, 66: 466-500.

91. Patel DA, Patel MR, Patel KR, Patel NM. (2012) Buccal mucosa as a route for systemic drug delivery: A review. Int J Drug Dev Res, 4: 99-116.

92. Patel VF, Liu F, Brown MB. (2011) Advances in oral transmucosal drug delivery. J Control Release**,** 153: 106-116.

93. Pawar RR, Raut DB, Karde VK, Wadikar JC, Jadhav AS, Chintale AG. (2013) Mucoadhesive buccal drug delivery system: A review. Res J Pharm Technol, 6: 506-515.

94. Rathbone MJ, Drummond BK, Tucker IG. (1994) The oral cavity as a site for systemic drug delivery. Adv Drug Deliv Rev, 13: 1-22.

95. Kazsoki A, Szabó P, Süvegh K, Vörös T, Zelkó R. (2017) Macro- and microstructural tracking of ageing-related changes of papaverine hydrochloride-loaded electrospun nanofibrous buccal sheets. J Pharm Biomed Anal, 143: 62-67.

96. Hertz H. (1881) Über die berührung fester elastischer körper. J. für die Reine und Angew Math, 92: 156.

97. Moraes CM, Abrami P, de Araujo DR, Braga AFA, Issa MG, Ferraz HG, de Paula E, Fraceto LF. (2007) Characterization of lidocaine:hydroxypropyl-β-cyclodextrin inclusion complex. J Incl Phenom Macrocycl Chem, 57: 313-316.

98. Masuda K, Kaji H, Horii F. (2000) CP/MAS 13C NMR analyses of hydrogen bonding and the chain conformation in the crystalline and noncrystalline regions for poly(vinyl alcohol) films. J Polym Sci B Polym Phys, 38: 1-9.

99. Yamaura K, Tada M, Tanigami T, Matsuzawa S. (1986) Mechanical properties of films of poly(vinyl alcohol) derived from vinyl trifluoroacetate. J Appl Polym Sci , 31: 493-500.

100. Mohammad Mahdi Dadfar S, Kavoosi G, Mohammad Ali Dadfar S. (2014) Investigation of mechanical properties, antibacterial features, and water vapor permeability of polyvinyl alcohol thin films reinforced by glutaraldehyde and multiwalled carbon nanotube. Polym Compos, 35: 1736-1743.

101. Fukumori T, Nakaoki T. (2013) Significant Improvement of Mechanical Properties for Polyvinyl Alcohol Film Prepared from Freeze/Thaw Cycled Gel. Open J Org Polym Mater, 04: 7.

102. Wei H, Xingguo Y, Jiawen Z, Huige X, Jian X. (2013) Experimental research on the mechanical properties of PVA fiber reinforced concrete. Res J Appl Sci Eng Tech, 5: 4563-4567.

103. Fujiwara H, Shibayama M, Chen JH, Nomura S. (1989) Preparation of high-strength poly(vinyl alcohol) fibers by crosslinking wet spinning. J Appl Polym Sci, 37: 1403-1414.

104. Domján A, Bajdik J, Pintye-Hódi K. (2009) Understanding of the Plasticizing Effects of Glycerol and PEG 400 on Chitosan Films Using Solid-State NMR Spectroscopy. Macromolecules, 42: 4667-4673.

105. Bajdik J, Marciello M, Caramella C, Domján A, Süvegh K, Marek T, Pintye-Hódi K. (2009) Evaluation of surface and microstructure of differently plasticized chitosan films. J Pharm Biomed Anal, 49: 655-659.

8. BIBLIOGRAPHY OF THE CANDIDATE'S PUBLICATIONS

8.1. Publication relevant to the dissertation

I. **Kazsoki A**, Szabó P, Zelkó R. (2017) Prediction of the hydroxypropyl cellulose—poly(vinyl alcohol) ratio in aqueous solution containing papaverine hydrochloride in terms of drug loaded electrospun fiber formation. J Pharm Biomed Anal, 138: 357-362. IF(2017): 2.831

II. **Kazsoki A**, Szabó P, Süvegh K, Vörös T, Zelkó R. (2017) Macro- and microstructural tracking of ageing-related changes of papaverine hydrochloride-loaded electrospun nanofibrous buccal sheets. J Pharm Biomed Anal, 143: 62-67. IF(2017): 2.831

III. **Kazsoki A**, Domján A, Süvegh K, Zelkó R. (2018) Microstructural characterization of papaverine-loaded HPC/PVA gels, films and nanofibers. Eur J Pharm Sci, 122: 9-12. IF(2018): 3.532

IV. **Kazsoki A**, Szabó P, Domján A, Balázs A, Bozó T, Kellermayer M, Farkas A, Balogh-Weiser D, Pinke B, Darcsi A, Béni S, Madarász J, Szente L, Zelkó R. (2018) Microstructural Distinction of Electrospun Nanofibrous Drug Delivery Systems Formulated with Different Excipients. Mol Pharm, 15: 4214-4225. IF(2017): 4.396

8.2. Further related publications

V. **Kazsoki A**, Szabó P, Zelkó R. (2016) Nano- és mikroszálas rendszerek gyógyászati alkalmazási lehetőségei. Acta Pharm Hung, 86:2. IF(2016): -

VI. Sipos E, Kósa N, **Kazsoki A**, Szabó Z-I, Zelkó R. (2019) Formulation and Characterization of Aceclofenac-Loaded Nanofiber Based Orally Dissolving Webs. Pharmaceutics, 11: 417. IF(2019): 4.421

VII. Kovács A, **Kazsoki A**, Démuth B, Szirányi B, Madarász J, Süvegh K, Zelkó R. (2020) Influence of Aqueous Solubility-Enhancing Excipients on the Microstructural Characteristics of Furosemide-Loaded Electrospun Nanofibers. Pharmaceutics, 12: 385. IF(2019): 4.421

VIII. Sipos E, Csatári T, **Kazsoki A**, Gergely A, Bitay E, Szabó Z-I, Zelkó R. (2020) Preparation and Characterization of Fenofibrate-Loaded PVP Electrospun Microfibrous Sheets. Pharmaceutics, 12:612. IF(2019): 4.421

8.3. Other, not related publications

IX. Arany P, Róka E, Mollet L, Coleman AW, Perret F, Kim B, Kovács R, **Kazsoki A**, Zelkó R, Gesztelyi R, Ujhelyi Z, Fehér P, Váradi J, Fenyvesi F, Vecsernyés M, Bácskay I. (2019) Fused Deposition Modeling 3D Printing: Test Platforms for Evaluating Post-Fabrication Chemical Modifications and In-Vitro Biological Properties. Pharmaceutics, 11: 277. IF(2019): 4.421

X. Fejős I, He Y, Völgyi G, **Kazsoki A**, Sun J, Chen W, Sohajda T, Szente L, Jiang X, Béni S. (2014) Tapentadol enantiomers: Synthesis, physico-chemical characterization and cyclodextrin interactions. J Pharm Biomed Anal, 88: 594-601. IF(2014): 2.979

XI. Fejős I, **Kazsoki A**, Sohajda T, Márványos E, Volk B, Szente L, Béni S. (2014) Interactions of non-charged tadalafil stereoisomers with cyclodextrins: Capillary electrophoresis and nuclear magnetic resonance studies. J Chrom A, 1363: 348-355. IF(2014): 4.169

XII. **Kazsoki A**, Fejős I, Sohajda T, Zhou W, Hu W, Szente L, Béni S. (2016) Development and validation of a cyclodextrin-modified capillary electrophoresis method for the enantiomeric separation of vildagliptin enantiomers. Electrophoresis, 37: 1318-1325. IF(2016): 2.744

DOI:10.14753/SE.2020.2446

9. ACKNOWLEDGEMENTS

First of all, I would like to express my deepest gratitude to my supervisor, Professor Romána Zelkó for her endless support, encouragement and guidance.

Special thanks should be given to Diána Balogh for her professional advice, selfless help and much encouragement. I am endlessly grateful for the fate, that we have met, and I wish to thank her for everything I could learn from her.

I am extremely grateful to SpinSplit Ltd. for ensuring the use of its electrospinning device during my second project.

I am also indebted to the following people, co-authors who helped me during my work: Dr. Péter Szabó, Dr. Attila Domján, Dr. Károly Süvegh, Dr. Attila Farkas, Dr. Tamás Bozó, Dr. Miklós Kellermayer, Dr. András Darcsi, Dr. Szabolcs Béni, Dr. Tamás Vörös, Dr. János Madarász, Attila Balázs, Balázs Pinke and Dr. Lajos Szente.

Furthermore, I am grateful to all colleagues at the University Pharmacy Department of Pharmacy Administration.

Last, but not least, I would like to express my deepest gratitude to my parents and my twin brother for everything that I have been receiving throughout the course of my study.

Journal of Pharmaceutical and Biomedical Analysis 134 (2017) 357–362
DOI:10.14753/SE.2020.2446

Contents lists available at ScienceDirect

Journal of Pharmaceutical and Biomedical Analysis

journal homepage: www.elsevier.com/locate/jpba

Prediction of the hydroxypropyl cellulose—poly(vinyl alcohol) ratio in aqueous solution containing papaverine hydrochloride in terms of drug loaded electrospun fiber formation

Adrienn Kazsoki, Péter Szabó, Romána Zelkó *

University Pharmacy Department of Pharmacy Administration, Semmelweis University, Hőgyes Endre St. 7-9, H-1092 Budapest, Hungary

ARTICLE INFO

Article history:
Received 31 December 2016
Received in revised form 14 February 2017
Accepted 15 February 2017
Available online 22 February 2017

Keywords:
Papaverine hydrochloride
Hydroxypropyl cellulose
Polyvinyl alcohol
Nanofibers
Storage and loss moduli
Molar reflectance

ABSTRACT

Papaverine hydrochloride loaded electrospun fibers were prepared for buccal drug delivery with the aim of improving the oral bioavailability of the crystalline drug, which can be achieved by the increased solubility and by the circumvention of the intensive first pass metabolism. The water soluble hydroxypropyl cellulose (HPC) was chosen as a mucoadhesive polymer. In order to improve the electrospinnability of HPC, the also mucoadhesive poly(vinyl alcohol) (PVA) was used. During the experiments, the total polymer concentration was kept constantly at 15% (w/w), and only the ratio of the two polymers was changed. Five different HPC:PVA ratios (5:5, 6:4, 7:3, 8:2, 9:1) were examined. Combination of rheological measurements and molar reflectance characterization with scanning electron microscopy was applied for the determination of the optimum composition of the gels for fiber formation. The crystalline-amorphous transition of papaverine hydrochloride was also tracked by Fourier transform infrared spectroscopy. A correlation was found between the macrostructural properties of the polymer solutions and their electrospinnability and the consequent morphology of the resultant samples. Along with the changes of the polymer ratio, the corresponding morphology of the electrospun samples also varied. With decreasing HPC ratio of the system, a transition from the spray-dried film-like structure through fibrous film to fibers was observed. Polymer solutions of the lowest elasticity and smallest intermolecular interactions contributed to the best fiber characteristics of the samples. The results enable the determination of the polymer ratio for the formation of applicable quality of electrospun fibers. According to the results 5:5 and 6:4 polymer ratios enabled the best fiber performance.

1. Introduction

Cardiovascular diseases are among the leading causes of death in the world. Cerebral ischaemia represents one of the major cardiovascular health concerns because of not only the morbidity but its role in the development of dementia and other disabilities. Considering the effect of cerebral ischaemia on overall public health, it is obvious that proper management of such conditions is essential to achieve the best possible outcome, therefore prompt and targeted treatment can enormously contribute to both public and individual health [1]. However, pharmacodynamic properties of papaverine are beneficial for the treatment of stroke; its unfavourable biopharmaceutical behavior confines the clinical applicability. The benzylisoquinoline-type opium alkaloid papaverine (Fig. 1) has a non-specific direct relaxant effect on smooth muscle. The vasodilation is resulted by the inhibition of phosphodiesterase enzymes and the direct actions on calcium channels [2].

Orally administered papaverine has been shown to increase regional cerebral blood flow in humans. Papaverine hydrochloride is slightly soluble in water, and its poor peroral bioavailability is associated with high intra- and interindividual variability. This variation can be explained by the extensive first pass metabolism and the inadequate absorption depending on incomplete *in vivo* drug release [3]. Furthermore, the utilization of alternative administration routes is hastened by tha fact that papaverine has been reported to carry the risk of potential liver damage [4,5]. As a result of these properties, papaverine can only be administered parenterally in emergency cases, such as cerebral ischemia in order to ensure the therapeutic drug levels in the brain and the rapid onset. Since the administration of invasive parenteral dosage forms has several unfavourable features, these problems can be addressed by

Abbreviations: HPC, hydroxypropyl cellulose; PVA, poly(vinyl alcohol).

* Corresponding author.
E-mail address: zelko.romana@pharma.semmelweis-univ.hu (R. Zelkó).

http://dx.doi.org/10.1016/j.jpba.2017.02.030
0731-7085/

DOI:10.14753/SE.2020.2446

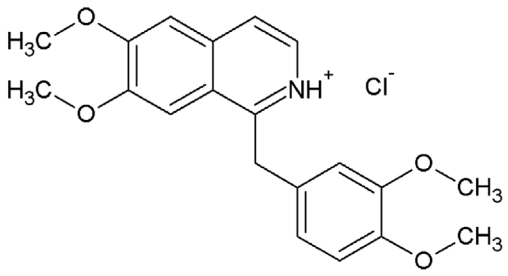

Fig. 1. Chemical structure of papaverine hydrochloride.

using alternative dosage forms, such as inhalation or buccal, rectal or transdermal administration routes [6].

Nanofibers have been successfully applied in various fields of the medicine, such as tissue engineering scaffolds, in wound healing, vascular graft implants and drug delivery [7–9] because of their pharmaceutically luring advantages, such as high surface area to volume ratio and very high porosity [10,11].

Electrospinning represents the most commonly used fiber forming technique, which utilizes electrical forces to produce nanofibers from polymers [12]. Wide variety of polymers can be used to control the drug release kinetics or to modify the dissolution [13]. The incorporation of poorly water-soluble drugs into polymer-based nanofibers is of special interest because of the increased solubility and the consequent improved oral bioavailability. Such improvement in the solid state properties can be enabled by the high amorphization efficacy of the fiber forming process and by the unique characteristics of the formed fibrous system [14–16].

The oral cavity is a possible site for the delivery of drugs. With the mucosal delivery local pharmacological effects can be achieved. For this application, the residence time and the local drug concentration are the most important factors, influencing the amount of absorbed drug [17]. Systemic effects can also be achieved via transmucosal routes, which is due to the highly vascularized, rich blood supplied and relatively permeable properties of the mucosa. Permeation and consequently the bioavailability can increase by using enhancers (for example polysorbate, sodium lauryl sulfate) [18,19]. Because of the advantages provided by buccal formulations, such as rapid onset of effect, good bioavailability, elimination of hepatic first-pass metabolism and consequently the reduced amount of drug, the buccal delivery could be an alternative administration of the parenteral routes [20–26].

Chemically-modified cellulose derivatives (ethers and esters) are commonly used for buccal drug delivery [20]. The first generation of mucoadhesive polymers such as the hydroxypropyl cellulose (HPC) and poly(vinyl-alcohol) (PVA) are able to form non-covalent bonds with the mucosa, thus ensuring a better oral residence and drug release at the absorption site. HPC presents high mucoadhesive potential and its further advantage is the aqueous solubility, thus avoiding the need of the use of organic solvents during production [27–29]. Most of the natural and semisynthetic polymers exhibit poor spinnability thus the application of polymer of good spinnability could improve fiber forming capability. The combination of two polymers enables adequate composite fiber performance.

The fiber forming mechanism is very complex and the electrospinnability of polymer gels is widely studied, but still not completely understood. The surface tension, conductivity, entanglement concentration, viscosity and the dynamic moduli: storage (G') and loss (G") modulus are the most commonly examined properties. The conductivity measurement could be informative when the polymer solutions containing ionogenic polymer in different concentrations and then the conductivity can correlate with the polymer concentration. In case of the total mass of the uncharged polymers and the active pharmaceutical ingredients are the same, the conductivity and the surface tension remain unchanged [7,30–35].

Molar refraction was successfully used to examine the intermolecular forces between polymer and plasticizer [36]. Determination of molar refractions could be applied to examine the interactions between the polymers. Best of our knowledge the molar refraction effect on the fiber forming process has not been published yet.

The primary aim of the present study was to prepare papaverine hydrochloride loaded buccal nanofibrous films, and to determine the optimum composition of HPC-PVA aqueous solutions for electrospun fiber formation based on the rheological and molar reflectance characterization of the system. With this formulation intended for transmucosal drug administration, the unique properties of the nanofibrous sheets and the benefits of the buccal formulation could be combined preferably.

2. Materials and methods

2.1. Materials

Hydroxypropyl cellulose (Klucel EXF Pharm, Ashland, USA; Mw ~ 80000; the moles of substitution = 3.8) and poly(vinyl alcohol) (18-88 Ph. Eur., Merck, Darmstadt, Germany) polymers, polysorbate 20 (Ph. Eur., Molar chemicals, Hungary) and distilled water were used for the preparation of gels. The model drug was papaverine hydrochloride (Ph. Eur.).

2.2. Preparation of papaverine-HCl gels

Papaverine-HCl stock solution was prepared by dissolving 0.6 g drug in 18.8 g of distilled water in the presence of 0.6 g polysorbate 20 (3% w/w) applying a few minutes of heating. The clear solution was cooled to room temperature and then it was diluted to 20.0 g with distilled water. The gels were prepared by the addition of the necessary amount of HPC, PVA and 30 mg/g papaverine-HCl aqueous stock solution. The total polymer concentration of the gels was 15% (w/w). The HPC: PVA mass ratios were 5:5, 6:4, 7:3, 8:2, 9:1 which corresponded to 7.5, 12.2, 10.5, 9 and 13.5 HPC concentration (% w/w), respectively with the final polymer concentration of 15% (w/w). The required amount of PVA and stock solution was measured into a beaker, than it was heated on 80–90 °C and stirred on magnetic stir plate until a homogenous gel was achieved. The gels were cooled to the room temperature and finally the necessary amount of the HPC was added and it was also stirred until homogenous gel was achieved. The samples were stored at room temperature (25 ± 2 °C).

2.3. Calculation of the molar refraction

The molar refraction values were calculated by the Lorentz-Lorenz equation [36]:

$$R = V_m - \mathrm{r} \quad (1)$$

where V_m is the molar volume ($dm^3 mol^{-1}$) and r is the space-filling factor. V_m was calculated as

$$V_m = M/\rho \quad (2)$$

where M is the molecular weight ($g\,mol^{-1}$) and ρ is the volumetric mass density of the gels ($g\,cm^{-3}$).

Density values were determined with calibrated flask method. In case of molecular weight calculations, the mass ratios of the components (papaverine-HCl, polysorbate 20, PVA and HPC) were considered.

DOI:10.14753/SE.2020.2446

The space-filling factor (r), which denotes the fraction of the molar volume actually occupied by the molecules [36], is calculated as

$$r = (n^2 - 1)/(n^2 + 2) \quad (3)$$

where n is the refractive index, which was determined at 22.6 ± 0.1 °C by Krüss Refractometer (Germany).

2.4. Rheological properties of the gels

The rheological properties of the gels were carried out with Kinexus Pro rheometer (Malvern Instruments Ltd, UK). Measured data were registered with rSpace for Kinexus Pro 1.3 software. Samples were measured using parallel plates geometry (50 mm diameter) in constant 25 ± 0.1 °C temperature. The gap between the plates was 0.0300 mm.

Storage and loss moduli were determined by oscillatory tests. The elastic or storage modulus (G'), which represents the ability of the materials to store energy, was calculated as

$$G' = (\tau_a/\gamma_a)_* cos\delta$$

and the viscous or loss modulus (G''), which can be defined as the ability of the material to dissipate energy, was calculated as

$$G'' = (\tau_a/\gamma_a)_* \sin\delta,$$

where τ_a is the shear stress, γ_a is the deformation and δ is the phase shift angle [37].

The oscillatory shear measurements were performed at amplitude within the linear region which was chosen to 40% within the viscoelastic region and the frequency was in the range of 0.1–10 s^{-1}. Three parallels were measured of each gel in both tests.

2.5. Electrospinning

The prepared gels were transferred into plastic syringes and then the syringes were vented. After all, a metallic needle with 1.2 mm inner diameter was attached through a silicon tube. The syringe was put into a syringe pump which provided the controlled polymer gel flow.

The applied voltage was examined in three levels: 20, 25 and 30 kV. The needle to collector distance was 5, 10 and 15 cm. The flow rate was 0.2 or 0.3 ml/h. In the course of the 10 min continuous apparatus operation, the fibers were collected on aluminum foil.

2.6. Fourier transform infrared (FT-IR) spectroscopy

Physicochemical properties of the fibers were examined using Jasco FT/IR-4200 spectrophotometer which was equipped with Jasco ATR PRO470-H single reflection accessory. The measurements were performed in absorbance mode. The spectra were collected over a wavenumber range of 4000 and 1800 cm^{-1}. After 50 scans, the measurements were evaluated with the FT-IR software (Spectra Manager-II, Jasco).

2.7. Preparation of physical mixtures

Physical mixtures of the components of the drug loaded nanofiber in the same concentration were made by the manual combination of papaverine-HCl, PVA and HPC in a pestle and mortar. After the PVA was milled, the substance was homogenized. The mixture was used as control for the FT-IR examinations.

Table 1
The measured (R_m) and the calculated (R_c) molar refractions, the space-filling factors (r) and the Lorentz-Lorenz plot (R_m-R_c)/R_m values (%) in case of the different HPC:PVA mass ratio.

HPC:PVA mass ratio	r	R_m	R_c	$(R_m-R_c)/R_m$*100
5:5	0.2224	75.2288	75.2392	−0.0139
6:4	0.2223	71.6466	71.6357	0.0153
7:3	0.2223	67.9983	68.0322	−0.0498
8:2	0.2225	64.5054	64.4286	0.1191
9:1	0.2225	60.7817	60.8251	−0.0714

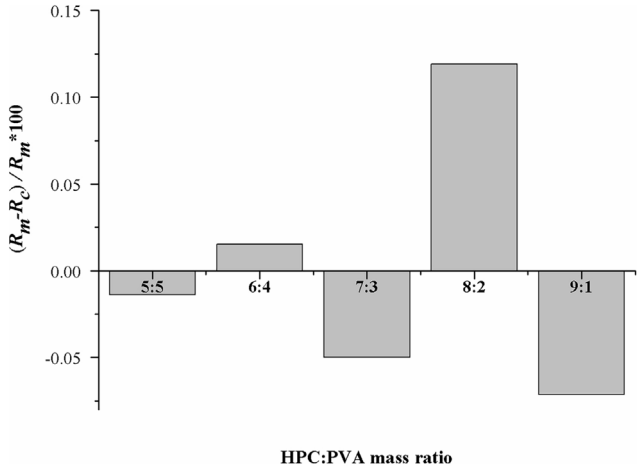

Fig. 2. Lorentz-Lorenz plot values of papaverine-HCl loaded gels (R_m is a measured- and R_c is a calculated molar refraction index).

2.8. Scanning electronmicroscopic analysis (SEM)

Detailed morphology of the fibers was characterized by scanning electron microscope (SEM). SEM studies were performed by a Hitachi S-4300 instrument equipped with a Bruker energy dispersive X-ray spectroscope (Hitachi Science Systems, Ltd., Japan). The surfaces of samples were covered by a sputtered gold conductive layer, and 5–10 kV accelerating voltage was used for taking high resolution electron micrographs.

3. Results

3.1. The Lorentz-Lorenz analysis

Density and refractive index were determined in case of each gels. R_m values and space-filling factors were calculated using Eqs. (1 and 3), respectively. R_m values were plotted as a function of PVA concentrations (% w/w) and a linear was fitted. The slope of linear regression was 2.4024 and the linear regression accuracy values (R^2) was 0.9999. According to the regression lines, R_c values were calculated. Table 1 summarizes the measured (R_m) and the calculated (R_c) molar refractions, the space-filling factors and the Lorentz-Lorenz plot (R_m-R_c)/R_m values (%). The nearly unchanged space-filling factor values refer to almost equal molecular mobility. Lorentz-Lorenz plot values of the papaverine-HCl loaded gels as function of HPC:PVA mass ratio are shown in Fig. 2. According to the results, along with increasing HPC ratio, R_m and R_c values are continuously decreasing, which indicates the lack of specific intermolecular interaction between the polymers. However, the divergence, which is the highest in case of HPC:PVA 8:2, 9:1 and 7:3 mass ratio, indicates slight, non-specific intermolecular interaction e.g hydrogen bonding or altered chain entanglement.

DOI:10.14753/SE.2020.2446

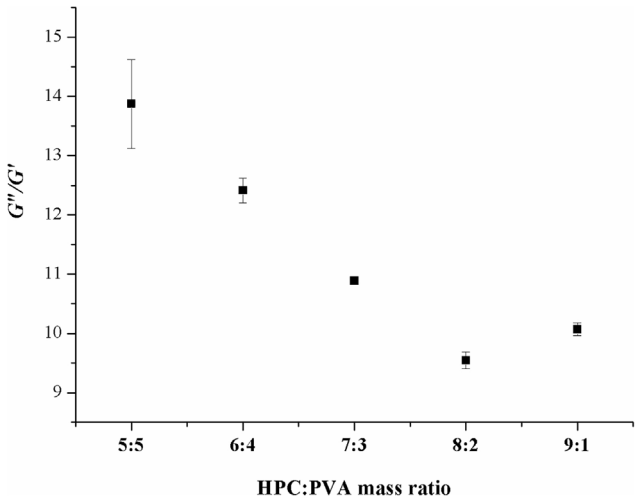

Fig. 3. Ratio of storage (G') and loss (G") moduli of papaverine-HCl loaded gels as a function of HPC:PVA mass ratio (dynamic moduli measured at a frequency 1.995 Hz).

3.2. Rheological measurements

The viscoelasticity of gels influences the jet formation and the jet stability, so it is one of the most critical parameters for the successful electrospinning process. Oscillatory test was used to determine the storage and loss moduli. The tests were compared at different frequency values. The results of *G"/G'* values displayed the same tendency at the different frequency values, therefore only the results corresponding to 1.998 s^{-1} value were presented in Fig. 3.

A local minimum was observed in the dynamic modulus ratio of HPC:PVA = 8:2 sample. The modulus ratio decreases monotonically reaching a minimum value and following the increase. The smallest ratio refers to the most elastic behavior of the composite gel compare to the other HPC:PVA ratios. The latter suggests that the preponderant viscoelasticity of the sample could be disadvantageous from the point of fiber formation, since the electrical forces cannot be effectively transferred to the viscoelastic elongation of the polymer jets in the course of the fiber formation.

3.3. Morphology study of the samples

The electrospinning of papaverine-HCl containing gels resulted in a well-defined, more or less round shaped samples on the aluminum foil. Most of the prepared samples could be easily peeled off from the aluminum foil, which is beneficial for the further studies and also for the final applications. Only the sample of HPC:PVA 9:1 mass ratio was the exception, since the firm adhesion inhibited its removal.

The morphology of the prepared samples was tracked by SEM measurements. The results indicate that with increasing HPC ratio to PVA the morphology was changed; transition from spray-dried film-like structures through fibrous films to fibers can be observed which is illustrated by Fig. 4.

Partially spray-dried films and beaded fibers were formed in case of HPC:PVA 9:1 mass ratio, which can be observed in Fig. 4E. The simultaneous electrostatic spraying and electrospinning of the viscous polymer solution resulted in the appearance of films and beaded fibers.

In case of 8:2 ratio, a fibrous film morphology can be observed (Fig. 4D), while at 7:3 ratio also the fibrous film formation is dominant (Fig. 4C), but in the latter case the fibrous structure characterizes the whole sample. At 5:5 and 6:4 HPC:PVA mass ratio (Fig. 4A and B) clearly fibrous systems, without beads can be observed.

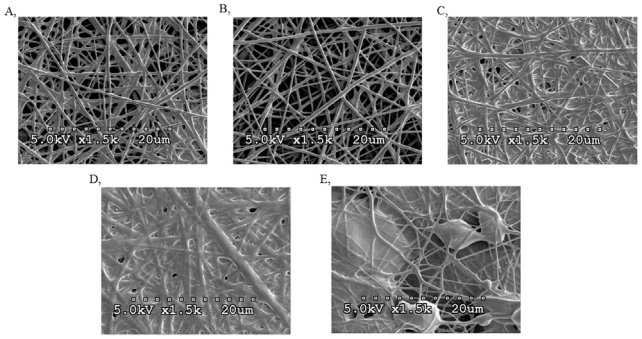

Fig. 4. SEM photos of the spray-dried film-to-fiber transition as a function of HPC:PVA mass ratio 5:5 (**A**), 6:4 (**B**), 7:3 (**C**), 8:2 (**D**), 9:1 (**E**).
(The total polymer concentration was 15% (w/w). During the fiber forming process 30 kV voltage was applied. The flow rate was 0.2 ml/h and needle to collector distance was 15 cm.)

With the decreasing HPC ratio the fibrous morphology will become the dominant feature. The transition from film formation to the mainly fibrous system is initiated at 8:2 mass ratio and completed by 6:4 ratio. Along with the decrease of HPC ratio the proportion of the fibrous parts in the electrospun samples increased.

3.4. FT-IR analysis

The FT-IR spectra of various samples, physical mixture and the components are presented in Fig. 5. The characteristic peak of the model drug around at 2300–2700 cm^{-1} can be observed clearly in the physical mixture. Another characteristic peaks of the papaverine-HCl were overlapped with peaks from functional group of the polymers, so that to verify the amorphous transition of the drug the 2300–2700 cm^{-1} wavenumber range was evaluated. In contrast to crystalline materials, where the limited rotational-vibrational transitions are allowed, in amorphous materials several transitions can take place. Since the absorbed energy is dissipated among the numerous transitions, broadening and merging of the spectrum is a common phenomenon as a result of crystalline-amorphous transition.

The lack of the high intensity characteristic peaks of various fiber samples indicates that the papaverine-HCl was incorporated into the nanofibers in an amorphous state as a result of the electrospinning process.

4. Discussion

There is a desired chain entanglement density, which is necessary to produce electrospun fibers [30]. The optimal change entanglement, where overlapping of polymeric chains renders a flexible supramolecular structure to the gels, is developed at a given concentration range resulting in good fiber forming properties. If the chain entanglement become too extensive, in other words unfavourable overlapping of polymeric chains takes place, instead of the formation of defect-free individual fibers the fibrous film formation is dominant. Alteration of polymeric chain entanglement, thus the change of polymeric chain overlapping can be explained by the obtained results, since molar reflectance and rheological parameters also depend on the inter- and intrachain interaction of polymers. The molar reflectance characterization results indicated that the increase in HPC content resulted in the enhanced entanglements of polymer chains, which is disadvantageous in the course of the fiber forming process. Generally, spinnable solutions should exhibit viscoelastic properties, but the too high elasticity is objectionable during the fiber forming process. In the case of the

DOI:10.14753/SE.2020.2446

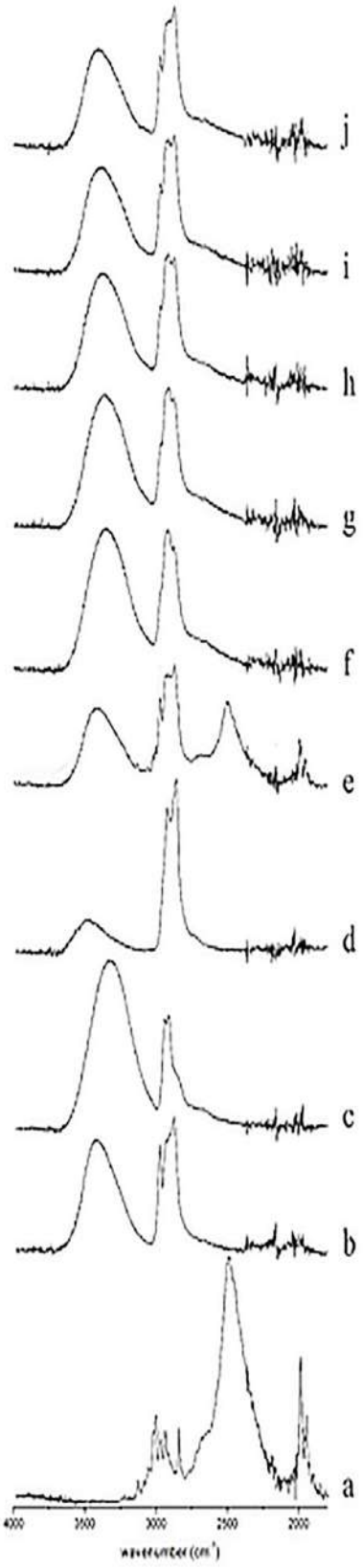

Fig. 5. FTIR spectra of papaverine-HCl (**a**), hydroxypropyl cellulose (HPC) (**b**), poly(vinyl alcohol) (PVA) (**c**), polysorbate 20 (**d**), physical mixture (**e**), fibers (**f–j**):15% (w/w) polymer, 3% (w/w) polysorbate 20, 30 kV voltage, 15 cm distance, 0.2 ml/h flow rate between 4000 and 1800 cm^{-1} wavenumber. (HPC:PVA = 5:5 (**f**), HPC:PVA = 6:4 (**g**), HPC:PVA = 7:3 (**h**), HPC:PVA = 8:2 (**i**), HPC:PVA = 9:1(**j**)).

most elastic behavior (smallest *G"/G'* ratio) of the polymeric solution the film formation was the dominant process, while the less elastic behavior of the samples resulted in more fibrous structure. The observed phenomenon is in good agreement with the authors' previous studies, where the adhesiveness and the viscosity values had a local minimum, which could lead to higher productivity of the fiber formation process and optimum micromorphology of the emitted fibers [38].

5. Conclusion

Papaverine-HCl loaded HPC-PVA composite nanofibrous systems were prepared successfully by electrospinning process. The optimum composition of HPC-PVA fibers was determined based on the rheological and molar reflectance characterization of their solution.

This formulation could enable the transmucosal amorphous drug delivery, thus improving the oral bioavailability of the poorly soluble crystalline papaverine-HCl, meanwhile avoiding its first pass metabolism.

Appendix A. Supplementary data

Supplementary data associated with this article can be found, in the online version, at http://dx.doi.org/10.1016/j.jpba.2017.02.030.

References

[1] E.P. Soler, V.C. Ruiz, Epidemiology and risk factors of cerebral ischemia and ischemic heart diseases: similarities and differences, Curr. Cardiol. Rev. 6 (3) (2010) 138–149.
[2] Papaverine A2 – Aronson, J.K, Meyler's Side Effects of Drugs (Sixteenth Edition), Elsevier Oxford, 2016, pp. 471–472.
[3] G. Berg, K.-Å. Jönsson, M. Hammar, B. Norlander, Variable bioavailability of papaverine, Pharmacol. Toxicol. 62 (1988) 308–310.
[4] V. Rønnov-Jessen, A. tjernlund hepatotoxicity due to treatment with papaverine, New Engl. J. Med. 281 (1969) 1333–1335.
[5] E. Poncin, C. Silvain, G. Touchard, J. Barbier, M. Beauchant, Papaverine-induced chronic liver disease, Gastroenterology 90 (1986) 1051–1053.
[6] S.M. Pond, T.N. Tozer, First-Pass elimination basic concepts and clinical consequences, Clin. Pharmacokinet. 9 (1984) 1–25.
[7] J. Pelipenko, P. Kocbek, J. Kristl, Critical attributes of nanofibers: preparation, drug loading, and tissue regeneration, Int. J. Pharm. 484 (2015) 57–74.
[8] R. Rošic, P. Kocbek, J. Pelipenko, J. Kristl, S. Baumgartner, Nanofibers and their biomedical use, Acta Pharm. 295 (2013).
[9] A. Kazsoki, P. Szabó, R. Zelkó, Nano- és mikroszálas rendszerek gyógyászati alkalmazási lehetőségei, Acta Pharm. Hung. 86 (2016) 53–59.
[10] T.J. Sill, H.A. von Recum, Electrospinning: applications in drug delivery and tissue engineering, Biomaterials 29 (2008) 1989–2006.
[11] C.P. Barnes, S.A. Sell, E.D. Boland, D.G. Simpson, G.L. Bowlin, Nanofiber technology: designing the next generation of tissue engineering scaffolds, Adv. Drug Deliv. Rev. 59 (2007) 1413–1433.
[12] N. Bhardwaj, S.C. Kundu, Electrospinning: a fascinating fiber fabrication technique, Biotechnol. Adv. 28 (2010) 325–347.
[13] I. Sebe, P. Szabó, B. Kállai-Szabó, R. Zelkó, Incorporating small molecules or biologics into nanofibers for optimized drug release: a review, Int. J. Pharm. 494 (2015) 516–530.
[14] G. Verreck, I. Chun, J. Rosenblatt, J. Peeters, A.V. Dijck, J. Mensch, M. Noppe, M.E. Brewster, Incorporation of drugs in an amorphous state into electrospun nanofibers composed of a water-insoluble, nonbiodegradable polymer, J. Controlled Release 92 (2003) 349–360.
[15] M.E. Brewster, G. Verreck, I. Chun, J. Rosenblatt, J. Mensch, A. Van Dijck, M. Noppe, A. Ariën, M. Bruining, J. Peeters, The use of polymer-based electrospun nanofibers containing amorphous drug dispersions for the delivery of poorly water-soluble pharmaceuticals, Die Pharmazie – Int. J. Pharm. Sci. 59 (2004) 387–391.
[16] G.L. Amidon, H. Lennernäs, V.P. Shah, J.R. Crison, A theoretical basis for a biopharmaceutic drug classification: the correlation of in vitro drug product dissolution and in vivo bioavailability, Pharm. Res. 12 (1995) 413–420.
[17] P. Szabó, T.B. Daróczi, G. Tóth, R. Zelkó, In vitro and in silico investigation of electrospun terbinafine hydrochloride-loaded buccal nanofibrous sheets, J. Pharm. Biomed. Anal. 131 (2016) 156–159.
[18] B.J. Aungst, N.J. Rogers, Comparison of the effects of various transmucosal absorption promoters on buccal insulin delivery, Int. J. Pharm. 53 (1989) 227–235.
[19] I.A. Siegel, H.P. Gordon, Surfactant-induced increases of permeability of rat oral mucosa to non-electrolytes in vivo, Arch. Oral Biol. 30 (1985) 43–47.

DOI:10.14753/SE.2020.2446

[20] P. Chinna Reddy, K.S.C. Chaitanya, Y. Madhusudan Rao, A review on bioadhesive buccal drug delivery systems: current status of formulation and evaluation methods, DARU J. Pharm. Sci. 19 (2011) 385–403.
[21] V.F. Patel, F. Liu, M.B. Brown, Advances in oral transmucosal drug delivery, J. Controlled Release 153 (2011) 106–116.
[22] P. Mahajan, A. Kaur, G. Aggarwal, S.L. Harikumar, Mucoadhesive drug delivery system: a review, Int. J. Drug Dev. Res. 5 (2013) 11–20.
[23] S.D. Manohar, D.A. Sridhar, S.C. Mallikarjuna, Drug delivery from the oral cavity: a focus on mucoadhesive buccal drug delivery systems, PDA J. Pharm. Sci. Technol. 66 (2012) 466–500.
[24] D.A. Patel, M.R. Patel, K.R. Patel, N.M. Patel, Buccal mucosa as a route for systemic drug delivery: a review, Int. J. Drug Dev. Res. 4 (2) (2012) 99–116.
[25] R.R. Pawar, D.B. Raut, V.K. Karde, J.C. Wadikar, A.S. Jadhav, A.G. Chintale, Mucoadhesive buccal drug delivery system: a review, Res. J. Pharm. Technol. 6 (2013) 506–515.
[26] M.J. Rathbone, B.K. Drummond, I.G. Tucker, The oral cavity as a site for systemic drug delivery, Adv. Drug Deliv. Rev. 13 (1994) 1–22.
[27] E. Russo, F. Selmin, S. Baldassari, C.G.M. Gennari, G. Caviglioli, F. Cilurzo, P. Minghetti, B. Parodi, A focus on mucoadhesive polymers and their application in buccal dosage forms, J. Drug Deliv. Sci. Technol. 32 (Part B) (2016) 113–125.
[28] S. Punitha, Y. Girish, Polymers in mucoadhesive buccal drug delivery system – a review, Int. J. Res. Pharm. Sci. 1 (2010) 170–186.
[29] A. Sosnik, J. das Neves, B. Sarmento, Mucoadhesive polymers in the design of nano-drug delivery systems for administration by non-parenteral routes: a review, Prog. Polym. Sci. 39 (2014) 2030–2075.
[30] S.L. Shenoy, W.D. Bates, H.L. Frisch, G.E. Wnek, Role of chain entanglements on fiber formation during electrospinning of polymer solutions: good solvent, non-specific polymer–polymer interaction limit, Polymer 46 (2005) 3372–3384.
[31] C.J. Angammana, S.H. Jayaram, Analysis of the effects of solution conductivity on electrospinning process and fiber morphology, IEEE Trans. Ind. Appl. 47 (2011) 1109–1117.
[32] R.R. Klossner, H.A. Queen, A.J. Coughlin, W.E. Krause, Correlation of Chitosan's rheological properties and its ability to electrospin, Biomacromolecules 9 (2008) 2947–2953.
[33] O. Regev, S. Vandebril, E. Zussman, C. Clasen, The role of interfacial viscoelasticity in the stabilization of an electrospun jet, Polymer 51 (2010) 2611–2620.
[34] W.K. Son, J.H. Youk, T.S. Lee, W.H. Park, The effects of solution properties and polyelectrolyte on electrospinning of ultrafine poly(ethylene oxide) fibers, Polymer 45 (2004) 2959–2966.
[35] J.H. Yu, S.V. Fridrikh, G.C. Rutledge, The role of elasticity in the formation of electrospun fibers, Polymer 47 (2006) 4789–4797.
[36] J. Dredán, R. Zelkó, Z. Á. Dávid, I. Antal, Quantitative estimation of film forming polymer–plasticizer interactions by the Lorentz–Lorenz law, Int. J. Pharm. 310 (2006) 25–30.
[37] M. Gašperlin, L. Tušar, M. Tušar, J. Šmid-Korbar, J. Zupan, J. Kristl, Viscosity prediction of lipophilic semisolid emulsion systems by neural network modelling, Int. J. Pharm. 196 (2000) 37–50.
[38] P. Szabó, B. Kállai-Szabó, N. Kállai-Szabó, I. Sebe, R. Zelkó, Preparation of hydroxypropyl cellulose microfibers by high-speed rotary spinning and prediction of the fiber-forming properties of hydroxypropyl cellulose gels by texture analysis, Cellulose 21 (2014) 4419–4427.

DOI:10.14753/SE.2020.2446

Journal of Pharmaceutical and Biomedical Analysis 144 (2017) 62–67

Contents lists available at ScienceDirect

Journal of Pharmaceutical and Biomedical Analysis

journal homepage: www.elsevier.com/locate/jpba

Macro- and microstructural tracking of ageing-related changes of papaverine hydrochloride-loaded electrospun nanofibrous buccal sheets

Adrienn Kazsoki [a], Péter Szabó [a], Károly Süvegh [b], Tamás Vörös [c], Romána Zelkó [a,*]

[a] University Pharmacy Department of Pharmacy Administration, Semmelweis University,Hőgyes Endre St. 7-9, H-1092 Budapest, Hungary
[b] Laboratory of Nuclear Chemistry, Eötvös Loránd University/HAS Chemical Research Center, P.O. Box 32, H-1518 Budapest, Hungary
[c] Doctoral School of Chemistry, Eötvös Loránd University, Pázmány Péter Prom. 1/A, H-1117 Budapest, Hungary

ARTICLE INFO

Article history:
Received 21 April 2017
Received in revised form 15 May 2017
Accepted 17 May 2017
Available online 27 May 2017

Keywords:
Papaverine-hydrochloride
Nanofibrous system
Accelerated stability
Physical ageing
Recrystallization
Ortho-positronium lifetime distribution

ABSTRACT

Electrospun papaverine hydrochloride-loaded nanofibrous sheets consist of hydroxypropyl cellulose/poly(vinyl alcohol) composite were prepared for buccal administration for cerebral ischemia. The nanofibrous drug delivery system was subjected to accelerated stability test for four weeks in order to scrutinize the solid state changes relating to the stress induced (40 ± 2 °C/75 ± 5% relative humidity) physical ageing. Micro- and macrostructural alterations were detected using scanning electron microscopy (SEM), Raman spectroscopy, Fourier transform infrared spectroscopy (FTIR) and positron annihilation lifetime spectroscopy (PALS). Significant changes were revealed at both supramolecular and macroscopic levels. Microscopic morphology uncovered major morphological transitions. Subtle variations of Raman and FTIR spectra indicated that the local chemical environment of papaverine was altered suggesting a partial phase transition of the active. Discrete o-Ps lifetimes and lifetime-distributions unveiled a two-step ageing process of the drug carrier. In addition to the tracking of the glassy-to-rubbery transition of the fiber forming polymers, the Raman spectroscopy enabled monitoring the kinetics of the phase transition observed.

1. Introduction

The opium alkaloid papaverine exerts a non-specific direct relaxant effect on smooth muscles, including the dilatation of blood vessels [1]. These pharmacodynamic properties make it a potential candidate for the treatment of cerebral ischaemia, but its unpleasant physicochemical and biopharmaceutical properties (such as slight water solubility, poor peroral bioavailability, high pharmacokinetic intra- and interindividual variability) restrict the *per os* administration [2,3]. These unfavourable features can be addressed with the combination of a nanofibrous and a buccal formulation. The former targets the solubility related issues, whilst the latter aims at the concerns associated with first pass metabolism and the consequential oral bioavailability. The rapid onset of effect and the reduced inter-and intraindividual varieties are also representing the favourable expectations of this formulation [4,5].

In our previous study, hydroxypropyl cellulose (HPC)- and polyvinyl alcohol (PVA) based papaverine hydrochloride loaded nanofibrous sheets were prepared for buccal application. During the preformulation study the ratio of the two polymer was varied (HPC:PVA = 5:5, 6:4, 7:3, 8:2, 9:1) and the total polymer concentration was kept constantly at 15% (w/w). HPC:PVA 6:4 composite mass ratio resulted the best fiber forming characteristics [6], so in the following, only this sample ratio was examined. Fourier transform infrared (FTIR) measurements suggested that the drug went through a solid state phase transition (presumably crystalline-amorphous transition) as a result of the electrospinning process. Although, amorphous form represent an effective means of dissolution enhancement, the thermodynamically metastable nature of such systems is a real headache for researchers [7]. High enthalpy of amorphous materials is considered as the main reason for spontaneous transition into a lower enthalpy correspondent crystalline form. Such transitions can be efficiently tracked by volume- and enthalpy relaxation measurements [8,9]. The amorphous polymers might undergo physical ageing, which can be accompanied with

Abbreviations: FTIR spectroscopy, Fourier transform infrared spectroscopy; HPC, hydroxypropyl cellulose; o-Ps, ortho-positronium; PVA, poly(vinyl alcohol); PALS, positron annihilation lifetime spectroscopy; SEM, scanning electronmicroscopy.

* Corresponding author.
E-mail address: zelko.romana@pharma.semmelweis-univ.hu (R. Zelkó).

http://dx.doi.org/10.1016/j.jpba.2017.05.035
0731-7085/

DOI:10.14753/SE.2020.2446

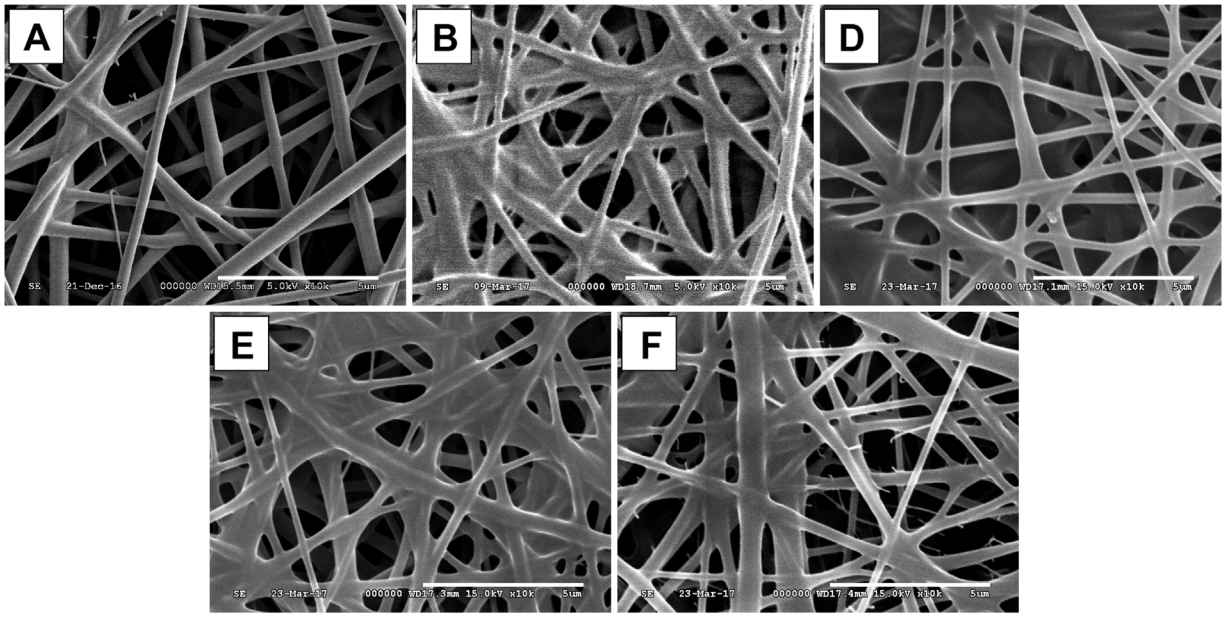

Fig. 1. SEM morphology of the freshly prepared (A) and the stored samples (week 1(B), week 2 (C), week 3 (D), week 4 (E)).

supramolecular changes in the polymers. The moisture- and CO_2 absorption from the surrounding air is one of the possible explanations for this phenomenon [10,11]. It has been well documented that solid dispersions possess higher physical stability than that of the raw amorphous material itself. The possibilities for the formation of drug-polymer interactions (e.g hydrogen-bond formation) decrease the recrystallization tendency of amorphous actives [12].

The supramolecular structure and the solid state characteristics of a polymeric drug delivery system influence the drug release characteristics, which have a major impact on peroral bioavailability. The monitoring of the solid state stability and the supramolecular changes of the amorphous drug loaded polymer-based nanofibrous system is of special interest, since these are crucial factors from the point of long term stability [13].

The different types of solid state characterization methods can be classified in three groups: imaging techniques (e.g. scanning electron microscopy (SEM) and atomic force microscopy (AFM)), macrostructural (e.g. FTIR spectroscopy, Raman spectroscopy, differential scanning calorimetry (DSC) and power X-ray diffraction (PXRD)) and microstructural (e.g. positron lifetime spectroscopy (PALS), solid-state nuclear magnetic resonance (ssNMR)) characterization methods [13]. The ssNMR is very sensitive to molecular conformation in solid-state systems, but with this technique the free volumes remain invisible [14–18]. PALS is a sensitive method to determine size distribution of free volume holes through *ortho*-positronium (o-Ps) lifetime distributions, which is in strong correlation with the physical ageing of the polymers [10,19–21].

The aim of the present study was to monitor the supramolecular changes of the papaverine-HCl-loaded hydroxypropyl cellulose-poly(vinyl alcohol) nanofibrous system, through positronium lifetime distribution and tracking the physical stability of the delivery system with FTIR and Raman spectroscopy in the course of the four weeks long storage under stress condition.

2. Materials and methods

2.1. Materials

For the fiber forming process hydroxypropyl cellulose (Klucel EXF Pharm, Ashland, USA; Mw ~80000; the moles of substitution = 3.8), poly(vinyl alcohol) (18–88 Ph. Eur., Merck, Darmstadt, Germany) and polysorbate 20 (Ph. Eur., Molar chemicals, Hungary) were used. The active pharmaceutical ingredient was papaverine hydrochloride (Ph. Eur.).

2.2. Fiber preparation

Papaverine-HCl containing gel of 15% (w/w) total polymer concentration and HPC: PVA 6:4 mass ratio, was prepared by the addition of the necessary amount of HPC, PVA and 30 mg/g papaverine-HCl aqueous stock solution (according to [6]) applying gentle heat and magnetic stirring. The gel was then transferred into a plastic syringe equipped with a metallic needle (1.2 mm inner diameter). In our previously published paper the effect of the applied voltage and the needle to collector distance on the fibers morphology was studied. The applied voltage was examined in three levels: 20, 25 and 30 kV. The needle to collector distance was 5, 10 and 15 cm. The best fiber characteristics were achieved in case of 15 cm distance and better fiber characteristic was found with the increasing voltage.

So that, for the electrospinning process the voltage was set to 30 kV. The distance between the spinneret and the collector was 15 cm. The fibers were collected on aluminum foil in the course of the 45 min spinning duration.

2.3. Storage conditions

The accelerated stability test was done based on the standard protocol to follow the quality changes of the product and determine recommended storage conditions. The nanofibrous samples were stored in closed containers at $40 \pm 2\,^{\circ}C$ and $75 \pm 5\%$ relative humidity for four weeks.

2.4. Scanning electron microscopic analysis (SEM)

The morphology changes of the nanofibrous systems were followed with scanning electron microscope (SEM). SEM studies were performed by a Hitachi S-4300 instrument equipped with a Bruker energy dispersive X-ray spectroscope (Hitachi Science Systems, Ltd., Japan). The surfaces of samples were covered by a sputtered

DOI:10.14753/SE.2020.2446

gold conductive layer, and 5–10 kV accelerating voltage was used for taking high resolution electron micrographs.

2.5. Fourier transform infrared (FTIR) spectroscopy

Physicochemical properties of the fibers were examined using Jasco FT/IR-4200 spectrophotometer which was equipped with Jasco ATR PRO470-H single reflection accessory. The measurements were performed in absorbance mode and spectra were collected over a wavenumber range of 4000 and 1800 cm^{-1}. 100 scans were performed at a resolution of 2 cm^{-1}. The measurements were evaluated with the FTIR software (Spectra Manager-II, Jasco).

2.6. Raman spectroscopy

The MI-Raman spectra were recorded by a FRA 106 extension of a Bruker IFS 55 Fourier-transform infrared (FT-IR) spectrometer using a 100 mW 1064 nm Nd:YAG laser and a liquid nitrogen cooled Ge detector. The MI-Raman spectra were recorded at 2 cm^{-1} instrumental resolution and 512 scans were accumulated.

2.7. Positron annihilation lifetime spectroscopy (PALS)

For positron lifetime measurements, a positron source made of carrier-free ^{22}NaCl was used. Its activity was around 10^6 Bq and the active material was sealed between two very thin Kapton® foils. The source was put between two layers of nanofibrous sheets which were peeled off from the aluminum foil. Lifetime spectra were measured with a fast–fast coincidence system based on BaF_2/XP2020Q detectors and Ortec® electronics. Three parallel spectra were measured from each sample.

Firstly, the spectra were evaluated by the RESOLUTION computer code. Three lifetime components were found in all samples, where the longest component was identified as o-Ps lifetime. The MELT code was used to extract lifetime distributions from the spectra [22,23]. These latter evaluations were used to characterize the size distribution of the free-volume holes in the samples throughout the o-Ps lifetime [10].

3. Results and discussion

3.1. Morphology study of the samples

SEM images are summarized in Fig. 1 indicating a time dependent progression in the morphology. However, the basic fibrous structure was retained by the end of the stability test, significant structural changes can be observed. Stress induced deterioration of fibrous structure can be divided in two major steps. At first, a fiber-film like transition was commenced, which was manifested in the merging and broadening of individual fibers. After all, fragmentation took place, i.e. tenuous initiative scraps were formed. Furthermore, signs of surface crystallization of the active could also be noticed.

Previous works suggested that one of the possible reasons for the film formation could be the glassy-to-rubbery transition of the polymeric carriers. This alteration could be the consequence of the plasticization effect of the polysorbate 20 and also the elevated temperature during the storage. The moisture absorbed from the environment acts also as a plasticizer leading to significant decrease of the T_g of the fiber-forming polymers [10,24], but since the samples stored in airtight containers, the latter effect can be neglected.

3.2. FT-IR analysis

Fig. 2 shows the FTIR spectra of papaverine-HCl loaded nanofibrous sheets as a function of storage time. In the case of the fresh fibrous sample, the lack of high intensity characteristic peak of papaverine-HCl around at 2500 cm^{-1} is obvious. The broadening and merging of the spectrum could refer to the physical state related changes of the active, conceivably to a crystalline-amorphous transition.

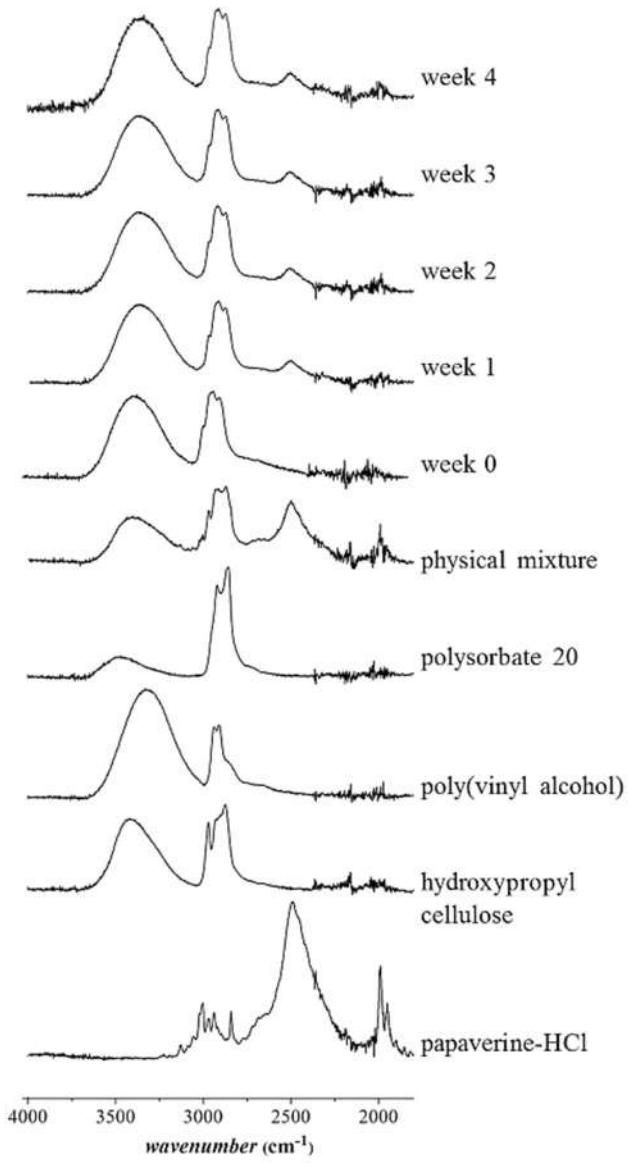

Fig. 2. FTIR spectra of the components and the stored samples.

After one week of storage, a peak appeared at 2500 cm^{-1} related possibly to the active which was persistent throughout the remaining sampling points. It should be noted that the relative peak intensity was almost constant in all cases. It can be inferred that the latter phenomenon is the consequence of the recrystallization of the active material. This is in accordance with the observations of the morphological evaluation.

Elevated temperature and exposition to high humidity have a substantial impact on molecular mobility and secondary intermolecular interactions, notably increasing the former and decreasing the latter. These changes can make a drug delivery system more prone to solid state modifications, and the escalation of the molecular mobility sharply boosts the chances that molecules or clusters of amorphous actives start to form crystals. In our preliminary study, we demonstrated that there only weak

DOI:10.14753/SE.2020.2446

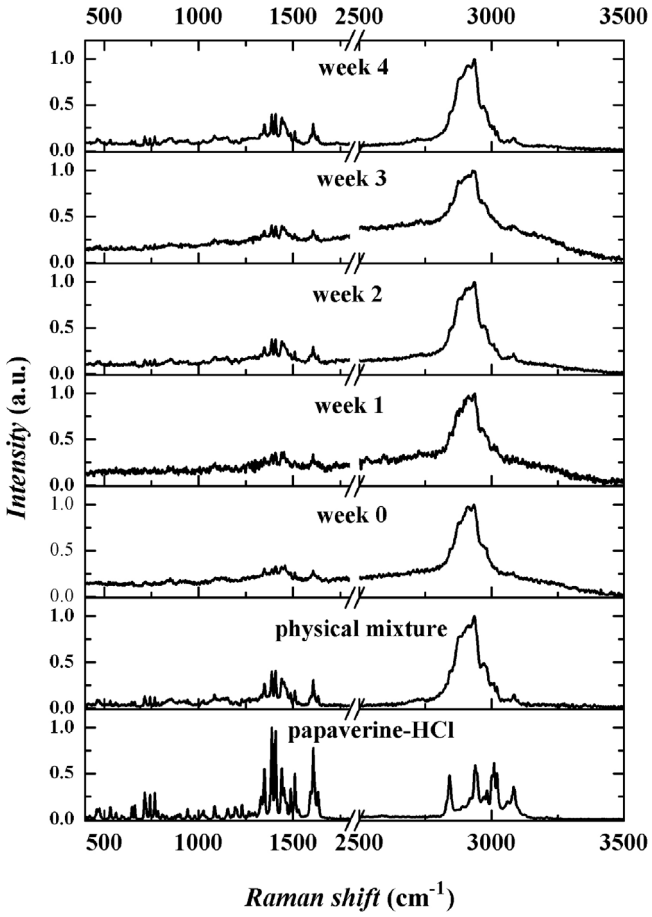

Fig. 3. Raman spectra of the samples between 400 and 3500 cm^{-1}.

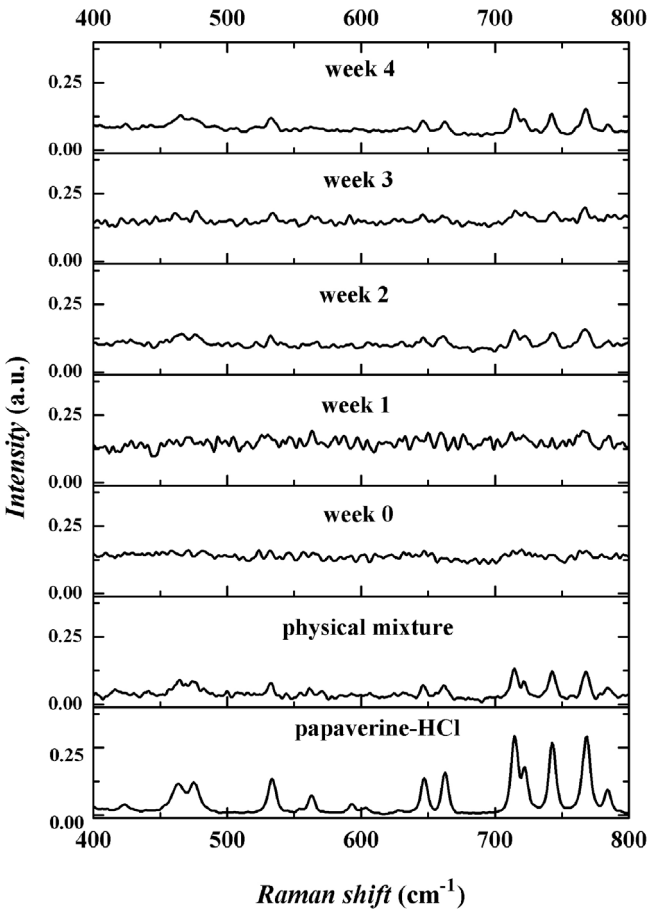

Fig. 4. Raman spectra of the samples between 400 and 800 cm^{-1}.

secondary inter- and intramolecular interactions existed between the polymers, which also confirm that even a subtle elevation of temperature can be sufficient to overcome these attractive forces. Although, the presence of weak secondary interactions is considered beneficial from the point of fiber formation, because optimum molecular entanglement can be achieved, but, on the other hand, this can be a drawback for the solid state stability, since these interactions are not strong enough to keep the active in an amorphous state.

3.3. Raman spectroscopy

Vibrational characterization of the samples is represented in Figs. 3 and 4. As seen in Fig. 3, characteristic peaks of the active are well recognizable in the spectrum of the physical mixture suggesting the active being in a crystalline state. Considering the spectrum of fresh samples, significant merging can be observed, but the spectra of the stored samples underwent a progressive evolution until a spectrum resembling the physical mixture was achieved, which refers to a time-dependent process. Significant peak shifts were only observed in the CH-stretching vibrations of papaverine-HCl around 2938 cm^{-1}. The observed peak shifts, were as follows: week 0: −4.9 cm^{-1}, week 1: −1.9 cm^{-1}, week 2: −2.9 cm^{-1}, week 3: −2.9 cm^{-1} and week 4: −2.9 cm^{-1}. Taking a closer look at the region of 50–200 cm^{-1} assigned as lattice vibration, a time-dependent process emerges strongly relating to the solid state changes of the drug loaded polymeric systems. As represented in Fig. 5**A** and **B** the shape and the integrated area of the designated region increasingly approximate the characteristics of the physical mixture, suggesting that recrystallization of papaverine took place as a result of the stress conditions. Similarly, characteristic peaks in the region between 700 and 780 cm^{-1} attributed to the benzene and isoquinoline ring out of plane deformation and the C—C—C bond (connecting the two ring systems) deformation merged into the baseline and then re-separation of these peaks was noticeable. This was also noticeable in the region between 430 and 700 cm^{-1}, where peaks of the wagging vibrations of methoxy moieties (463 cm^{-1} and 473 cm^{-1}), out of plane deformations of the rings (533 cm^{-1}, 563 cm^{-1}), in plane and out of pane deformations of the rings and twisting vibrations of methoxy moieties (647 and 662 cm^{-1}, respectively) can be found (Fig. 4) [25]. This phenomenon can be explained by the limited conformational and molecular mobility of the moieties and the active in a crystalline form, which led to sharp characteristics peak. In an amorphous state, the energy is distributed between the numerous allowed conformations resulting the merging and broadening of the peaks.

3.4. PALS measurements

Fig. 6 illustrates the average discrete o-Ps lifetimes as a function of storage time indicating a two-step process in supramolecular restructuring. At first, one week exposition to stress condition resulted in the increase of the o-Ps lifetime value and, consequently, larger free volume holes. This was followed by a sharp drop and then a successive marked rise of o-Ps lifetime values. Distributions of o-Ps lifetimes also confirm the two-step ageing process, suggesting multiple supramolecular restructuring throughout the stability test (Fig. 7). The first storage week induced a pronounced change in the distribution in terms of the width as well in the average values.

DOI:10.14753/SE.2020.2446

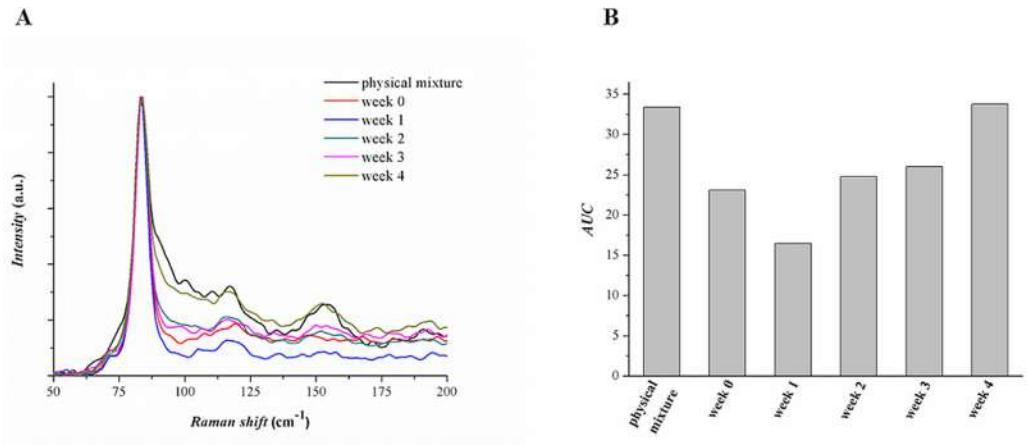

Fig. 5. The shape (**A**) and the integrated area [26] (**B**) of the region between 50 and 200 cm^{-1}.

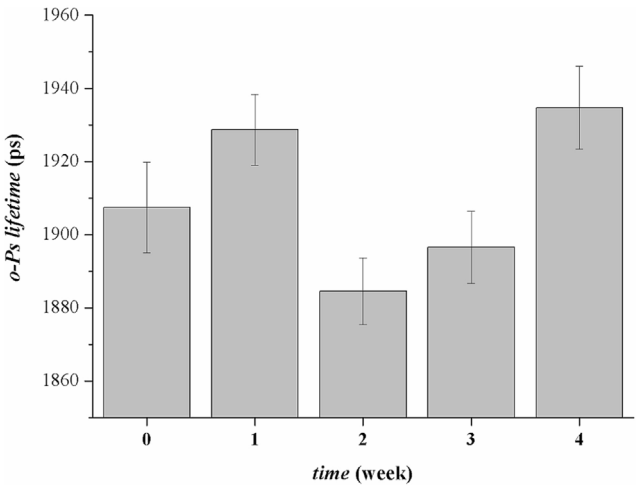

Fig. 6. Average discrete o-Ps lifetimes of the nanofibers as a function of storage time.

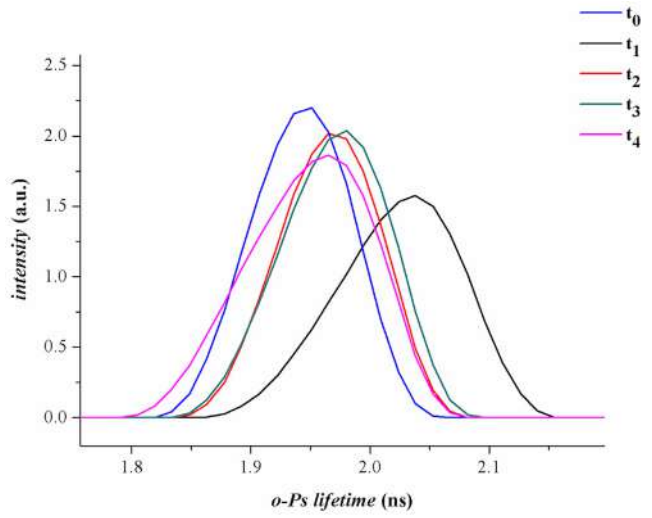

Fig. 7. The o-Ps lifetime distributions in papaverine-HCl-loaded nanofibrous system after 0, 1, 2, 3, 4 weeks of storage (t_0, t_1, t_2, t_3, t_4).

This process was pursued by a second rearrangement, as indicated by the backward shift and narrowing of the distributions.

These observations can be traced back to several reasons including the phase transition and redistribution of the active ingredient, the supramolecular rearrangement of polymeric chains and final fragmentation of the fibers. After 1 week, the elevated temperature during the storage increased the molecular mobility of polymer chains thus destroying the original polymeric structure and creating new vacancies (t_1). Similarly, the reduction in the intensity of the lattice vibrations shown in Fig. 5**b** also refers to the enhanced molecular mobility of the active, which leads to enthalpy relaxation by recrystallization.

However, later on (after 2 weeks), a new structure was formed, possibly involving hydrogen bonds between the polymeric chains. During storage, the peak at 1.951 ns, indicative of o-Ps atoms situated in holes between polymeric chains, shifted towards longer lifetimes (o-Ps = 2.038 ns after 1 week), demonstrating the relaxation of the structure and the increase of free volume holes in size. This was most probably due to the storage under stress conditions resulting in the glassy-to-rubbery transition of the polymer fibers. This transition can be tracked clearly on the SEM photos.

A longer exposure of fibers to elevated temperature leads to different structures in samples stored for 2–4 weeks. The temperature driven mobility increase does not possess enough strength to overpower the binding force of hydrogen bonds between the chains. The result is an intermediate structure: the size distribution of free volume holes widens but does not shift towards larger holes (t_1-t_3). The widening of the distribution after 4 weeks of storage suggests that a large fraction of "crosslinks" was ruined by the enhanced molecular mobility and the crystallization of the papaverine caused inhomogeneity in the free volume size distributions.

4. Conclusions

The combination of non-invasive spectroscopic methods – FTIR, Raman spectroscopy and PALS –, enable sensitive means for the detection and the prediction of possible supramolecular interactions initiated by stress conditions during storage. The applied experimental setup represented a useful approach to track how the ageing of the polymeric carrier reflected in the solid-state changes of the active. The latter could be of impact from the point of the physical stability of polymer-based drug delivery systems.

Acknowledgement

The authors are grateful to Tünde Rente for the Scanning Electron Microscopic images.

DOI:10.14753/SE.2020.2446

References

[1] Papaverine A2 – Aronson, J.K, Meyler's Side Effects of Drugs, sixteenth ed., Elsevier, Oxford, 2016.
[2] E.R. Garrett, H. Roseboom, J.R. Green, W. Schuermann, Pharmacokinetics of papaverine hydrochloride and the biopharmaceutics of its oral dosage forms, Int. J. Clin. Pharmacol. Biopharm. 16 (1978) 193–208.
[3] G. Berg, K.-Å. Jönsson, M. Hammar, B. Norlander, Variable bioavailability of papaverine, Pharmacol. Toxicol. 62 (1988) 308–310.
[4] V.F. Patel, F. Liu, M.B. Brown, Advances in oral transmucosal drug delivery, J. Control. Release 153 (2011) 106–116.
[5] D.A. Patel, M.R. Patel, K.R. Patel, N.M. Patel, Buccal mucosa as a route for systemic drug delivery: a review, Int. J. Drug Dev. Res. 4 (2012) 99–116.
[6] A. Kazsoki, P. Szabó, R. Zelkó, Prediction of the hydroxypropyl cellulose—poly(vinyl alcohol) ratio in aqueous solution containing papaverine hydrochloride in terms of drug loaded electrospun fiber formation, J. Pharm. Biomed. Anal. 138 (2017) 357–362.
[7] N. Shahrin, Solubility and dissolution of drug product: a review, Int. J. Pharm. Life Sci. 2 (2013) 33–41.
[8] J.M.G. Cowie, R. Ferguson, Physical ageing of poly(methyl methacrylate) from enthalpy relaxation measurements, Polymers 34 (1993) 2135–2141.
[9] B.C. Hancock, G. Zografi, Characteristics and significance of the amorphous state in pharmaceutical systems, J. Pharm. Sci. 86 (1) (1997) 1–12.
[10] K. Süvegh, R. Zelkó, Physical aging of poly(vinylpyrrolidone) under different humidity conditions, Macromolecules 35 (3) (2002) 795–800.
[11] S. Yoshioka, Y. Aso, Correlations between molecular mobility and chemical stability during storage of amorphous pharmaceuticals, J. Pharm. Sci. 96 (2007) 960–981.
[12] A. Lust, C.J. Strachan, P. Veski, J. Aaltonen, J. Heinämäki, J. Yliruusi, K. Kogermann, Amorphous solid dispersions of piroxicam and Soluplus®: Qualitative and quantitative analysis of piroxicam recrystallization during storage, Int. J. Pharm. 486 (2015) 306–314.
[13] P. Szabó, R. Zelkó, I. Antal, The role of solid state characterization in predicting stability of solid dosage forms, Curr. Pharm. Des. 22 (2016) 5019–5028.
[14] A. Ito, T. Watanabe, S. Yada, T. Hamaura, H. Nakagami, K. Higashi, K. Moribe, K. Yamamoto, Prediction of recrystallization behavior of troglitazone/polyvinylpyrrolidone solid dispersion by solid-state NMR, Int. J. Pharm. 383 (2010) 18–23.
[15] T.N. Pham, S.A. Watson, A.J. Edwards, M. Chavda, J.S. Clawson, M. Strohmeier, F.G. Vogt, Analysis of amorphous solid dispersions using 2D solid-state NMR and 1H T1 relaxation measurements, Mol. Pharm. 7 (2010) 1667–1691.
[16] D.M. Schachter, J. Xiong, G.C. Tirol, Solid state NMR perspective of drug–polymer solid solutions: a model system based on poly(ethylene oxide), Int. J. Pharm. 281 (2004) 89–101.
[17] B. Brettmann, E. Bell, A. Myerson, B. Trout, Solid-state NMR characterization of high-loading solid solutions of API and excipients formed by electrospinning, J. Pharm. Sci. 101 (2012) 1538–1545.
[18] B.K. Brettmann, A.S. Myerson, B.L. Trout, Solid-state nuclear magnetic resonance study of the physical stability of electrospun drug and polymer solid solutions, J. Pharm. Sci. 101 (2012) 2185–2193.
[19] V. Szente, K. Süvegh, T. Marek, R. Zelkó, Prediction of the stability of polymeric matrix tablets containing famotidine from the positron annihilation lifetime distributions of their physical mixtures, J. Pharm. Biomed. Anal. 49 (2009) 711–714.
[20] B. Szabó, K. Süvegh, R. Zelkó, Effect of storage on microstructural changes of Carbopol polymers tracked by the combination of positron annihilation lifetime spectroscopy and FT-IR spectroscopy, Int. J. Pharm. 416 (2011) 160–163.
[21] D. Kiss, K. Süvegh, R. Zelkó, The effect of storage and active ingredient properties on the drug release profile of poly(ethylene oxide) matrix tablets, Carbohydr. Polym. 74 (2008) 930–933.
[22] P. Kirkegaard, M. Eldrup, O.E. Mogensen, N.J. Pedersen, Program system for analysing positron lifetime spectra and angular correlation curves, Comput. Phys. Commun. 23 (1981) 307–335.
[23] A. Shukla, M. Peter, L. Hoffmann, Analysis of positron lifetime spectra using quantified maximum entropy and a general linear filter, Nucl. Instrum. Methods Phys. Res. A 335 (1993) 310–317.
[24] M.A. Repka, T.G. Gerding, S.L. Repka, J.W. McGinity, Influence of plasticizers and drugs on the physical-mechanical properties of hydroxypropylcellulose films prepared by hot melt extrusion, Drug. Dev. Ind. Pharm. 25 (1999) 625–633.
[25] N. Leopold, J.R. Baena, M. Bolboacă, O. Cozar, W. Kiefer, B. Lendl, Raman, IR, and surface-enhanced Raman spectroscopy of papaverine: an automated setup for in situ synthesis of the silver substrate and recording of the SER spectra, Vib. Spectrosc. 36 (2004) 47–55.
[26] E. Poncin, C. Silvain, G. Touchard, J. Barbier, M. Beauchant, Papaverine-induced chronic liver disease, Gastroenterology 90 (1986) 1051–1053.

European Journal of Pharmaceutical Sciences 120 (2018) 9–12
DOI:10.14753/SE.2020.2446

Contents lists available at ScienceDirect

European Journal of Pharmaceutical Sciences

journal homepage: www.elsevier.com/locate/ejps

Microstructural characterization of papaverine-loaded HPC/PVA gels, films and nanofibers

Adrienn Kazsoki[a], Attila Domján[b], Károly Süvegh[c], Romána Zelkó[a,*]

[a] University Pharmacy Department of Pharmacy Administration, Semmelweis University, Hőgyes Endre utca 7-9, H-1092 Budapest, Hungary
[b] Institute of Organic Chemistry, Research Centre for Natural Sciences, Hungarian Academy of Sciences, Magyar tudósok körútja 2, H-1117 Budapest, Hungary
[c] Laboratory of Nuclear Chemistry, Eötvös Loránd University/HAS Chemical Research Center, P.O. Box 32, H-1518 Budapest 112, Hungary

ARTICLE INFO

Keywords:
Hydroxypropyl cellulose
Poly(vinyl alcohol)
Papaverine hydrochloride
Positron Annihilation Lifetime Spectroscopy (PALS)
Solid-state magic angle spinning (MAS)
Gel-film transition
Electrospun nanofibers

ABSTRACT

Papaverine hydrochloride loaded gels, films and electrospun fibers were prepared for buccal drug delivery with the aim of improving the oral bioavailability of the crystalline drug, which can be achieved by the increased solubility and by the circumvention of the intensive first pass metabolism. The water soluble hydroxypropyl cellulose (HPC) was chosen as a mucoadhesive polymer. In order to improve the electrospinnability of HPC, the similarly mucoadhesive poly(vinyl alcohol) (PVA) was used. Since the drying of gels is of decisive role in either the formation of drug-loaded cast films or electrospun fibers, a real time ortho-positronium (o-Ps) tracking of gels was applied in order to obtain information about the supramolecular changes of the drying-induced gel-film transition. An anomalous increase of o-Ps lifetime value in the gel-film transition region was observed which refers to the remaining intramolecularly bound water in the drug-loaded polymeric gel matrix. The latter could provide information about the characteristics of polymer-water interactions in the phase transition, consequently the storage stability of the formulated solid system.

1. Introduction

The vast majority of newly developed drugs are poorly water soluble. If the drug is a part of dispersion system, it may exist as an amorphous solid in polymeric system which enables improved solubility and dissolution rate compared to the crystalline form (Horvat et al., 2018). Solubility and dissolution rate enhancements are generally accepted as a useful ways for the formulation of pharmaceuticals involved in biopharmaceutical drug classification system (BCS) class II, where oral bioavailability is confined by the limited aqueous solubility (Nagy et al., 2012; Nagy et al., 2010).

During the past decade, several studies have been dealing with this issue, most of them using solid dispersions. Recently, an increasing interest has been paid to polymeric micro- and nanofibers as potential drug delivery systems owing to their high specific surface area, high porosity, and the ability to incorporate pharmaceuticals in amorphous state (Szabó et al., 2015).

Gel polymers including various polysaccharides have been extensively studied for the development of drug delivery systems. Due to their properties, such as bioavailability, biodegradability, stability, availability, renewability, low toxicity, they can be applied as independent solid matrices in different forms, e.g., micro- or nanofibers. Their functionality-related properties are affected by the polymer structure, the plasticizer concentration, the solvent and some other factors related to dissolution, permeability and diffusion properties of the film. Gels are formed by crosslinking polymer chains through physical, ionic or covalent interactions and are well known for their ability to absorb water. In the course of the formulation of solid dosage forms, drying of the gels is necessary to eliminate excess solvent from the gel structure. As the solvent is removed from the polymer solution, the structure of the polymer may change dramatically, for example, from randomly dissolved polycrystalline structures or from colloidal dispersion to continuous film (Davidovich-Pinhas and Bianco-Peled, 2010; Sriamornsak and Kennedy, 2008; Szabó et al., 2012).

The main factors determining the drug release properties of a dosage form based on a hydrophilic polymer are the swellability and erosibility of the polymeric matrix, as well as, the diffusibility of drug molecules in the matrix (Borgquist et al., 2006). Swellability and the erosibility of the matrix depend on the hydration tendency of the polymer and the interaction between the polymer and the embedded drug and the water molecules. In the case of amorphous or partly amorphous drugs and polymers, this latter property can strongly be

Abbreviations: HPC, hydroxypropyl cellulose; PVA, poly(vinyl alcohol); PALS, Positron Annihilation Lifetime Spectroscopy; MAS, solid-state magic angle spinning; NMR, nuclear magnetic resonance; FT-IR, Fourier Transform Infrared Spectroscopy

* Corresponding author.
E-mail address: zelko.romana@pharma.semmelweis-univ.hu (R. Zelkó).

https://doi.org/10.1016/j.ejps.2018.06.020
Received 24 February 2018; Received in revised form 19 June 2018; Accepted 19 June 2018
Available online 20 June 2018

influenced by a phenomenon known as physical ageing. As the constituents of the dosage form are usually not in equilibrium below their glass transition temperature, usually undergo spontaneous, although slow, transformations towards low-energy equilibrium states. The natural humidity of air initiates these processes and the plasticization effects of water, CO_2 or other excipients are enough to change the crystallinity of the polymer and the embedded drug (Süvegh and Zelkó, 2002; Szente et al., 2011).

The authors developed a real time method that can provide molecular level understanding of gel-film transition of polymers based on the o-Ps lifetime changes (Szabó et al., 2012). The latter enabled the exact detection of the transition from a polymer-in-water system to a water-in-polymer system and the determination of the end point of the process of film forming. In the present study the same real time o-Ps tracking of polymer gels was applied in order to obtain information about the supramolecular changes of the gel-film or gel-fiber transition in the course of drying. The latter could provide information about the characteristics of polymer-water interactions in the phase transition, which has a decisive impact on the storage stability of the formulated solid system.

The aim of this work was to show and study the effects of different formulation processes (film and fiber forming) on the morphology of papaverine in gel matrix. To gain a detailed picture of these effects, we have combined several structural characterization methods for the investigation of fibers and films.

2. Materials and methods

2.1. Materials

For the fiber forming process, hydroxypropyl cellulose (Klucel EXF Pharm, Ashland, USA; Mw ~80,000; the moles of substitution = 3.8), poly(vinyl alcohol) (18-88 Ph. Eur., Merck, Darmstadt, Germany) and polysorbate 20 (Ph. Eur., Molar chemicals, Hungary) were used. The active pharmaceutical ingredient was papaverine hydrochloride (Ph. Eur.).

2.2. Papaverine-HCl containing gel and fiber preparation

Papaverine-HCl containing gels of 15% (w/w) total polymer concentration and HPC: PVA 5:5, 6:4, 7:3, 8:2 mass ratios, were prepared by the addition of the necessary amounts of HPC, PVA and 30 mg/g papaverine-HCl aqueous stock solution (according to (Kazsoki et al., 2017a; Kazsoki et al., 2017b)) applying gentle heat and magnetic stirring. The freshly prepared gels were then transferred into a plastic syringe equipped with a metallic needle (1.2 mm inner diameter). In our previously published paper the effect of the applied voltage and the needle to collector distance on the fibers morphology was studied. The applied voltage was examined in three levels: 20, 25 and 30 kV. The needle to collector distance was 5, 10 and 15 cm. The best fiber characteristics were achieved in case of 15 cm distance and 30 kV voltage (Kazsoki et al., 2017b). The fibers were collected on aluminum foil in the course of the 45 minute spinning duration.

2.3. o-Ps lifetime measurement setup and design

For positron lifetime measurements, a positron source made of carrier-free ^{22}NaCl was used. Its activity was around 10^5 Bq and the active material was sealed between two very thin kapton foils. Lifetime spectra were measured with a fast-fast coincidence system (MacKenzie, 1983) based on BaF_2/XP2020Q detectors and Ortec electronics. Every spectrum was recorded in 4096 channels of an analyzer card and each contained 10^5 coincidence events. The number of coincidence counts was much lower than normally. This was inevitable because of the requirements of the continuous real-time measurement. However, since we needed only the o Ps lifetime as observable quantity, the low count number has not increased the uncertainty of measurements beyond reasonable levels.

The detectors were arranged vertically in this experimental setup, which was previously published (Szabó et al., 2012). The upper detector was, at beginning of the measurement, over the surface of the polymer gel of 5 mm. An aluminum plate was placed on the lower detector. The positron source was placed on the plate and the gel-filled glass cylinder was put on the source. Although a great number of positrons were lost for the Al plate in this arrangement, the significant signal remained intact. As aluminum does not produce an o-Ps component, any signal in that certain lifetime range came from the gel. Although more than 50% of positrons annihilated in the aluminum plate and the foil covering the glass cylinder, o-Ps signals came exclusively from the gel. During the drying period (temperature: 22 ± 0.5 °C; relative humidity: 47 ± 3%) 12 parallel spectra were collected in every day. The fitting parameter (variance of the fit, chi square per degrees of freedom) is changing within 1.0 to 1.15 intervals in each parallel measurement. From the point of the comparison of samples these changes did not cause any artefact. All the lifetime spectra were evaluated individually by the RESOLUTION computer code (Kirkegaard et al., 1981).

2.4. Solid state magic nuclear magnetic resonance (NMR) measurement

Solid-state magic angle spinning (MAS) spectra of samples were recorded on a Varian NMR system operating at a ^{1}H frequency of 400 MHz (100 MHz for ^{13}C) with a Chemagnetics 4.0 mm narrow-bore double resonance T3 probe. The spinning rate of the rotor was 10 kHz in all cases. For the one-dimensional ^{13}C CP MAS (cross-polarization magic angle), 2000 transients were recorded with SPINAL-64 decoupling with a strength of 83 kHz and 1 ms of contact time. A recycle delay of 30 s was used for all experiments, which is 5 times larger than T_{1H} of the crystalline papaverine-HCl. The temperature of all the measurements was 20 °C. Adamantane was used as external chemical shift reference (38.55 and 29.50 ppm). The 90° pulse lengths were 3 μs for both the proton and the carbon channels for all the NMR experiments.

3. Results and discussion

Fig. 1 (blue line) illustrates the drying curve of the HPC:PVA gels of 6:4 ratio which was considered the best from the point of view of its spinning ability for the electrospinning process, and the corresponding o-Ps lifetime values as a function of drying time (black line). The comparison of the two curves is interesting, since the microstructural changes of the gel-film transition can be clearly tracked. The evaporation of the surface water content (linear phase of the drying curve) does not visibly affect o-Ps lifetime values (Fig. 1) and the corresponding free volumes of the polymer gel. The drying curve and the corresponding o-Ps lifetime values clearly illustrate that there is a shift between the loss of water and the consequent free volume decrease. The higher o-Ps lifetime values enable the sufficient mobility of the polymer chains to let the water diffuse out from the free volume holes. Most of the water evaporates in this linear part of the drying curve; meanwhile the o-Ps lifetime is almost constantly high. The evaporation of the remaining amount of water is much slower, that is in good agreement with the corresponding declining o-Ps lifetime values, and finally levels out to constant low value, which is characteristic to the polymer substance. The most important point of positronium lifetime data is this little delay they show compared to weight loss data. The latter indicates a slow rearrangement of molecules after losing the gross mass of water content. At this point, the polymer has already lost most of its water content and the swelling effect of water molecules should have already dropped dramatically. The polymer chains just undergo a transition process providing lower mobility of chains. After the transitional phase a polymeric film was formed containing residual water (equilibrium

DOI:10.14753/SE.2020.2446 European Journal of Pharmaceutical Sciences 122 (2018) 9–12

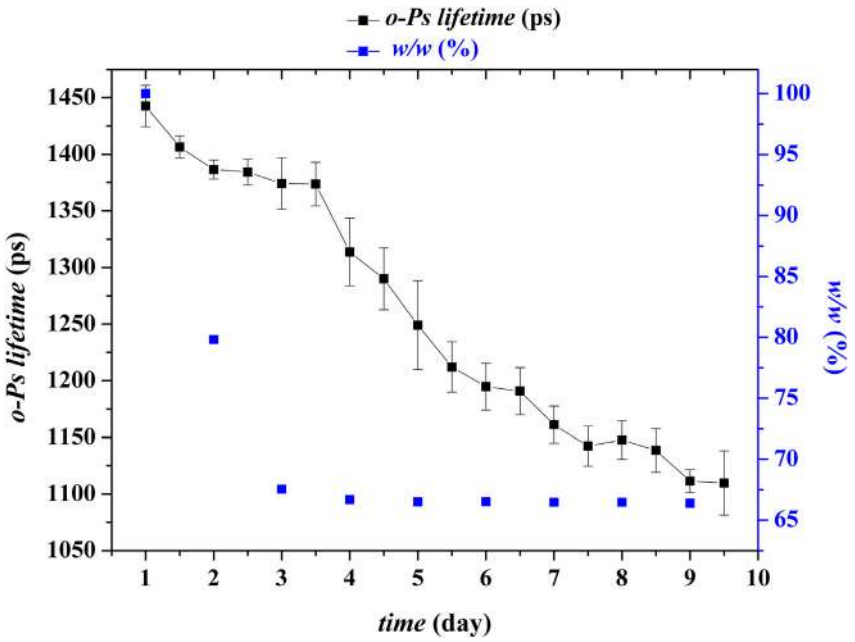

Fig. 1. Loss of weight and o-Ps lifetime values of HPC:PVA = 6:4 (m/m) gels as a function of drying time. (For interpretation of the references to colour in this figure, the reader is referred to the web version of this article.)

moisture content). The remaining water has a decisive impact on the water-induced amorphous-crystalline transition of the embedded papaverine hydrochloride in the course of storage of dried films and nanofibers, as well.

Note that this drying process, strictly speaking, characterizes only the slow film formation process. During electrospinning, the fiber formation takes place much more rapidly and the drying should be much faster. This is why the delayed structural change is so important. We discuss this below in details when we compare films, mixtures and fibers.

The occurrence of large scale structural changes during the film-formation process is supported by NMR-data. The polymer chains just undergo a transition process providing lower mobility of chains. Similar conformational rearrangement of polymer chains was found at low swelling rate by PALS and solid state NMR methods (Domján et al., 2012).

Fig. 2 represents the NMR-spectra of papaverine hydrochloride and that of the drug-loaded polymer film. In papaverine-containing films, papaverine is in a crystalline state, which is expected, as the secondary-bounded water molecules in the polymer composite stabilize the papaverine hydrochloride in a crystalline state forming a solid dispersion (which raises stability issues). Signals of papaverine are overlapped completely in the two spectra. Broadened signals of papaverine belonging to the amorphous phase are not present. However the intensity and the width of several signals are slightly different. These differences may indicate the formation of nanocrystalline morphology. Previous studies are also in good agreement with these results (Kazsoki et al., 2017b) where an amorphous-crystalline transition of papaverine hydrochloride was confirmed by various solid state characterization methods after a relatively short storage period of the drug-loaded nanofibers.

Please, note the scale difference here between the present NMR results and former FT-IR data (Kazsoki et al., 2017b) NMR spectroscopy reports the nanocrystals clearly, which formed in the drying process of films. On the other hand, exactly the same nanocrystals are below the detection limits of IR spectroscopy. So, IR data report amorphous state where NMR shows nanocrystals, thus the change of the morphology in the structure of papaverine is obvious. During the film-formation (or fiber-formation) process, its structure changed considerably. NMR and the positron lifetime date indicate this clearly. These changes might

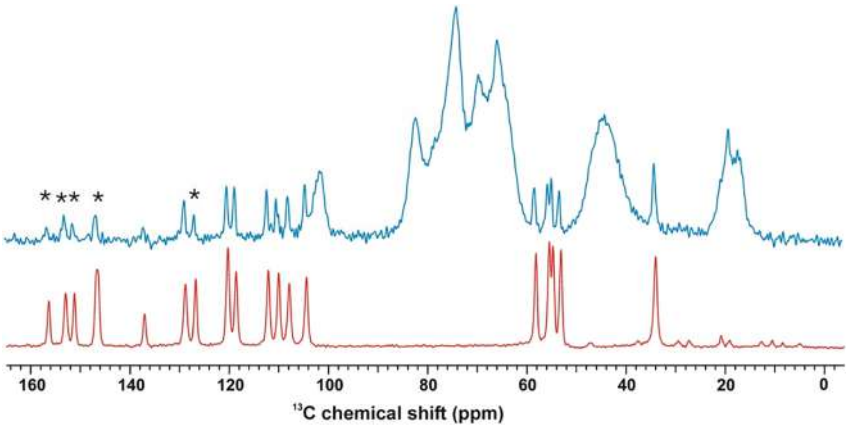

Fig. 2. Solid state ^{13}C CPMAS NMR spectra of papaverine hydrochloride (red) and drug-loaded film (blue). The most differing signals are noted with asterisks. (For interpretation of the references to colour in this figure legend, the reader is referred to the web version of this article.)

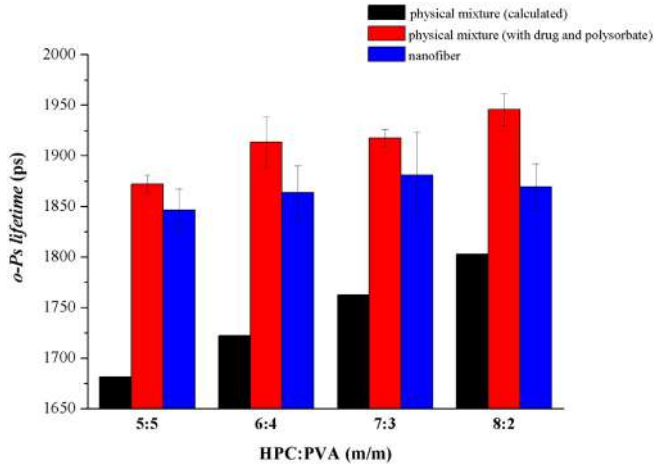

Fig. 3. o-Ps lifetime values of physical mixtures and corresponding drug-loaded fibers.

well modify not only the solid state characteristics but the absorption behavior of the active.

Fig. 3 shows the o-Ps lifetime values of the physical mixtures and the corresponding nanofibers of different HPC:PVA ratios. The fiber formation aligned the supramolecular structure of the polymer, which is indicated by the decreased o-Ps lifetime values of different samples. The denser structure might also indicate the formation of hydrogen bound complexes between the matrix and the drug. The presence of polysorbate plasticized the polymer composite either in the physical mixtures or in fibrous samples. The increased o-Ps lifetime values refer to enlarged molecular mobility and, thus, bigger free volume holes.

The open-air film formation is a slow process, it took few days. Even so, the structural change occurred only after the total weight loss at dried, glassy state. At this stage, the mobility of polymeric chains is low, so, the delay of the structural change is not surprising. However, this delay emphasizes the role of rapid drying in electrospinning fiber-formation. The structure of fibers should definitely be metastable, and we are planning additional study to investigate this metastability.

4. Conclusions

The results highlight the importance of supramolecular changes in the course of the drying-induced gel-film transition or gel-to-fiber formation. The anomalous gel-film transition refers to the presence of secondary bounded intramolecular water, which could initiate the amorphous-crystalline transition of the drug. It suggests that the mapping of the binding energies of polymer-drug and polymer-water would be essential for the selection of a polymer delivery base for a given drug in order reserve the functionality-related stability of the system.

Even if the mentioned H-bounded complex formation is limited (or does not appear at all), the hole size alone can have significant effect on drug release and, thus, on the pharmacokinetic properties of papaverine.

Acknowledgement

A part of the work was supported by the Hungarian Science Foundation (OTKA) under Grant K115939.

References

Borgquist, P., Körner, A., Piculell, L., Larsson, A., Axelsson, A., 2006. A model for the drug release from a polymer matrix tablet—effects of swelling and dissolution. J. Control. Release 113, 216–225.

Davidovich-Pinhas, M., Bianco-Peled, H., 2010. A quantitative analysis of alginate swelling. Carbohydr. Polym. 79, 1020–1027.

Domján, A., Fodor, C., Kovács, S., Marek, T., Iván, B., Süvegh, K., 2012. Anomalous swelling behavior of poly(N-vinylimidazole)-l-poly(tetrahydrofuran) amphiphilic conetwork in water studied by solid-state NMR and positron annihilation lifetime spectroscopy. Macromolecules 45, 7557–7565.

Horvat, G., Pantić, M., Knez, Ž., Novak, Z., 2018. Encapsulation and drug release of poorly water soluble nifedipine from bio-carriers. J. Non-Cryst. Solids 481, 486–493.

Kazsoki, A., Szabó, P., Süvegh, K., Vörös, T., Zelkó, R., 2017a. Macro- and microstructural tracking of ageing-related changes of papaverine hydrochloride-loaded electrospun nanofibrous buccal sheets. J. Pharm. Biomed. Anal. 143, 62–67.

Kazsoki, A., Szabó, P., Zelkó, R., 2017b. Prediction of the hydroxypropyl cellulose—poly (vinyl alcohol) ratio in aqueous solution containing papaverine hydrochloride in terms of drug loaded electrospun fiber formation. J. Pharm. Biomed. Anal. 138, 357–362.

Kirkegaard, P., Eldrup, M., Mogensen, O.E., Pedersen, N.J., 1981. Program system for analysing positron lifetime spectra and angular correlation curves. Comput. Phys. Commun. 23, 307–335.

MacKenzie, I.K., 1983. In: Brandt, W., Dupasquier, A. (Eds.), Experimental methods of annihilation time and energy spectrometry. Positron Solid-State Physics, North-Holland.

Nagy, Z.K., Nyul, K., Wagner, I., Molnar, K., Marosi, G., 2010. Electrospun water soluble polymer mat for ultrafast release of Donepezil HCl. Express Polym Lett 4, 763–772.

Nagy, Z.K., Balogh, A., Vajna, B., Farkas, A., Patyi, G., Kramarics, Á., Marosi, G., 2012. Comparison of electrospun and extruded Soluplus®-based solid dosage forms of improved dissolution. J. Pharm. Sci. 101, 322–332.

Sriamornsak, P., Kennedy, R.A., 2008. Swelling and diffusion studies of calcium polysaccharide gels intended for film coating. Int. J. Pharm. 358, 205–213.

Süvegh, K., Zelkó, R., 2002. Physical aging of poly(vinylpyrrolidone) under different humidity conditions. Macromolecules 35, 795–800.

Szabó, B., Süvegh, K., Zelkó, R., 2012. Real time positron annihilation lifetime spectroscopy for the detection of the hydrocolloid gel-film transition of polymers. Polym. Test. 31, 546–549.

Szabó, P., Sebe, I., Stiedl, B., Kállai-Szabó, B., Zelkó, R., 2015. Tracking of crystalline-amorphous transition of carvedilol in rotary spun microfibers and their formulation to orodispersible tablets for in vitro dissolution enhancement. J. Pharm. Biomed. Anal. 115, 359–367.

Szente, V., Baska, F., Zelkó, R., Süvegh, K., 2011. Prediction of the drug release stability of different polymeric matrix tablets containing metronidazole. J. Pharm. Biomed. Anal. 54, 730–734.

molecular pharmaceutics

DOI:10.14753/SE.2020.2446

Article

Cite This: *Mol. Pharmaceutics* 2018, 15, 4214–4225

pubs.acs.org/molecularpharmaceutics

Microstructural Distinction of Electrospun Nanofibrous Drug Delivery Systems Formulated with Different Excipients

Adrienn Kazsoki,[†] Péter Szabó,[†] Attila Domján,[‡] Attila Balázs,[‡] Tamás Bozó,[§] Miklós Kellermayer,[§] Attila Farkas,[∥] Diána Balogh-Weiser,[∥] Balázs Pinke,[⊥] András Darcsi,[#] Szabolcs Béni,[#] János Madarász,[▽] Lajos Szente,[○] and Romána Zelkó*[,†]

[†]University Pharmacy Department of Pharmacy Administration, Semmelweis University, Hőgyes Endre utca 7-9, H-1092 Budapest, Hungary

[‡]NMR Research Laboratory, Research Centre for Natural Sciences, Hungarian Academy of Sciences, Magyar tudósok körútja 2, H-1117 Budapest, Hungary

[§]Department of Biophysics and Radiation Biology, Semmelweis University, Tűzoltó utca 37-47, H-1094 Budapest, Hungary

[∥]Department of Organic Chemistry and Technology, Budapest University of Technology and Economics, Műegyetem rakpart 3, H-1111 Budapest, Hungary

[⊥]Department of Polymer Engineering, Faculty of Mechanical Engineering, Budapest University of Technology and Economics, Műegyetem rakpart 3, H-1111 Budapest, Hungary

[#]Department of Pharmacognosy, Semmelweis University, Üllői út 26, H-1085 Budapest, Hungary

[▽]Department of Inorganic and Analytical Chemistry, Budapest University of Technology and Economics, Szent Gellért tér 4, H-1111 Budapest, Hungary

[○]CycloLab, Cyclodextrin Research and Development Laboratory Ltd., Illatos út 7, H-1097 Budapest, Hungary

Supporting Information

ABSTRACT: The electrospun nanofiber-based orally dissolving webs are promising candidates for rapid drug release, which is due to the high surface area to volume ratio of the fibers and the high amorphization efficacy of the fiber formation process. Although the latter is responsible for the physical and/or chemical instability of these systems. The primary aim of the present study was to elucidate how the addition of polysorbate 80 (PS80) and hydroxypropyl-β-cyclodextrin (HP-β-CD) influenced the electrospinning process, the properties, and the behavior of the obtained nanofibers. In order to reveal any subtle changes attributable to the applied excipients, the prepared samples were subjected to several state of the art imaging and solid state characterization techniques at both macroscopic and microscopic levels. Atomic force microscopy (AFM) revealed the viscoelastic nature of the fibrous samples. At relatively low forces mostly elastic deformation was observed, while at higher loads plasticity predominated. The use of polysorbate led to about two times stiffer, less plastic fibers than the addition of cyclodextrin. The $^{1}H-^{13}C$ nuclear magnetic resonance (NMR) cross-polarization build-up curves pointed out that cyclodextrin acts as an inner, while polysorbate acts as an outer plasticizer and, due to its "liquid-like" behavior, can migrate in the polymer-matrix, which results in the less plastic behavior of this formulation. Positron annihilation lifetime spectroscopy (PALS) measurements also confirmed the enhanced mobility of the polysorbate and the molecular packing enhancer properties of the cyclodextrin. Solid-state methods suggested amorphous precipitation of the active ingredient in the course of the electrospinning process; furthermore, the nature of the amorphous systems was verified by NMR spectroscopy, which revealed that the use of the examined additives enabled the development of a molecularly dispersed systems of different homogeneities. An accelerated stability study was carried out to track physical state related changes of the incorporated drug and the polymeric carrier. Recrystallization of the active ingredient could not be observed, which indicated a large stress tolerance capacity, but time-dependent microstructural changes were seen

continued...

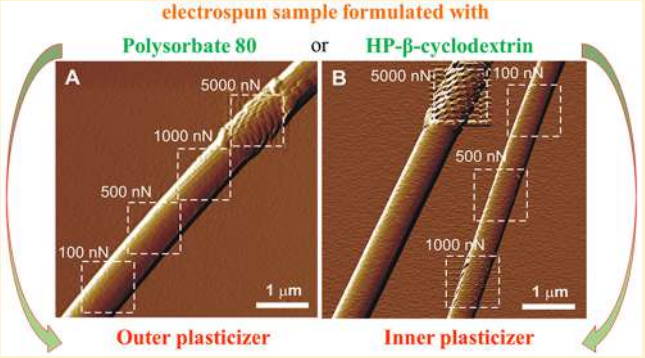

Received: June 20, 2018
Revised: July 13, 2018
Accepted: July 19, 2018
Published: July 19, 2018

DOI: 10.1021/acs.molpharmaceut.8b00646
Mol. Pharmaceutics 2018, 15, 4214–4225

DOI:10.14753/SE.2020.2446

in the presence of polysorbate. Raman mapping verified homogeneous drug distribution in the nanofibrous orally dissolving webs. The performed dissolution study indicated that the drug dissolution from the fibers was rapid and complete, but the formed stronger interaction in the case of the PVA-CD-MH system resulted in a little bit slower drug release, compared to the PS80 containing formulation. The results obviously show that the complex physicochemical characterization of the polymer-based fibrous delivery systems is of great impact since it enables the better understanding of material properties including the supramolecular interactions of multicomponent systems and consequently the rational design of drug-loaded nanocarriers of required stability.

KEYWORDS: *metoclopramide hydrochloride monohydrate, electrospun nanofiber, morphological and solid-state characterization, inner and outer plasticizer, accelerated stability test*

1. INTRODUCTION

Over the last few decades, the nanofibrous materials have shown a great interest due to their several potential medical and pharmaceutical applications. High surface area to volume ratio and high porosity of the prepared fibers are just a few examples of the numerous desirable characteristics, which make such formulations optimal candidates for drug delivery systems.

Electrospinning, the most frequently employed nanofiber production technique, where the fiber formation is carried out by applying high voltage. The possibility of fine-tailoring fiber characteristics through the optimal selection of process parameters has attracted a considerable attention in the past few years.[1−4]

High amorphization efficacy of the electrospinning process enables that the active ingredient can be incorporated in the polymer matrix in purely amorphous state, which may result in an enhanced apparent aqueous solubility and dissolution rate.[5] Apart from amorphization, solubility can be improved by using solubility enhancement excipients, like solubilizing agents. Polysorbate (PS) is a universal, polymeric nonionic surfactant capable of increasing the aqueous solubility of drugs.[6]

Cyclodextrins (CDs) and their derivatives are frequently applied, but not universal solubilizers.[7,8] The cyclic host molecules can form inclusion complexes or external adducts with drugs of appropriate size; therefore, CDs can improve solubility, enhance drug absorption and transport across biological membranes, and stabilize active pharmaceutical ingredients via specific, noncovalent bond formations.[9] For electrospinning process, mainly neutral CD derivatives are suitable,[10−14] but nanofibrous formulations of charged CDs, such as sulphobutyl-ether-β-CDs, have already been described.[15]

In addition, along with their ability to promote electrospinning process, they are well-known plasticizers that can modify the mechanical properties of the fibrous samples and thus the applicability of the orally dissolving webs.

The lack of long-range structural order and the need to overcome lattice energy are responsible for the enhanced apparent water solubility of amorphous materials. However, increased thermodynamic potential of amorphous systems and their higher molecular mobility make such systems prone to physical and/or chemical instability.[16]

Amorphous solid dispersions or molecularly dispersed solid solutions are useful to improve apparent aqueous solubility and to address stability issues.[17−19] Numerous excipients have been used in the formulation of such systems. For example, surfactants act as kinetic stabilizers, and selecting a polymeric matrix exhibiting strong intermolecular interactions (e.g., hydrogen bonds) may also lead to higher physicochemical stability.[20] A more complex molecular packing can be achieved, thus preventing amorphous drug from recrystallization as a result of the decreased molecular mobility, by combination of polymers with other excipients in the course of development of solid solutions or dispersions. Aging related processes do not encompass only the changes to the physical state of the active, but it can entail the physicochemical alterations of the polymer carrier as well. These two coexisting phenomena together determine the long-term stability of polymeric matrix-based amorphous drug delivery systems.[16]

As a model drug, metoclopramide hydrochloride (MH, 4-amino-5-chloro-*N*-[2-diethylamino)ethyl]-2-methoxybenzamide hydrochloride monohydrate) was chosen to gain a better insight into the reversible interactions, e.g., hydrogen bonding, that stabilize the metastable amorphous nanofibrous drug delivery systems, through the formation of secondary interactions. The structural features of the substituted benzamide derivate antiemetic drug (phenyl ring, aromatic primary amine, amide, tertiary amine) enable to establish various intermolecular interactions with the used excipients and the poly(vinyl alcohol) (PVA), which was chosen as the polymeric matrix base of the buccal formulation, because of its excellent electrospinability and good hydrogen bond formation ability.

The primary aim of the present study was to elucidate how the addition of polysorbate 80 (PS80) and hydroxypropyl-β-cyclodextrin (HP-β-CD) influenced the electrospinning process, the properties, and the behavior of the obtained nanofibers. In order to reveal any subtle changes attributable to the applied excipients, the prepared samples were subjected to several state of the art imaging and solid state characterization techniques at both macroscopic and microscopic levels.

2. EXPERIMENTAL SECTION

2.1. Materials. Metoclopramide hydrochloride monohydrate (MH, 336.26 g/mol, >98% purity) was purchased from Sigma-Aldrich. Hydroxypropyl-β-cyclodextrin (HP-β-CD, average degree of substitution (n) ≈ 4.5, (1135.0 + 58.1n) g/mol)) was kindly supplied by Cyclolab Ltd. (Budapest, Hungary). Polysorbate 80 (PS80, Ph. Eur., Molar Chemicals, Hungary), poly(vinyl alcohol) (PVA) (18−88 Ph. Eur., Merck, Darmstadt, Germany), and distilled water were used for the preparation of gels.

2.2. Methods. *2.2.1. Sample Preparation. 2.2.1.1. Metoclopramide Hydrochloride (MH)-Loaded Electrospun Fiber Formation.* Aqueous gels of two different compositions were prepared by using the listed gel components (the applied amounts are described in Table 1A) and the appropriate amount of distilled water with applying heating (80 °C) under magnetic stirring until a clear gel was obtained.

Prior to electrospinning (Unitronik Ltd., Nagykanizsa, Hungary, equipped with an NT-35 high voltage DC supply), the prepared gels cooled to room temperature were transferred into a 1 mL plastic syringe fitted with a metallic spinning tip of 1.2 mm inner diameter. The samples were collected on grounded aluminum plate covered with aluminum foil or parchment paper.

DOI: 10.1021/acs.molpharmaceut.8b00646
Mol. Pharmaceutics 2018, 15, 4214−4225

DOI:10.14753/SE.2020.2446

Table 1. Composition of the aqueous gels (A) and the electrospinning process parameters (B) of the samples

(A)	concentration (w/w %)			
sample name	metoclopramide-HCl (MH)	polysorbate[a] (PS)	cyclodextrin[b] (CD)	poly(vinyl alcohol) (PVA)
PVA-PS[c]	0	1	0	13
PVA-PS-MH[d]	3	1	0	13
PVA-CD[e]	0	0	14	10
PVA-CD-MH[f]	3	0	14	10
(B)	electrospinning process parameters			
sample name	voltage (kV)	flow rate (mL/min)	emitter to collector distance (cm)	
PVA-PS[c]	25	0.05	15	
PVA-PS-MH[d]	30	0.05	15	
PVA-CD[e]	27	0.065	15	
PVA-CD-MH[f]	27	0.065	15	

[a]Polysorbate 80. [b]Hydroxypropyl-β-cyclodextrin [c]Poly(vinyl alcohol)-based, polysorbate 80 containing formulation without metoclopramide-HCl. [d]Poly(vinyl alcohol)-based, polysorbate 80 and metoclopramide-HCl containing formulation. [e]Poly(vinyl alcohol)-based, hydroxypropyl-β-cyclodextrin containing formulation without metoclopramide-HCl. [f]Poly(vinyl alcohol)-based, hydroxypropyl-β-cyclodextrin and metoclopramide-HCl containing formulation.

The latter enabled to peel samples more easily off. Table 1B shows the final parameters applied in the electrospinning process. The experiments were performed in a well-controlled room at ambient temperature (23−26 °C) and 35 ± 5% relative humidity. The prepared samples were also stored at room temperature for the further studies.

2.2.1.2. Preparation of Physical Mixtures. Physical mixtures corresponding to the compositions of the drug loaded nanofibers (MH, milled PVA, either PS80 or HP-β-CD) were prepared and used as control for the physicochemical measurements.

2.2.2. Scanning Electron Microscopy (SEM) Imaging. The samples were fixed by a conductive double-sided carbon adhesive tape and then coated with a gold layer (JEOL JFC-1200 Fine Coater, JEOL Ltd., Tokyo, Japan). SEM images were taken with JEOL JSM-6380LA scanning electron microscope (JEOL Ltd., Tokyo, Japan). The acceleration voltage and the working distance were 15 kV and 10 mm, respectively.

Diameters of 100 individual fibers were measured by ImageJ software (US National Institutes of Health). For statistical assessment, SPSS 20.0 software package (SPSS Inc., Chicago IL, USA) was used. Qualitative statistical analysis, Kolgomorov−Smirnov test, and analysis of variance were done to determine the fiber diameter distributions and to compare samples.

2.2.3. Atomic Force Microscopy (AFM). 2.2.3.1. Sample Preparation for AFM Imaging. For AFM imaging, fibers were collected on freshly cleaved mica discs (Grade V1, Ted Pella Inc., Redding, CA) attached to the aluminum foil-covered collector. In order to obtain a sparse surface coverage with the least overlap between fibers, the mica discs were positioned off-center on the collector, and electrospinning was done briefly (for 10 s). Fibers collected on mica discs were subjected to AFM measurements within 24 h.

2.2.3.2. AFM Imaging and Force Spectroscopy. AFM images were collected in noncontact mode with a Cypher S instrument (Asylum Research, Santa Barbara, CA) at 1−2 Hz line-scanning rate in air, using a silicon cantilever (OMCL AC-160TS, Olympus, Japan, typical spring constant: 20−25 N/m) oscillated at its resonance frequency (300−320 Hz). In order to explore the mechanical characteristics of nanofibers, force volume maps, i.e., 100 force curves in a 10 × 10 matrix of a 1 μm^2 predefined area, were collected in contact mode. The AFM tip was moved toward the sample with 1 μm/s velocity until reaching a predefined load (100 nN−5 μN), then the tip was immediately retracted with the same speed. Samples were rescanned after force spectroscopy to assess the effects of mechanical manipulation on fiber morphology. AFM cantilevers were calibrated by using the thermal method.[21] Temperature during the measurements was 29 ± 1 °C.

2.2.3.3. Analysis of AFM Images and Force Spectra. AFM images and force spectra were analyzed by using the built-in algorithms of the AFM driver software (IgorPro, WaveMetrics Inc., Lake Oswego, OR). Amplitude-contrast images are shown throughout this Article. Topographical height was measured in height-contrast images. To obtain the Young's modulus, force curves taken at 100 nN maximum load were fitted with the Hertz model of elasticity,[22] assuming the AFM tip to be a spherical indenter (r = 10 nm) with a modulus of 167 GPa and Poisson ratio of 0.27,[23] while Poisson ratio of PVA fibers was estimated to be 0.45.[24] Plasticity of the fibers was calculated (eq 1) from force curves taken at 5 μN maximum load, as

$$\text{plasticity} = (\text{AUC}_a - \text{AUC}_r)/\text{AUC}_a \quad (1)$$

where AUC_a and AUC_r are the area under approach and retraction force curves, respectively. To discriminate between data collected from the fiber surface and that from the fiber side or the substrate, only those force curves were taken into analysis, which were recorded at locations with the height of at least 85% of the maximum height of the examined region of the fiber. Young's modulus and plasticity histograms were created in Origin 8.6 software (OriginLab Corp., Northampton, MA). For Young's modulus determination, n = 118 (PVA-PS-MH fibers) and n = 304 (PVA-CD-MH fibers) force curves were analyzed. Plasticity of PVA-PS-MH and PVA-CD-MH fibers was derived from n = 57 and n = 38 force spectra, respectively.

2.2.4. Power X-ray Diffraction (XRD). X-ray diffraction patterns of the samples were recorded by X'pert Pro MDP X-ray diffractometer (PANalytical, Amelo, Netherlands). Cu−K α radiation (1.542 Å) and a Ni filter were used. The applied voltage was 40 kV, and the current was 30 mA. The samples were examined between 4° and 40° 2θ.

2.2.5. Positron Annihilation Lifetime Spectroscopy (PALS). For positron lifetime measurements, a positron source made of carrier-free ^{22}NaCl with ∼10^6 Bq activity was used, which was sealed between two thin Kapton foils. The fibrous samples or the physical mixtures were placed at either side of the source

DOI: 10.1021/acs.molpharmaceut.8b00646
Mol. Pharmaceutics 2018, 15, 4214−4225

(forming a sandwich structure), and finally, it was wrapped in aluminum foil. Lifetime spectra were measured with a fast−fast coincidence system based on BaF_2 XP2020Q detectors and Ortec electronics. From each sample, three parallels were measured. The spectra were evaluated by the RESOLUTION computer code.[25] Three lifetime components were found in each sample. The longest component was identified as orthopositronium (*o*-Ps) lifetime, which is related to the annihilation of the *o*-Ps atoms.

2.2.6. Solution-State Nuclear Magnetic Resonance (NMR) Spectroscopy. The solution-state NMR experiments were carried out in D_2O at 25 °C on a 600 MHz Varian DDR NMR spectrometer (Agilent Technologies, Palo Alto, CA, USA), equipped with a 5 mm inverse-detection gradient (IDPFG) probehead. Standard pulse sequences and processing routines available in VnmrJ 3.2C/Chempack 5.1 were used. The complete resonance assignments of metoclopramide and HP-*β*-CD were achieved by using direct $^1H-^{13}C$, long-range $^1H-^{13}C$, and scalar spin−spin connectivities, derived from 1D ^1H, 2D gCOSY, zTOCSY or ROESY, $^1H,^{13}C$-gHSQCAD, or gHMBCAD ($^nJ_{CH}$ = 8 Hz) experiments, respectively. ^1H chemical shifts in all experiments were referenced to the HOD (δ = 4.65 ppm) signal. The intermolecular interactions were investigated by nuclear Overhauser effect (NOE) type experiment with 1:1.5 (MH: HP-*β*-CD) molar ratio, in neutral D_2O solution. Two-dimensional ROESY spectra with 512 increments were recorded using a mixing time of 300 ms during a spin-lock of 2.2 kHz.

2.2.7. Solid-State Nuclear Magnetic Resonance (ssNMR) Spectroscopy. ssNMR spectra were recorded on a Varian NMR system operating at a ^1H frequency of 400 MHz (100 MHz for ^{13}C) with a Chemagnetics 4.0 mm narrow-bore double resonance T3 probe. The spinning rate of the rotor was 9 kHz in all cases. For the one-dimensional ^{13}C cross-polarization (CP) MAS, 4−6000 transients were recorded with SPINAL-64 decoupling with a strength of 83 kHz and 0.5 ms of contact time with 20 s of recycle delay, which is 5 times larger than T_{1H} of the crystalline metoclopramide hydrochloride monohydrate. CP ^{13}C spectra were collected by varying the contact time to gain the cross-polarization build-up curves. The temperature of all the measurements was 20 °C. Adamantane was used as external chemical shift reference (38.55 and 29.50 ppm). The 90° pulse lengths were 3 μs for both the proton and the carbon channels for all the ssNMR experiments.

2.2.8. Accelerated Stability Test. Drug-loaded and drug-free nanofibrous samples were peeled off from the parchment paper, then repacked into aluminum foil and transferred into closed plastic containers to be stored in a stability chamber (Sanyo type 022, Leicestershire, UK) for 4 weeks at 40 ± 2 °C, 75 ± 5% RH. Morphological and physicochemical changes of the samples were analyzed by SEM, FT-IR, XRD, and PALS.

2.2.9. Metoclopramide Hydrochloride (MH) Content of the Fibrous Formulations. MH content of the fibers was measured by Jasco 530 UV−vis spectrophotometer (Agilent 8453 UV−vis Diode Array System, USA for MD) at 309 nm. MH aqueous standard stock solution (SSS) of 1 mg/mL was prepared in a calibrated volumetric flask. A working standard solution (WSS) of 50 μg/mL was prepared by diluting SSS with phosphate buffer (pH 6.8, 0.05 M, Ph. Eur. 8). Solutions of nine concentrations, in a 2.5−25 μg/mL concentration range, were used for the calibration. Solutions were diluted from the WSS.

2.2.10. Raman Mapping. The Raman spectroscopy measurements were carried out using LabRAM system (Horiba Jobin-Yvon, Lyon, France) coupled with an external 532 nm Nd:YAG laser source (Sacher Lasertechnik, Marburg, Germany) and an Olympus BX-40 optical microscope (Olympus, Hamburg, Germany). Objective of 100× magnification (numerical aperture (NA) = 0.9) was used for optical imaging. A 1800 groove/mm grating monochromator and charge-coupled-device (CCD) detector were used for dispersion and detection of Raman photons, and during the measurements of the physical mixtures, intensity filter (D = 0.6) was applied as MH shows intensive Raman activity. The spectra were collected over a spectral range of 346−1790 cm $^{-1}$ at 5 cm^{-1} resolution. The maps of the fibrous samples were collected with 2 μm step size in both direction and consisted of 29 × 29 points. In the case of the physical mixtures, the step size was 5 μm and 45 × 45 points were investigated. One spectrum acquisition took 20 s and accumulated 3 times in each mapping point. The nanofibrous samples were investigated without any sample preparation, while the physical mixtures were pressed slightly (50 bar) with hydraulic pressure (Manfredi, OL 57) to get flat surface. The component concentrations were determined with the Classical Least Squares (CLS) method using the pure components as reference materials during the evaluation of the physical mixtures, while in the case of the nanofibrous samples the spectra of the neat-fibrous samples and the extract amorphous MH were used as a reference. In the latter case for the pure spectrum extraction, the Multivariate Curve Resolution-Alternating Least Squares (MCR-ALS) method[26] was used.

2.2.11. Dissolution Test. In order to mimic the small-volume dissolution in the oral cavity, dissolution tests of MH-loaded fibrous films were carried out in a beaker using 20 mL of dissolution medium. The dissolution medium was phosphate buffer (pH 6.8, 0.05 M, Ph. Eur. 8). The fibrous samples were put into a sinker along with a stirring bar, which was then placed into the dissolution fluid tempered to 37 ± 1 °C. Stir rate was set to 50 rpm. The dissolution was followed for 15 min. At predetermined time points, 200 μL of samples were taken, which were immediately diluted to 2.5 mL. MH concentration was determined spectrophotometrically on the basis of calibration curve recorded earlier.

3. RESULTS AND DISCUSSION

3.1. Results. *3.1.1. Fiber Morphology and Topography.* Optimizing the electrospinning process parameters and the compositions, well-defined, round-shaped samples resulted on the collector. As illustrated in Figure 1A,B, a clear fibrous structure without any beads and film-like areas was obtained in each sample. SEM morphology substantiated the absence of any visible sign of heterogeneity in both samples, e.g., surface crystallization of the active ingredient. It is noteworthy that fiber formation could be carried out using a lower voltage when HP-*β*-CD was present in the gel.

Average fiber diameter values (mean ± SD) were 336 ± 88 and 323 ± 62 nm for PVA-PS-MH and PVA-CD-MH fibers, respectively. The distribution of PVA-PS-MH fibers is wider than that of the PVA-CD-MH fibers with a more uniform structure (Figure 1C,D).

Fiber diameter distributions of the two samples were investigated using Kolmogorov−Smirnov test. Statistical analyses of fiber diameters indicated that distributions of PVA-PS-MH and PVA-CD-MH were normal (p = 0.844 and 0.416, respectively). A one-way analysis of variance (ANOVA) pointed out that there was no significant difference between the diameter of the two formulations (p = 0.211).

DOI: 10.1021/acs.molpharmaceut.8b00646
Mol. Pharmaceutics 2018, 15, 4214−4225

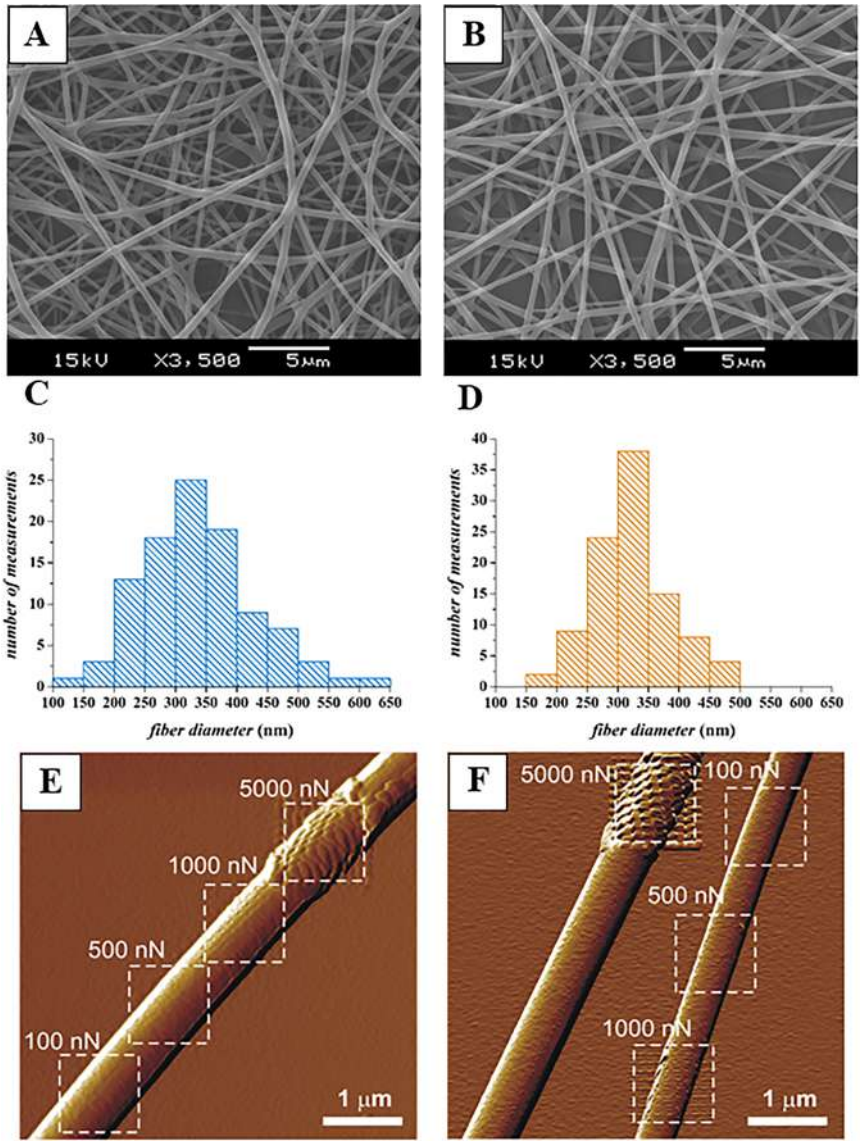

Figure 1. SEM photos of the poly(vinyl alcohol)-based, metoclopramide-HCl-loaded electrospun sample either containing polysorbate 80 (PVA-PS-MH) (A) or hydroxypropyl-β-cyclodextrin (PVA-CD-MH) (B) (magnification: 3500×). Histograms of the fiber diameter distribution of PVA-PS-MH (C) and PVA-CD-MH (D) fibers. Effect of mechanomanipulation: AFM−amplitude contrast images of PVA-PS-MH (E) and PVA-CD-MH (F) nanofibers taken after force spectroscopy. White dashed rectangles indicate areas where force maps (10 × 10 force curves) were taken from. Maximum load applied in each region is written next to the rectangles.

AFM topography of both PVA-PS-MH (Figure S1) and PVA-CD-MH (Figure S2) nanofibrous sample appeared similar to those seen in scanning electron micrographs (Figure 1A,B). Fibers appeared as long, curved, continuous, cylinders, although certain regions of PVA-PS-MH fibers exhibited a ribbon-like, flat structure (see top left and bottom right corners in Figure S1A). The height of the examined fiber regions varied between approximately 330−360 and 300−450 nm for PVA-PS-MH and PVA-CD-MH fibers, respectively. The surface of both fibers was relatively smooth with only a few nm height variations. The height profile of PVA-PS-MH fibers (Figure S1D) showed sharper peaks than that of the more rounded profile plot of PVA-CD-MH fibers (Figure S2D), indicating that PVA-PS-MH fibers display a bit coarser surface.

To assess the mechanical characteristics of PVA nanofibers, we applied 100 nN, 500 nN, 1 μN, and 5 μN loads at well-defined points of fiber surface, pressing and retracting the AFM tip into them at a constant 1 μm/s velocity. After rescanning the manipulated area, no noticeable alterations were found in regions loaded with 100 nN forces (Figure 1E,F). At 500 nN load, no effect for PVA-PS-MH but few small depressions were detected for PVA-CD-MH fibers, while at 1 and 5 μN loads, permanent surface depressions were seen in both compositions; thus, these forces enabled plastic deformation. Depressions were shallower and blurred in PVA-PS-MH fibers (Figure 1E), while they were deeper and had a more definite profile reflecting the shape of AFM tip in PVA-CD-MH fibers (Figure 1F).

Representative force curves taken at different maximum loads are shown in Figure S3. In the low force regime (100 nN maximum load, Figure S3A, E) a considerable attractive interaction between the fibers and the tip can be inferred from the negative peak in approach curves. After reaching the fiber surface (distance = 0 nm), the force followed an apparent linear increase up to the threshold load (≈ 100 nN), a sign of elastic response. As the tip was retracted, the force decreased, and this region of the retraction curve was roughly parallel to the approach curve

DOI: 10.1021/acs.molpharmaceut.8b00646
Mol. Pharmaceutics 2018, 15, 4214−4225

with a very small hysteresis between them, implying there was almost no plastic deformation at this load. Large negative force peak in retraction curve is due to tip−fiber adhesion and then the force reached 0 as the tip was drawn farther from fiber surface.

The ascending force region of approach curves was fitted with the Hertz model of elasticity[22] adapted to AFM force spectroscopy (Figure S3A,E dotted lines). Distributions of Young's modulus calculated from the fits showed an apparent normal distribution for both polymers, with mean ± SD values of 3.26 ± 1.74 and 1.48 ± 0.90 GPa for PVA-PS-MH and PVA-CD-MH fibers, respectively (Figure S4A).

As the load was increased, hysteresis area between approach and retraction curves became larger (Figure S3) indicating plastic deformation of the fibers. PVA-CD-MH expressed larger hysteresis area than PVA-PS-MH at each applied load; thus, it is more plastic (see plasticity distributions at 5 μN load in Figure S4B), as it was concluded from Figure 1E,F.

3.1.2. Solid-State Characterization of the Fibrous Samples. PALS measurements were carried out with the aim of monitoring the supramolecular alterations through *o*-Ps lifetime changes of physical mixtures, the electrospun neat and drug loaded fibrous samples. The *o*-Ps lifetimes of the physical mixtures, regardless of the used excipients, were found to be approximately same. This increased *o*-Ps lifetime values of PVA-PS and PVA-PS-MH nanofibrous samples in contrast to the physical mixture (Figure 2).

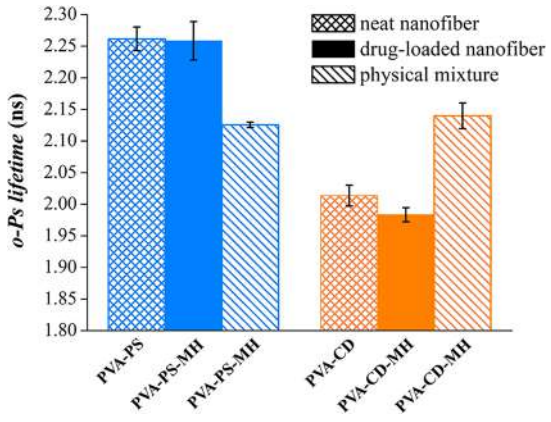

Figure 2. Discrete orthopositronium (*o*-Ps) lifetimes of either polysorbate or cyclodextrin containing neat samples, drug-loaded nanofibers, and related physical mixtures.

The presence of the active pharmaceutical ingredient could not modify substantially the average free volume holes and thereby the supramolecular structure. The *o*-Ps lifetimes of CD containing neat (PVA-CD) and drug-loaded (PVA-CD-MH) fibrous samples were remarkably decreased compared to the physical mixture. The presence of the active pharmaceutical ingredient caused a further slight, but not remarkable, reduction in *o*-Ps lifetime.

In the X-ray diffractograms of physical mixtures, characteristic peaks of the MH are clearly observable with the broad peak of the PVA and CD (Figure 3A,B). Only diffuse peaks with the lack of any high intensity peaks belonging to MH characterize the XRD patterns of the fibrous samples.

Inclusion complexation of the substituted benzamide derivative, local anesthetic lidocaine with HP-β-CD, has already been described in the literature.[27] As the MH and lidocaine structure is very similar, 2D ROESY NMR measurement was carried out at neutral pH with the aim of analyzing hypothesized interactions between MH and the randomly substituted HP-β-CD at an atomic level. A partial ROESY spectrum of the MH/HP-β-CD system is shown in Figure 4A. Intense cross-peaks can be observed between the aromatic ^{1}H resonances of MH and the inner cavity protons of HP-β-CD (CD-H3 and CD-H5). The resonances of the aromatic moiety of MH also show cross-peaks with the hydroxypropyl chains.

In order to characterize the polymer-based macromolecular systems, ssNMR measurements were carried out. MH gives a well resolved NMR spectrum typical for crystalline materials built up of small molecules. All the resonances could be assigned to one carbon atom, as it was proven in a single pulse experiment with 600 s of recycle delay. The *N*-ethyl groups have a different environment in the crystalline structure; therefore, their signals notably differed from the signals obtained in the solution NMR spectra, enabling their differentiation and assignation. Signals of the methyl groups at 9.9 and 3.7 ppm are extremely sensitive indicators to detect even low ratio of crystalline ordering in the complex matrix structure. In the spectra (Figure 4B, blue and orange lines) of multicomponent fiber samples only a broadened signal was obtained in a wide range. Resonances of MH overlapped with the signals of polymeric matrices except for the methyl and some aromatic signals of MH. Merging and broadening of these sharp MH signals unambiguously shows that the MH has no crystalline structure. Instead of two methyl resonances, only a slightly shifted signal could be detected; hence, even a short-range order could be excluded on a nm scale.

The analysis of the shapes of the CP build-up curves, which are constructed by varying the contact time and plotting signal intensity vs contact time, can provide information on the proton environment of the carbon atoms, and their mobility could be evaluated. Fitting of the build-up curves by a simplified expression determination of changes in the chemical environment and relaxation of carbons (according to the eq 2) was possible:

$$M(t) = \lambda^{-1} M_0[1 - \exp(-\lambda t/T_{CH})] \exp(-t/T_{1\rho}) \quad (2)$$

where $\lambda = 1 + (T_{CH}/T_{1\rho}) - (T_{CH}/T_{1\rho})$, $M(t)$ is the magnetization at contact time t, M_0 is the initial magnetization, T_{CH} is the time coefficient of the CP (the time it takes for magnetization to be transferred from ^{1}H to ^{13}C), and $T_{1\rho}$ is the relaxation time of the carbon in the rotating frame. This equation is valid only in a regime of fast molecular motion, but it qualitatively describes the experimental CP build-up curves and permits comparison of the fitted parameters. The more mobile a carbon, the more slowly it relaxes, so the plasticizing effect of the excipients could be efficiently tracked. Because of the numerous overlaps of the signals, only the signal of PVA at 43.3 ppm was analyzed in details. The resonance (at 75.3 ppm) attributed to the crystalline PVA decreases or even disappears in the plasticized samples.[28] This effect is clearly observable on the ^{13}C NMR spectra of PVA-PS-MH sample (Figure S5), but it is not recognizable on the PVA-CD sample because of the overlapping signals.

The hydrogen environment did not change significantly around the CH_2 groups because the H-bond structure remains unaltered; thus, the T_{CH} parameter did not change remarkably. H-bonds between adjacent chains are replaced in the plasticized PVA fibers by H-bonds between PVA and plasticizer molecules. Change in the mobility is more pronounced; thus, the plasticization effect reflected in the T_{1rho} relaxation parameter is obvious (Figure 5). Mobility of PVA chains is very similar in PVA-CD and PVA-PS fibrous samples. Surprisingly, the chain

DOI: 10.1021/acs.molpharmaceut.8b00646
Mol. Pharmaceutics 2018, 15, 4214−4225

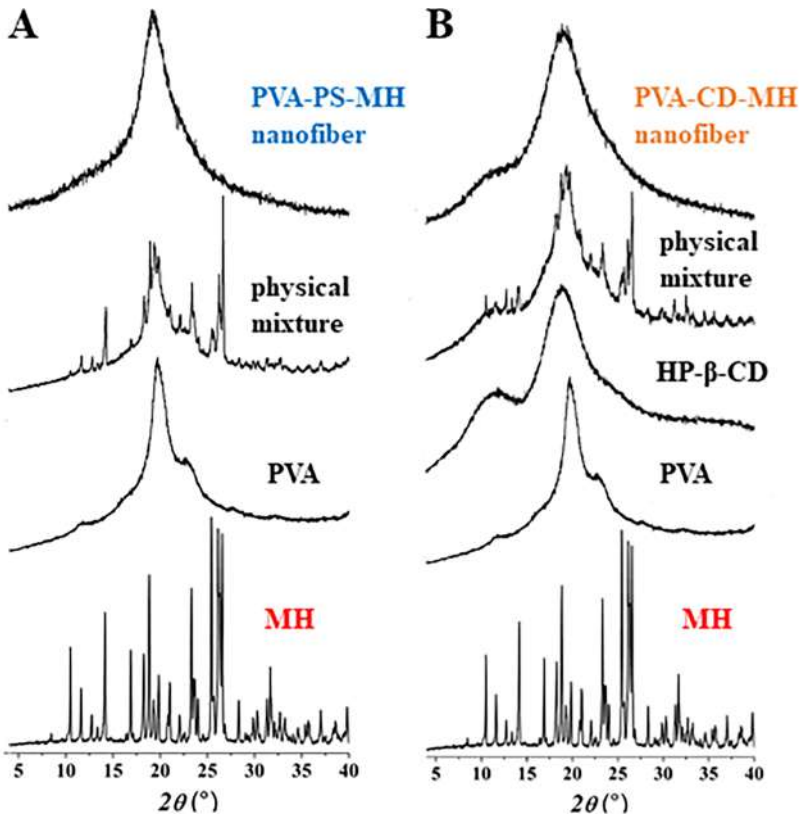

Figure 3. Power X-ray patterns of the components, physical mixture, and drug-loaded polysorbate (PVA-PS-MH) (A) or hydroxypropyl-β-cyclodextrin containing (PVA-CD-MH) (B) formulation.

mobility increases further in the MH containing samples, implying that MH acts also as a plasticizer.

ssNMR was utilized in the in depth characterization of the amorphous nature of the samples through the tendency of T_{1rho} values. The difference of PVA-CD and PVA-CD-MH samples was not explicitly smaller that the PS containing formulations, while the relaxation time difference between the neat (PVA-PS) and drug-loaded (PVA-PS-MH) samples was remarkably higher.

3.1.3. Accelerated Stability Test. One of the most urging issues with amorphous drug-loaded nanofibrous systems is their thermodynamically metastable nature; therefore, the physicochemical stabilization of such formulations to achieve long-term stability is of special interest.

Stress induced macrostructural changes of the fibrous samples were tracked by SEM measurements, and significant morphological changes were not observed (Figure 6A for PVA-PS-MH and Figure 6B for PVA-CD-MH). For fiber-to-film morphological transition, fragmentation has not been detected. The integrity of the fibrous structure has been retained throughout the entire course of the stability test. Slightly merged regions and a subtle broadening of the fibers were noticeable in the SEM image taken at week 4 of PVA-PS-MH sample.

The solid-state alterations were tracked by XRD. Figure 6C,D indicate that the diffractograms were not changed remarkably, i.e., characteristic peaks of the active cannot be observed in the course of the storage.

PALS is a sensitive tool to detect aging related changes of the drug carrier. Along with the storage time, the differences of the *o*-Ps values between neat and drug-loaded PS containing samples became larger: 0.046, 0.059, 0.062, and 0.072 ns for weeks 1, 2, 3, and 4 respectively (Figure 6E). In contrast to the HP-β-CD containing samples, the *o*-Ps lifetime and thus the average free volumes holes (between the standard deviations) remained nearly constant (Figure 6F) during the four week storage period.

3.1.4. Drug Distribution and in Vitro Dissolution Study. The measured drug content was 16.45 ± 0.25% (w/w) and 14.24 ± 0.27% (w/w) for PVA-PS-MH and PVA-CD-MH fibrous samples, respectively.

Raman mapping analyses were also carried out with the aim to monitor the distribution of the MH in the nanofiber-based orally dissolving webs and in the physical mixtures, which could be the base of the tablets. The amorphous form of the MH was not available, but with MCR-ALS method, it could be extracted. Figure S6 shows the Raman spectra of crystalline (A) and amorphous (B) MH. In the latter case, the broadened and merged signals could be tracked obviously.

Figure 7A,B show the Raman map of the MH-loaded PS80 containing electrospun sample and the corresponding physical mixture, respectively, while Figure 7C,D shows the HP-β-CD containing ones. The maps demonstrate the calculated concentrations of MH (between 0 and 1) in each sampling point, which were determined by Classical Least Squares (CLS) method using the appropriate reference spectra. In the case of the electrospun samples, regardless of the used excipient, slight fluctuation of the relative concentration values were obtained in each sampling point, while in the case of the physical mixtures MH concentration changed remarkable.

Figure 8 summarizes the results of the dissolution test of MH containing fibrous samples. The *in vitro* MH release was rapid and complete from the PS containing formulation (Figure 8A), which was similar to the results published in our previous study.[29] The rate of dissolution of the PVA-CD-MH sample was a bit slower than the PVA-PS-MH, but it was also complete (Figure 8B).

DOI: 10.1021/acs.molpharmaceut.8b00646
Mol. Pharmaceutics 2018, 15, 4214−4225

DOI:10.14753/SE.2020.2446

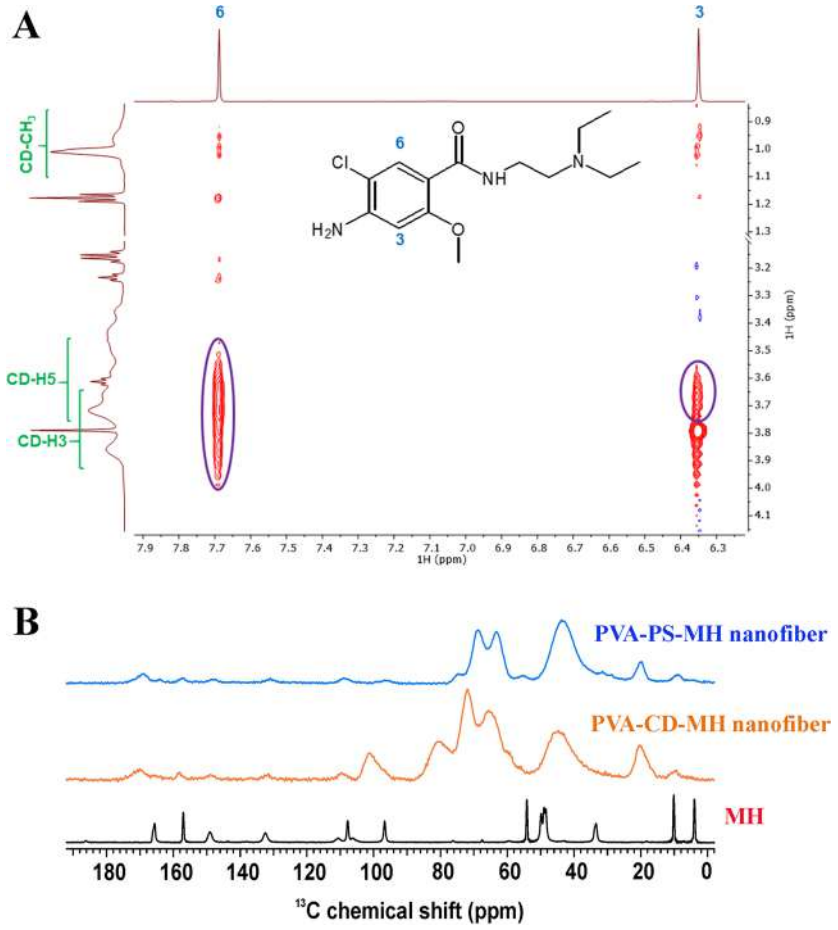

Figure 4. (A) Partial 2D ROESY NMR spectrum of metoclopramide-HCl and randomly substituted hydroxypropyl-β-cyclodextrin (HP-β-CD) and (B) solid-state NMR spectra of metoclopramide-HCl (MH) and the nanofibers.

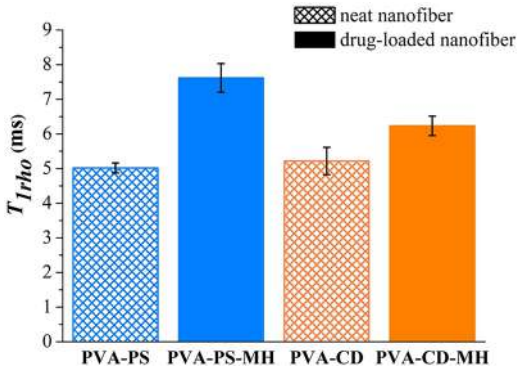

Figure 5. Solid-state NMR relaxation times of the neat- and MH-loaded polysorbate or cyclodextrin containing nanofibrous samples.

3.2. Discussion. SEM and AFM images clearly showed that in case of both formulations clearly fibrous structures with uniform surface were formed, which could refer that the PVA is a suitable polymer to incorporate MH.

AFM force spectroscopy results indicate that PVA fibers are viscoelastic materials. Loaded with relatively low forces (up to 100 nN), their deformation is largely elastic. Their Young moduli (mean ± SD values of 3.26 ± 1.74 and 1.48 ± 0.90 GPa for PVA-PS-MH and PVA-CD-MH fibers, respectively) are in well accordance with that of the previously reported trifluoroacetate-derived PVA films (1.5−3.75 GPa[30]). It should be noted that Young moduli of different PVA polymers available in the scientific literature vary in a very broad range (e.g., 6.4 MPa,[31] 1.8−4.7 GPa,[32] 32.6 GPa,[33] and 50 GPa[34]), which can be attributed to different compositions, preparation techniques, chemical modifications, and testing methods. Loading the fibers with higher forces (up to 5 μN), their deformation becomes predominantly plastic. Both the plasticity values calculated from force spectra and the observation that 500 nN load led to deformation only in PVA-CD-MH fiber indicates that PVA-CD-MH fibers are more plastic than PVA-PS-MH ones. Altogether, the use of PS80 led to about two times stiffer, less plastic PVA fibers than the addition of HP-β-CD.

The CP build-up curves showed that the HP-β-CD behaves similarly to PVA (Figure S7A), while in the case of PS80, liquid-like behavior was found (Figure S7B). The results suggest that HP-β-CD acts as an inner plasticizer, while PS80 acts an outer plasticizer.[35]

PALS results also disclosed differences in the plasticizing behavior of the excipients, and ssNMR showed mobility and diffusibility differences of the formulations, which was mainly manifested in the third lifetime values.[36] The o-Ps lifetime of PVA-PS-MH sample increased related to the physical mixture, which is due to the enhanced mobility and diffusibility of the PS80. The enormous reduction in o-Ps lifetimes of the HP-β-CD containing formulations, consequently in the average size of the free volume holes, indicated a more complex molecular packing due to the supramolecular ordering of the polymeric chains.

XRD implies the absence of a long-term ordering; thus, crystalline−amorphous transition of the active regardless of the

DOI: 10.1021/acs.molpharmaceut.8b00646
Mol. Pharmaceutics 2018, 15, 4214−4225

DOI:10.14753/SE.2020.2446

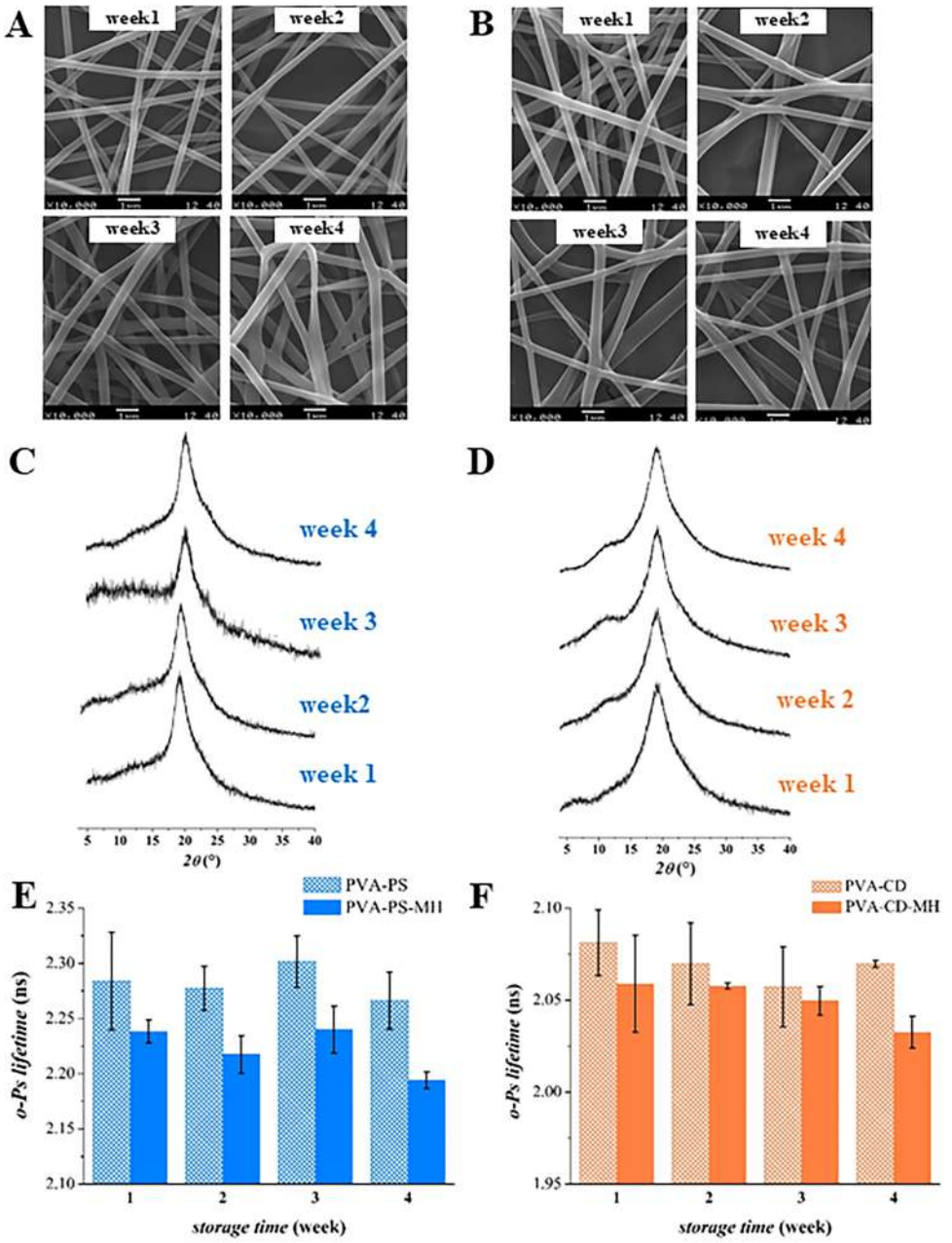

Figure 6. SEM photos (A), powder X-ray patterns (C), and discrete orthopositronium (o-Ps) lifetimes (E) of the stored (1−4 weeks) metoclopramide-HCl loaded polysorbate containing nanofibers. SEM photos (B), powder X-ray patterns (D), and discrete o-Ps lifetimes (F) of the stored (1−4 weeks) metoclopramide-HCl loaded hydroxypropyl-β-cyclodextrin containing nanofibers.

formulations took place as a result of the electrospinning process. ssNMR also confirmed the amorphous state of MH; furthermore, this technique could distinguish the amorphous nature of the active. Although it could be very useful during the formulation design, as the true solid solutions are stable thermodynamically alone, only a few literatures discuss the nature characterization of the amorphous drug delivery.[37,38] The comparison of T_{1rho} relaxation parameters of the neat fibers (matrix) and the drug-loaded ones indicated that the amorphous drug in PVA-CD-MH was molecularly dispersed. While the higher difference between the T_{1rho} relaxations of neat and drug-loaded PVA-PS-MH samples refers to the inhomogeneously distributed solid solution of MH, thus forming solid dispersion-like clusters.

The 2D ROESY measurements suggest that the aromatic moiety is in close proximity to the CD cavity, which refers to complex formation. The observed cross-peaks with the hydroxypropyl chains indicate that external complex formation also took place. From the complexation results of the concentrated liquid solution, we can conclude that the formed structure probably remained in solid state. Considering the chemical structure of the compounds of PVA-PS-MH samples, only a weaker interaction formation is possible. Altogether, in both formulations, the established intermolecular interactions were found strong enough to decrease the molecular mobility of the active and obstruct the enthalpy relaxation needed for its recrystallization, which explains why the amorphous state of MH did not considerably change until the end of the four-week long accelerated stability test.

PALS measurements indicate that the supramolecular structure of PVA-CD-MH samples did not change significantly

DOI: 10.1021/acs.molpharmaceut.8b00646
Mol. Pharmaceutics 2018, 15, 4214−4225

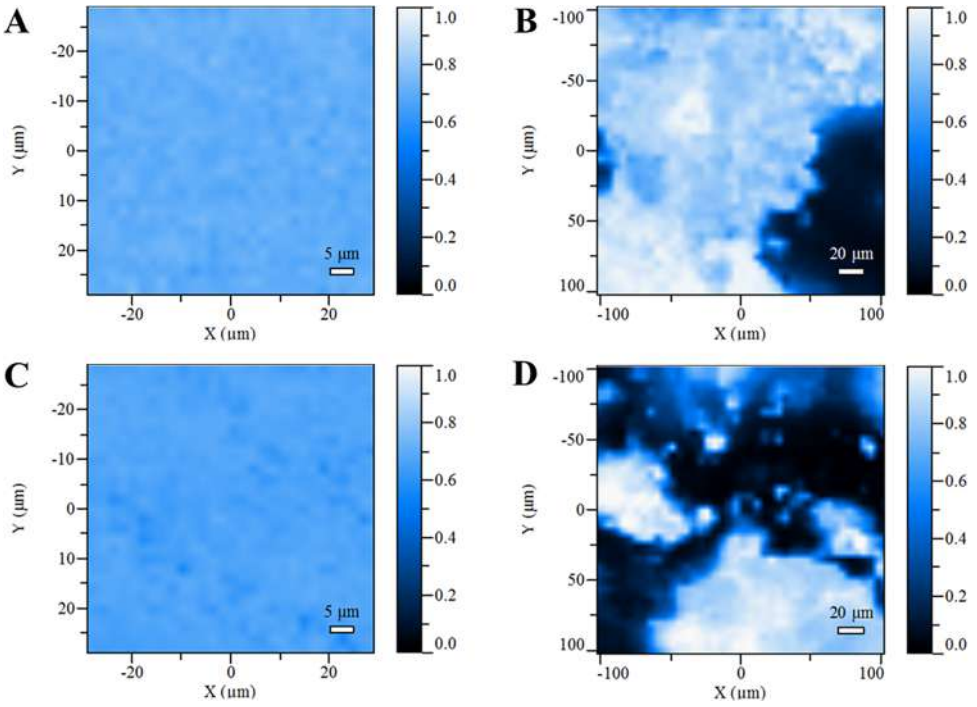

Figure 7. Raman maps of the polysorbate (A) and cyclodextrin (C) containing MH-loaded fibers and the corresponding physical mixtures (B,D).

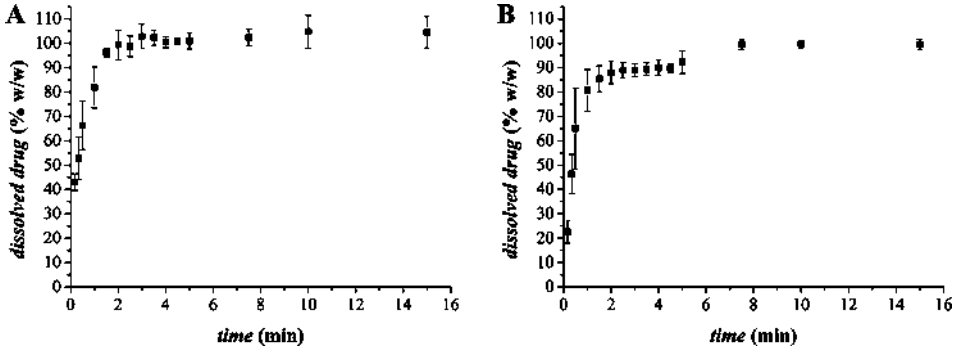

Figure 8. *In vitro* dissolution analysis of the polysorbate (A) and cyclodextrin (B) containing MH-loaded fibrous samples carried out at phosphate buffer of pH = 6.8, where the curves depict the average and deviation of the three parallel measurements.

during the storage, which could be a consequence of the formation of intermolecular interactions and the molecular packing enhancer property of the CD. The observed *o*-Ps values of the PVA-PS-MH reflect the weaker interactions and the fact that the liquid-like plasticizer can migrate in the fiber and could destroy the already formed secondary-bonds,[35] thus leading to time-dependent structural changes.

The measured drug content compared to the theoretical drug loading (latter can be calculated from the initial gel composition, assuming that all the solvent evaporated during the fiber formation process) indicated that almost the total amount of the active drug incorporated into the fibers. The drug distribution of the dosage forms plays a crucial role in formulation development. The Raman maps indicate that the distribution of MH in the electrospun fibrous sheets is homogeneous, which may be a result of the fast solvent evaporation of the electrospinning process. In contrast, the high variation in the MH concentration of the physical mixtures refers to the inhomogeneous drug distribution.

The enhanced apparent aqueous solubility of amorphous materials and the high surface area of fibrous sample, together with the surfactant wettability improving effect enabled fast and complete drug release from the PVA-PS-MH sample. The slightly slower release of MH from PVA-CD-MH nanofibers can be traced back to the secondary interactions between PVA-CD-MH. The increased molecular mobility of PVA may also play an important role in the achievement of a complete dissolution since the release of the active drug is beneficial from a more liquid-like polymer base.

4. CONCLUSION

Both HP-β-CD and PS80 enabled the formation of clear fibrous structure from MH containing PVA gels. A set of physicochemical measurements indicated the crystalline−amorphous transition of the active drug during the fiber formation, moreover, by means of ssNMR, even short-term ordering of MH could be excluded. ssNMR suggested that the use of PS80 or CD enabled the development of a molecularly dispersed system of different homogeneities. It was also pointed out that PS80 and CD render distinct mechanical properties of the fibers, as PS80 advances elastic behavior and CD promotes plastic features.

DOI: 10.1021/acs.molpharmaceut.8b00646
Mol. Pharmaceutics 2018, 15, 4214−4225

PS80 acts as external plasticizer with its liquid-like structure capable of migrating in the polymer matrix, thus resulting in a less plastic behavior of fibers. A similar observation was made during the accelerated stability test suggesting that the established interactions are strong enough to keep the drug in amorphous state until the end of the fourth week storage, even if time-dependent microstructural changes were observed in the presence of PS. CD acts as inner plasticizer and molecular packing enhancer. The amorphous drug is molecularly dispersed in the polymer matrix. Because of the MH-HP-β-CD complex formation, the amorphous nature of the active drug was maintained until the end of the accelerated stability test without any significant supramolecular changes, which together with the homogeneous drug distribution and the complete and fast dissolution makes this formulation promising from the point of both accessibility and stability.

■ ASSOCIATED CONTENT

Supporting Information

The Supporting Information is available free of charge on the ACS Publications website at DOI: 10.1021/acs.molpharmaceut.8b00646.

AFM amplitude-contrast images, representative force curves (taken at 100 nN, 500 nN, 1 μN, and 5 μN maximum loads), histogram of Young moduli and plasticity of the drug-loaded fibrous samples, Raman spectra of the pure amorphous drug extracted with the Multivariate Curve Resolution-Alternating Least Squares (MCR-ALS) method, and the ^{13}C cross-polarization magic angle spinning build-up curve of nanofibrous samples (PDF)

■ AUTHOR INFORMATION

Corresponding Author

*E-mail: zelko.romana@pharma.semmelweis-univ.hu. Tel/Fax: +36-1-2170927.

ORCID

Adrienn Kazsoki: 0000-0002-0611-3124
Tamás Bozó: 0000-0002-2643-0661
Miklós Kellermayer: 0000-0002-5553-6553

Author Contributions

A.K. designed and accomplished the gel preparation and formulated the electrospun fibrous mats, statistically analyzed the SEM results, performed and evaluated FT-IR and PALS measurements, evaluated the XRD results, performed the *in vitro* dissolution study, and wrote the manuscript. P.S. took part in the preformulation study and in the manuscript writing. A.D. and A.B. performed and evaluated the ssNMR measurements. T.B. and M.K. performed and evaluated the AFM measurements. A.F. performed the Raman spectroscopy measurements. D.B.-W. took part in the design of the experiments and in the sample preparation. B.P. performed the SEM measurements. A.D. and S.B. performed and evaluated the liquid-state NMR measurements. J.M. performed the XRD measurements. L.S. took part in the formulation. R.Z. finalized the manuscript.

Notes

The authors declare no competing financial interest.

■ ACKNOWLEDGMENTS

A part of the work was supported by grants from the Hungarian National Research, Development and Innovation Office (K115939; K124966; NVKP-16-1-2016-0017 National Heart Program).

■ REFERENCES

(1) Cramariuc, B.; Cramariuc, R.; Scarlet, R.; Manea, L. R.; Lupu, I. G.; Cramariuc, O. Fiber diameter in electrospinning process. *J. Electrost.* **2013**, *71* (3), 189−198.
(2) Koski, A.; Yim, K.; Shivkumar, S. Effect of molecular weight on fibrous PVA produced by electrospinning. *Mater. Lett.* **2004**, *58* (3), 493−497.
(3) Haider, A.; Haider, S.; Kang, I.-K. A comprehensive review summarizing the effect of electrospinning parameters and potential applications of nanofibers in biomedical and biotechnology. *Arabian J. Chem.* **2015**, DOI: 10.1016/j.arabjc.2015.11.015.
(4) Deitzel, J. M.; Kleinmeyer, J.; Harris, D.; Beck Tan, N. C. The effect of processing variables on the morphology of electrospun nanofibers and textiles. *Polymer* **2001**, *42* (1), 261−272.
(5) Pelipenko, J.; Kocbek, P.; Kristl, J. Critical attributes of nanofibers: Preparation, drug loading, and tissue regeneration. *Int. J. Pharm.* **2015**, *484* (1), 57−74.
(6) Rahma, A.; Munir, M. M.; Khairurrijal; Rachmawati, H. The Influence of Non-Ionic Surfactant on the Physical Characteristics of Curcumin-Loaded Nanofiber Manufactured by Electrospinning Method. *Adv. Mater. Res.* **2015**, *1112*, 429−432.
(7) Jambhekar, S. S.; Breen, P. Cyclodextrins in pharmaceutical formulations I: structure and physicochemical properties, formation of complexes, and types of complex. *Drug Discovery Today* **2016**, *21* (2), 356−362.
(8) Loftsson, T.; Hreinsdóttir, D.; Másson, M. Evaluation of cyclodextrin solubilization of drugs. *Int. J. Pharm.* **2005**, *302* (1−2), 18−28.
(9) Webber, M. J.; Langer, R. Drug delivery by supramolecular design. *Chem. Soc. Rev.* **2017**, *46* (21), 6600−6620.
(10) Uyar, T.; Besenbacher, F. Electrospinning of cyclodextrin functionalized polyethylene oxide (PEO) nanofibers. *Eur. Polym. J.* **2009**, *45* (4), 1032−1037.
(11) Zhang, W.; Chen, M.; Diao, G. Electrospinning β-cyclodextrin/poly(vinyl alcohol) nanofibrous membrane for molecular capture. *Carbohydr. Polym.* **2011**, *86* (3), 1410−1416.
(12) Bazhban, M.; Nouri, M.; Mokhtari, J. Electrospinning of cyclodextrin functionalized chitosan/PVA nanofibers as a drug delivery system. *Chin. J. Polym. Sci.* **2013**, *31* (10), 1343−1351.
(13) Kayaci, F.; Uyar, T. Encapsulation of vanillin/cyclodextrin inclusion complex in electrospun polyvinyl alcohol (PVA) nanowebs: Prolonged shelf-life and high temperature stability of vanillin. *Food Chem.* **2012**, *133* (3), 641−649.
(14) Canbolat, M. F.; Celebioglu, A.; Uyar, T. Drug delivery system based on cyclodextrin-naproxen inclusion complex incorporated in electrospun polycaprolactone nanofibers. *Colloids Surf., B* **2014**, *115*, 15−21.
(15) Borbás, E.; Balogh, A.; Bocz, K.; Müller, J.; Kiserdei, É.; Vigh, T.; Sinkó, B.; Marosi, A.; Halász, A.; Dohányos, Z.; Szente, L.; Balogh, G. T.; Nagy, Z. K. In vitro dissolution−permeation evaluation of an electrospun cyclodextrin-based formulation of aripiprazole using μFlux. *Int. J. Pharm.* **2015**, *491* (1), 180−189.
(16) Baghel, S.; Cathcart, H.; O'Reilly, N. J. Polymeric Amorphous Solid Dispersions: A Review of Amorphization, Crystallization, Stabilization, Solid-State Characterization, and Aqueous Solubilization of Biopharmaceutical Classification System Class II Drugs. *J. Pharm. Sci.* **2016**, *105* (9), 2527−2544.
(17) Chiou, W. L.; Riegelman, S. Pharmaceutical applications of solid dispersion systems. *J. Pharm. Sci.* **1971**, *60* (9), 1281−1302.
(18) He, Y.; Ho, C. Amorphous Solid Dispersions: Utilization and Challenges in Drug Discovery and Development. *J. Pharm. Sci.* **2015**, *104* (10), 3237−3258.
(19) Huang, Y.; Dai, W.-G. Fundamental aspects of solid dispersion technology for poorly soluble drugs. *Acta Pharm. Sin. B* **2014**, *4* (1), 18−25.

(20) Mah, P. T.; Peltonen, L.; Novakovic, D.; Rades, T.; Strachan, C. J.; Laaksonen, T. The effect of surfactants on the dissolution behavior of amorphous formulations. *Eur. J. Pharm. Biopharm.* **2016**, *103*, 13−22.
(21) Hutter, J. L.; Bechhoefer, J. Calibration of atomic-force microscope tips. *Rev. Sci. Instrum.* **1993**, *64* (7), 1868−1873.
(22) Hertz, H. Über die berührung fester elastischer körper. *Journal für die reine und angewandte Mathematik* **1881**, *92*, 156.
(23) Wang, B.; Wu, X.; Gan, T. H.; Rusinek, A. Finite Element Modelling of Atomic Force Microscope Cantilever beams with Uncertainty in Material and Dimensional Parameters. *Eng. Trans.* **2014**, *62*, 403−421.
(24) Lee, J.-H.; Lee, S.-S.; Chang, J.-D.; Thompson, M. S.; Kang, D.-J.; Park, S.; Park, S. A Novel Method for the Accurate Evaluation of Poisson's Ratio of Soft Polymer Materials. *Sci. World J.* **2013**, *2013*, 930798.
(25) Kirkegaard, P.; Eldrup, M.; Mogensen, O. E.; Pedersen, N. J. Program system for analysing positron lifetime spectra and angular correlation curves. *Comput. Phys. Commun.* **1981**, *23* (3), 307−335.
(26) Démuth, B.; Farkas, A.; Pataki, H.; Balogh, A.; Szabó, B.; Borbás, E.; Sóti, P. L.; Vigh, T.; Kiserdei, É.; Farkas, B.; Mensch, J.; Verreck, G.; Van Assche, I.; Marosi, G.; Nagy, Z. K. Detailed stability investigation of amorphous solid dispersions prepared by single-needle and high speed electrospinning. *Int. J. Pharm.* **2016**, *498* (1), 234−244.
(27) Moraes, C. M.; Abrami, P.; de Araujo, D. R.; Braga, A. F. A.; Issa, M. G.; Ferraz, H. G.; de Paula, E.; Fraceto, L. F. Characterization of lidocaine:hydroxypropyl-β-cyclodextrin inclusion complex. *J. Inclusion Phenom. Mol. Recognit. Chem.* **2007**, *57* (1), 313−316.
(28) Masuda, K.; Kaji, H.; Horii, F. CP/MAS 13C NMR analyses of hydrogen bonding and the chain conformation in the crystalline and noncrystalline regions for poly(vinyl alcohol) films. *J. Polym. Sci., Part B: Polym. Phys.* **2000**, *38* (1), 1−9.
(29) Szabó, P.; Daróczi, T. B.; Tóth, G.; Zelkó, R. In vitro and in silico investigation of electrospun terbinafine hydrochloride-loaded buccal nanofibrous sheets. *J. Pharm. Biomed. Anal.* **2016**, *131*, 156−159.
(30) Yamaura, K.; Tada, M.; Tanigami, T.; Matsuzawa, S. Mechanical properties of films of poly(vinyl alcohol) derived from vinyl trifluoroacetate. *J. Appl. Polym. Sci.* **1986**, *31* (2), 493−500.
(31) Mohammad Mahdi Dadfar, S.; Kavoosi, G.; Mohammad Ali Dadfar, S Investigation of Mechanical Properties, Antibacterial Features, and Water Vapor Permeability of Polyvinyl Alcohol Thin Films Reinforced by Glutaraldehyde and Multiwalled Carbon Nanotube. *Polym. Compos.* **2014**, *35*, 1736.
(32) Fukumori, T.; Nakaoki, T. Significant Improvement of Mechanical Properties for Polyvinyl Alcohol Film Prepared from Freeze/Thaw Cycled Gel. *Open J. Org. Polym. Mater.* **2013**, *03* (04), 110.
(33) Hu, W.; Yang, X.; Zhou, J.; Xing, H.; Xiang, J. Experimental research on the mechanical properties of PVA fiber reinforced concrete. *Res. J. Appl. Sci., Eng. Technol.* **2013**, *5* (18), 4563−4567.
(34) Fujiwara, H.; Shibayama, M.; Chen, J. H.; Nomura, S. Preparation of high-strength poly(vinyl alcohol) fibers by crosslinking wet spinning. *J. Appl. Polym. Sci.* **1989**, *37* (5), 1403−1414.
(35) Domján, A.; Bajdik, J.; Pintye-Hódi, K. Understanding of the Plasticizing Effects of Glycerol and PEG 400 on Chitosan Films Using Solid-State NMR Spectroscopy. *Macromolecules* **2009**, *42* (13), 4667−4673.
(36) Bajdik, J.; Marciello, M.; Caramella, C.; Domján, A.; Süvegh, K.; Marek, T.; Pintye-Hódi, K. Evaluation of surface and microstructure of differently plasticized chitosan films. *J. Pharm. Biomed. Anal.* **2009**, *49* (3), 655−659.
(37) Brettmann, B.; Bell, E.; Myerson, A.; Trout, B. Solid-state NMR characterization of high-loading solid solutions of API and excipients formed by electrospinning. *J. Pharm. Sci.* **2012**, *101* (4), 1538−1545.
(38) Brettmann, B. K.; Myerson, A. S.; Trout, B. L. Solid-state nuclear magnetic resonance study of the physical stability of electrospun drug and polymer solid solutions. *J. Pharm. Sci.* **2012**, *101* (6), 2185−2193.

DOI:10.14753/SE.2020.2446

Microstructural distinction of electrospun nanofibrous drug delivery systems formulated with different excipients

Figure S1

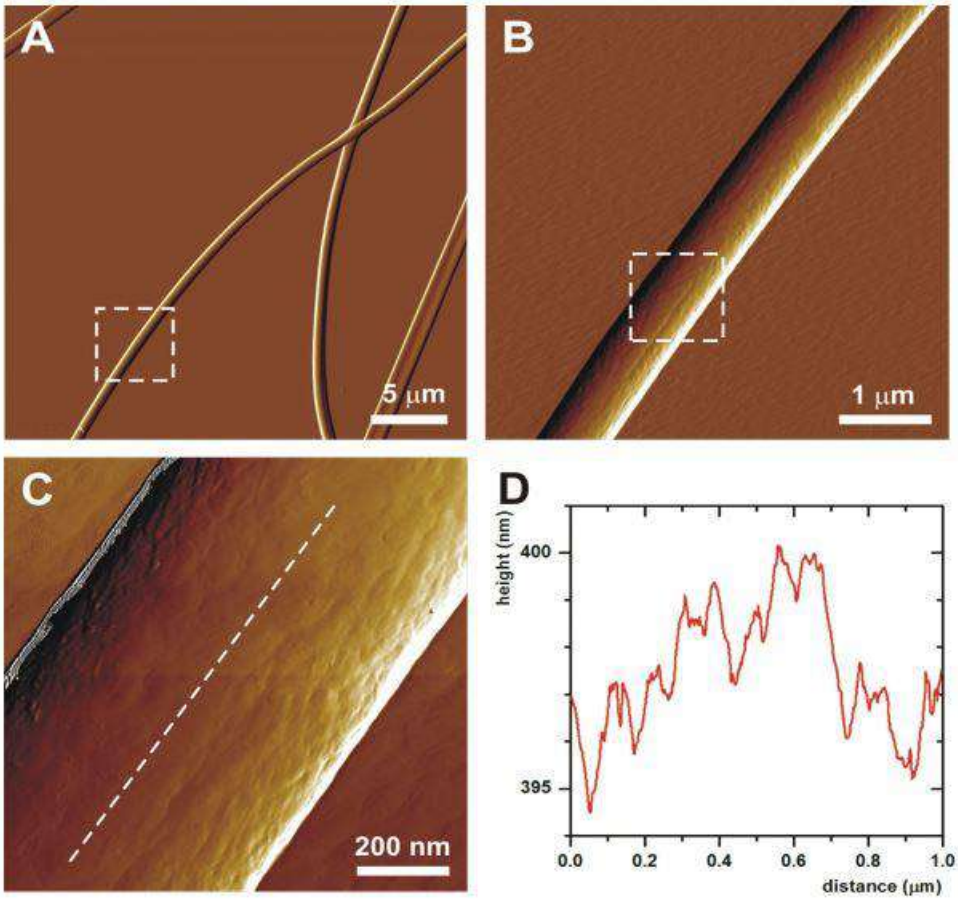

Figure S1. AFM amplitude-contrast images of poly(vinyl alcohol)-based, metoclopramide-HCl-loaded, polysorbate 80 containing (PVA-PS-MH) nanofibers. Panel (B) and (C) are higher resolution images of areas indicated by white, dashed rectangles on panel (A) and (B), respectively. (D) Height section taken alongside the white dashed line in panel (C).

DOI:10.14753/SE.2020.2446

Figure S2

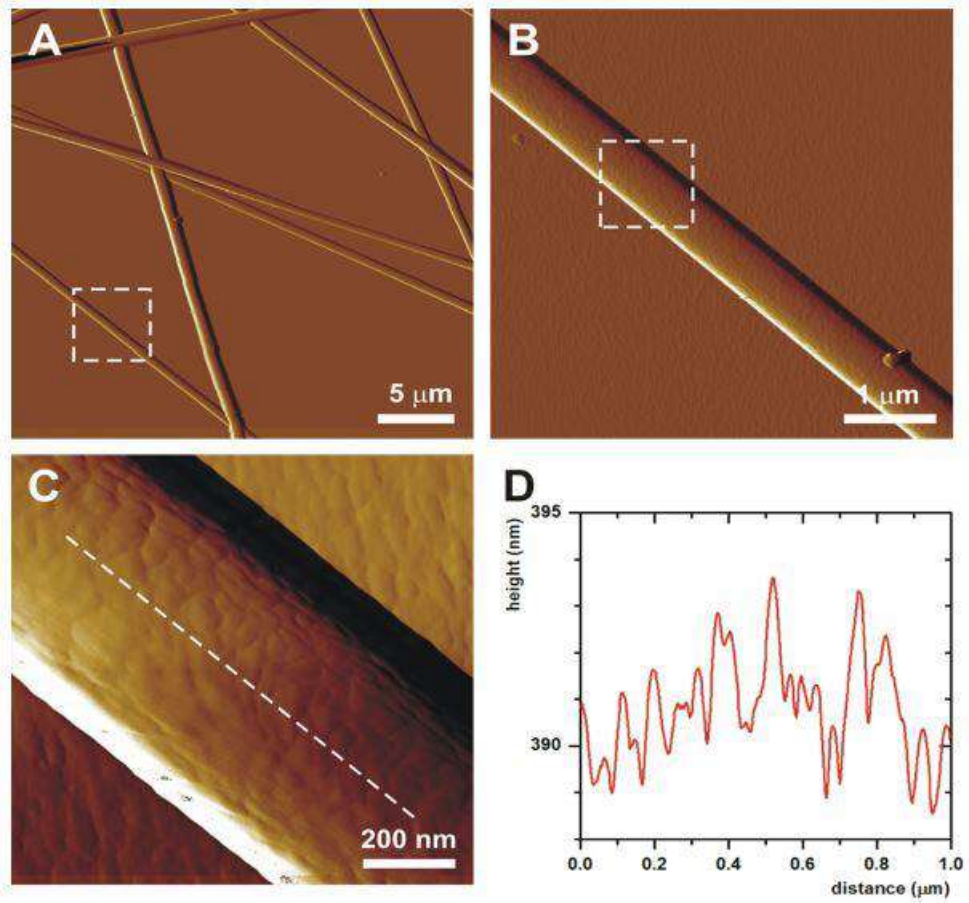

Figure S2. AFM amplitude-contrast images of poly(vinyl alcohol)-based, metoclopramide-HCl-loaded, hydroxypropyl-β-cyclodextrin containing (PVA-CD-MH) nanofibers. Panel (B) and (C) are higher resolution images of areas indicated by white, dashed rectangles on panel (A) and (B), respectively. (D) Height section taken alongside the white dashed line in panel (C).

DOI:10.14753/SE.2020.2446

Figure S3

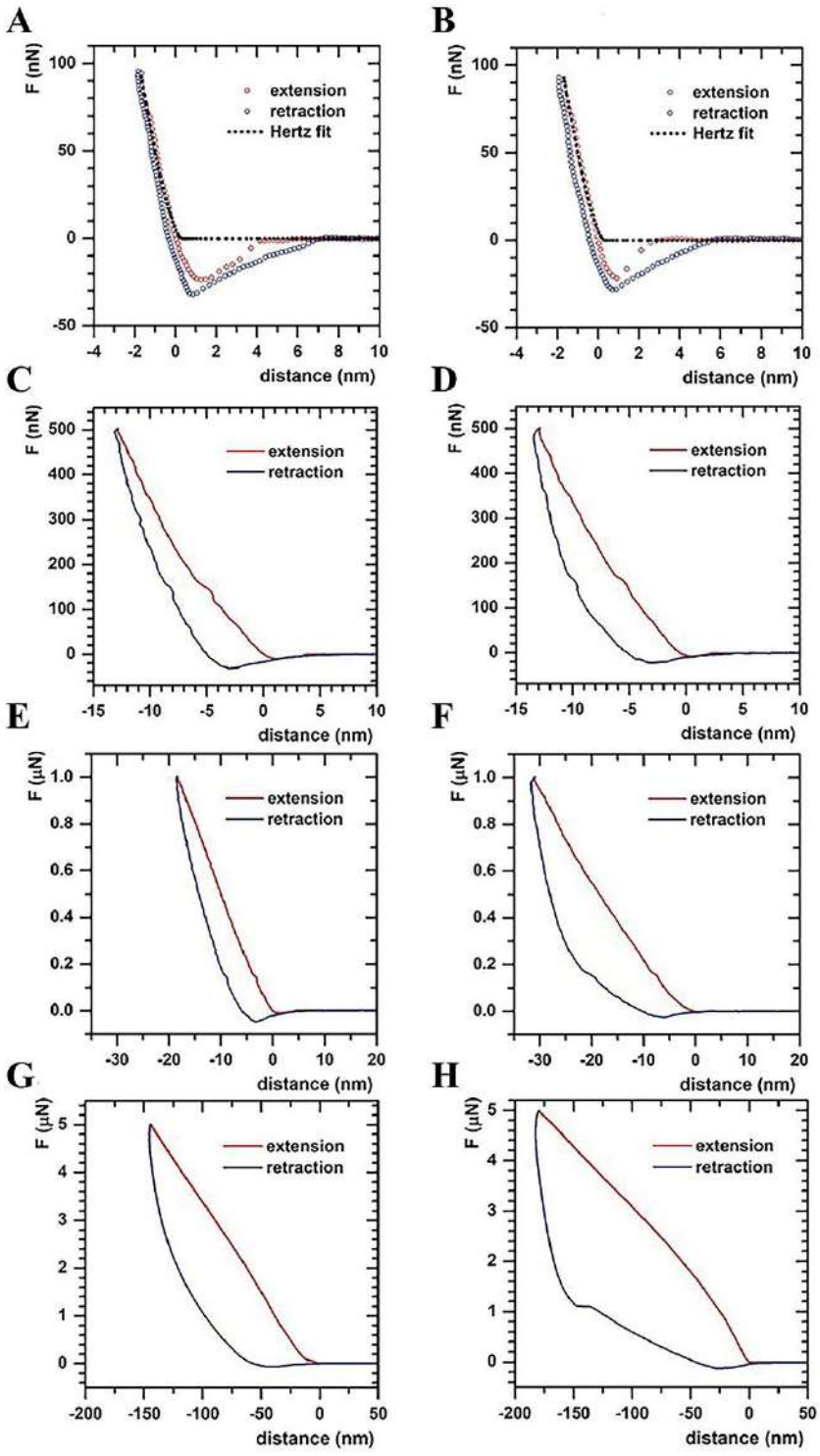

Figure S3 Representative force curves taken from metoclopramide-HCl-loaded either polysorbate 80 containing (left panels) or hydroxypropyl-β-cyclodextrin (right panels) nanofibers at 100 nN (A, B), 500 nN (C, D), 1 µN (E, F), 5µN (G, H) maximum loads. Horizontal axes show the distance from fiber surface.

DOI:10.14753/SE.2020.2446

Figure S4

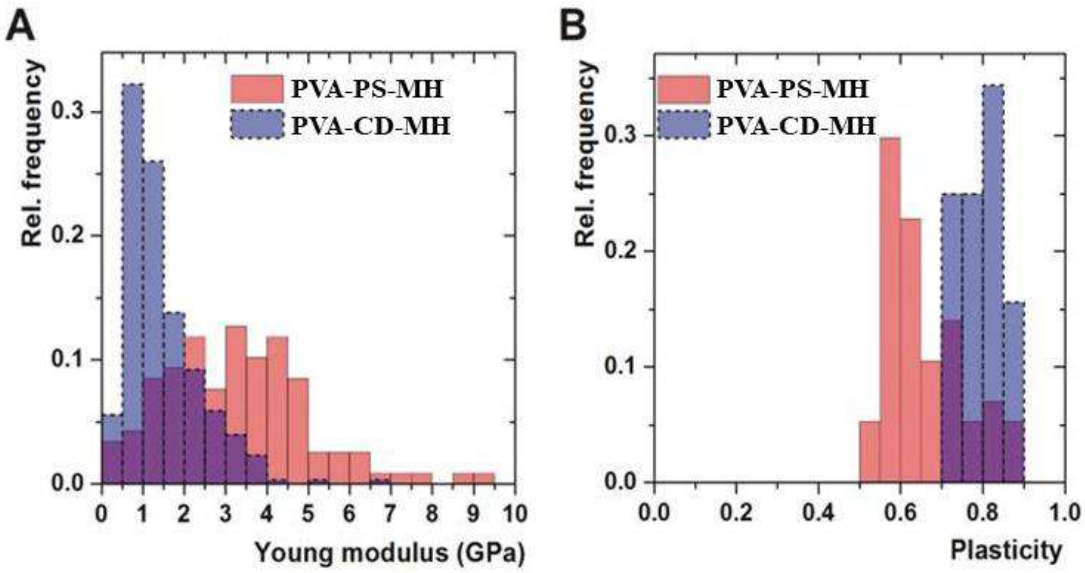

Figure S4 Histogram of (A) Young moduli and (B) plasticity of the metoclopramide-HCl-loaded fibers formed either polysorbate 80 (PVA-PS-MH) or HP-β-cyclodextrin (PVA-CD-MH)

DOI:10.14753/SE.2020.2446

Figure S5

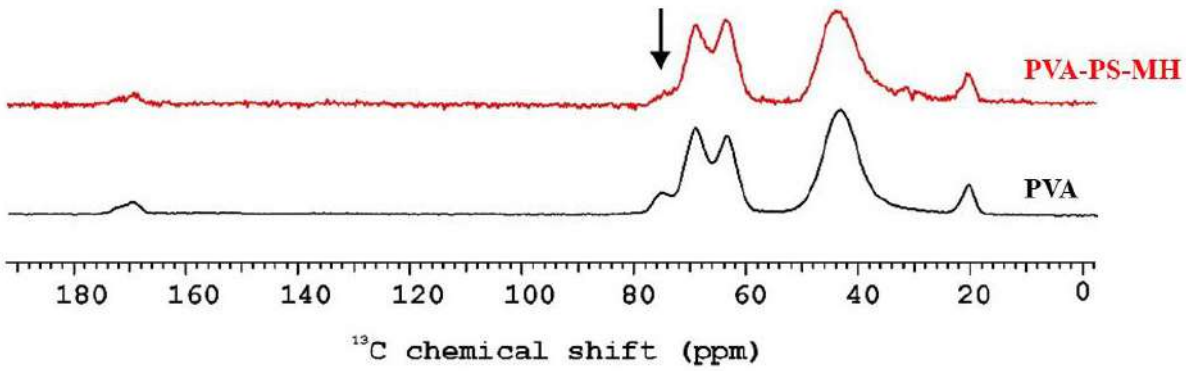

Figure S5 Solid-state NMR spectra of poly(vinyl alcohol) (PVA) and metoclopramide-hydrochloride-loaded, polysorbate 80 containing fibrous sample (PVA-PS-MH)

Figure S6

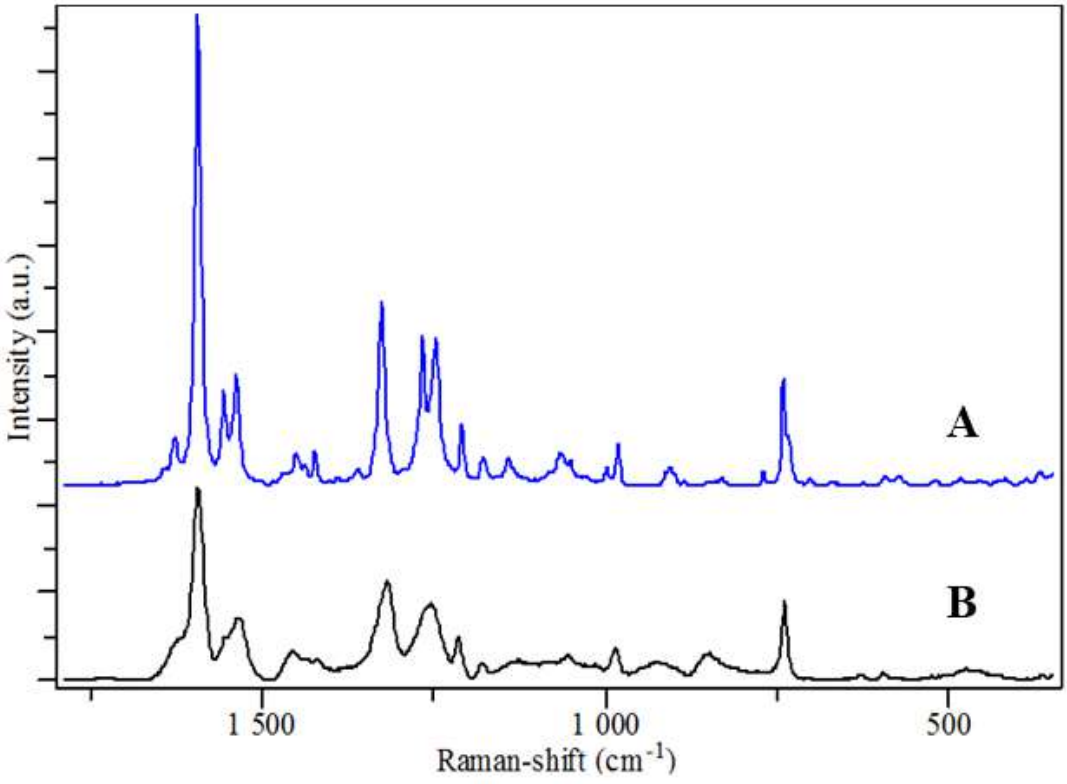

Figure S6 Raman spectra of crystalline (A) and amorphous (B) Metoclopramide-HCl

DOI:10.14753/SE.2020.2446

Figure S7

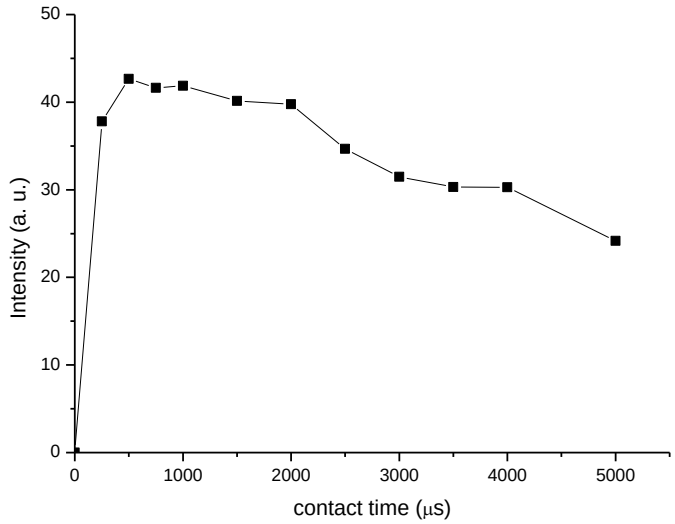

Figure S7 A ^{13}C cross polarization Magic Angle Spinning build-up curve of cyclodextrin in the nanofibrous (PVA-CD) sample

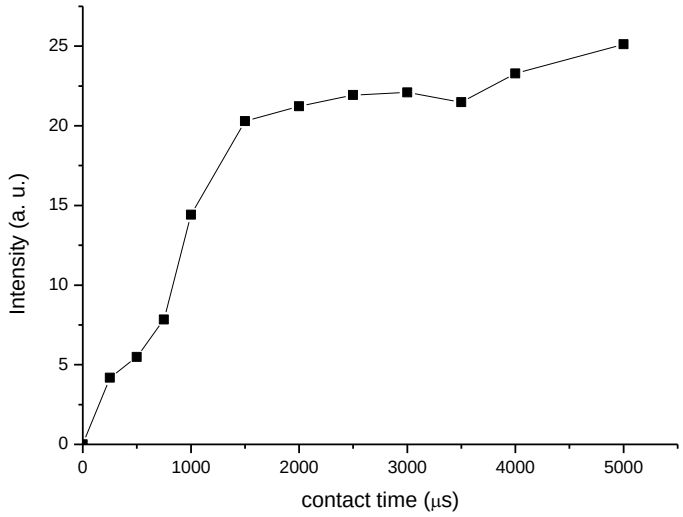

Figure S7 B ^{13}C cross polarization Magic Angle Spinning build-up curve of polysorbate in the nanofibrous (PVA-PS) sample